

Doctoral Theses at NTNU 2004:139

Petter Andreas Berthelsen

**An immersed interface method
for two-dimensional modelling
of stratified flow in pipes**



Department of Energy and Process Engineering
Norwegian University of Science and Technology
Trondheim, Norway, 2004

ISBN 82-471-6505-8 (printed ver.)
ISBN 82-471-6503-1 (electronic ver.)
ISSN 1503-8181

Abstract

This thesis deals with the construction of a numerical method for solving two-dimensional elliptic interface problems, such as fully developed stratified flow in pipes. Interface problems are characterized by its non-smooth and often discontinuous behaviour along a sharp boundary separating the fluids or other materials. Classical numerical schemes are not suitable for these problems due to the irregular geometry of the interface. Standard finite difference discretization across the interface violates the interfacial boundary conditions; therefore special care must be taken at irregular grid nodes.

In this thesis a decomposed immersed interface method is presented. The immersed interface method is a numerical technique formulated to solve partial differential equations in the presence of an interface where the solution and its derivatives may be discontinuous and non-smooth. Componentwise correction terms are added to the finite difference stencil in order to make the discretization well-defined across the interface. A method that approximates the correction terms is also proposed. Results from numerical experiments show that the rate of convergence is approximately of second order.

Moreover, the immersed interface method is applied to stratified multiphase flow in pipes. The flow is assumed to be fully developed and in steady-state. For turbulent flow, both a low Reynolds number turbulence model and a two-layer turbulence model are adopted in order to imitate turbulence in the flow field and in the vicinity of the boundaries. The latter turbulence model is modified accordingly to account for the effects of a wavy interface. In this case, the concept of interfacial roughness is used to model the wavy nature of the interface.

Numerical results are compared with analytical solutions for laminar flow and experimental data for turbulent flow. It is also demonstrated that the current numerical method offers more flexibility in simulating stratified pipe flow problems with complex shaped interfaces, including three-phase flow, than seen in any previous approach.

Acknowledgements

This work has been carried out for the period September 2000 – July 2004 at the Norwegian University of Science and Technology. The project was financed by the Norwegian Research Council. The funding provided by the Scandinavia-Japan Sasakawa Foundation for the participation at ICMF'04, Yokohama, Japan, is also gratefully acknowledged.

I am very thankful to my supervisor, Professor Tor Ytrehus, for his advice, for helpful discussions and his encouragement throughout my research at the Norwegian University of Science and Technology. I am also grateful to Zhi Lin Yang at SINTEF Material and Chemistry, Flow Technology Team, who motivated me to write my own codes, which gave me the necessary experience to develop the ideas that finally led to my results.

I wish to thank Ole Martin Hansen for his effort in getting our own local "super computer" Goliat. I appreciate his hard work to get Goliat up and running, and of course for giving me first priority access (as the only user). I realize now that without the computing power offered this work would have been impossible to finalize. I also wish to thank Reidar Kristoffersen for valuable discussions regarding numerical code development and for providing such a cheerful atmosphere among the research students.

I have also enjoyed the discussions, advice, encouragement and constructive criticism from Vidar Alstad, Gisle Otto Eikrem, Tore Flåtten, Bin Hu, and my fellow doctoral students at the "department of Mechanics", especially Alireza Ashrafian.

Finally, my family and friends have supported me through my studies. I owe them my sincere thanks for putting up with me this exciting, but stressful period, which had its ups and downs. I apologize to those who had to bear the brunt of that.

Petter Andreas Berthelsen
Trondheim, July 2004

Summary

This thesis consists of an introductory part accompanied by four papers, which are self-contained publications in journals and conference proceedings. The introductory part motivates the papers and introduces the underlying mathematical and numerical concepts.

The second part of the thesis consists of the following papers:

Paper I

Berthelsen, P. A. (2004), A decomposed immersed interface method for variable coefficient elliptic equations with non-smooth and discontinuous solutions, *Journal of Computational Physics* **197**(1), 364–386.

Paper II

Berthelsen, P. A. & Ytrehus, T. (2004), Stratified smooth two-phase flow using the immersed interface method, Submitted to *Computers & Fluids*.

Paper III

Berthelsen, P. A. & Ytrehus, T. (2004), Numerical modelling of stratified turbulent two- and three-phase pipe flow with arbitrary shaped interfaces, Presented at *The 5th International Conference on Multiphase Flow, ICMF'04*, Yokohama, Japan, May 30–June 4.

Paper IV

Berthelsen, P. A. & Ytrehus, T. (2004), Calculations of stratified wavy two-phase flow in pipes. Submitted to *International Journal of Multiphase Flow*.

Introductory Part

Table of Contents

1	Introduction	1
1.1	Background	1
1.2	Objective of this study	2
2	A Brief Review on Stratified Flow Models	5
2.1	Introduction	5
2.2	One-dimensional models	7
2.2.1	The Lockhart-Martinelli parameter	7
2.2.2	Mechanistic approach	7
2.3	Two-dimensional models	9
2.3.1	Laminar flow	9
2.3.2	Turbulent flow	9
3	Mathematical Formulation	13
3.1	Momentum equation	13
3.2	Level set formulation	14
3.3	Turbulence model	15
3.3.1	The two-layer model	15
3.3.2	The modified two-layer model	16
3.3.3	Equivalent interfacial roughness	18
3.4	Boundary conditions	19
4	The Grid Structure	21
4.1	Composite, overlapping grid	21
4.1.1	Discretization in computational space	22
4.2	Local grid refinement	23
4.2.1	Block-structured subgrids	24
4.2.2	The coarse/fine grid interface	25
4.3	Grid coupling	27

5	The Immersed Interface Method	31
5.1	Introduction	31
5.2	One-dimensional formulation	32
5.2.1	The Poisson equation	32
5.2.2	A variable coefficient linear equation	34
5.3	Two-dimensional formulation	36
5.3.1	Decomposing the jump conditions	36
5.3.2	Approximate correction terms	37
5.3.3	Curvilinear coordinates	38
6	Comments on the Papers	39
6.1	Paper I	39
6.2	Paper II	40
6.3	Paper III	41
6.4	Paper IV	41
6.5	Further work	42
A	The Mean Flow Equation	45
A.1	The Reynolds equations	45
A.2	Mean turbulent flow in a duct	46
	References	47

Chapter 1

Introduction

The introductory part of the thesis consist of six chapters. In this chapter, a brief introduction to the topic of the thesis is given. Background for the research project is provided, and the objective of the study is briefly stated. Then, in Chapter 2, a short literature review is given on modelling stratified two-phase flow in pipes, introducing the most common expressions and concepts. Chapter 3 presents the two-dimensional model describing stratified multiphase flow in pipes. In Chapter 4 the composite, overlapping grid framework used for the numerical discretization of the governing equations is described. Chapter 5 deals with the construction of a finite difference method for problems with non-smooth and discontinuous solutions. Finally, the papers are summarized and commented in Chapter 6, where concluding remarks are given and some possible directions for further work are suggested.

1.1 Background

In order to maintain a high level of oil production on the Norwegian continental shelf, it becomes increasingly important to devise new technical solutions for optimising the oil production of existing fields. For this particular reason, a jointly run doctoral research programme (PETRONICS), sponsored by the Norwegian Research Council (NFR), was established in 2000 by ABB, Norsk Hydro ASA and 5 departments at the Norwegian University of Science and Technology (NTNU). This collaboration is an interdisciplinary programme which combines the fields of engineering cybernetics, chemical engineering, fluid mechanics and production technology in order to focus on optimised production and automatic control of oil wells and fields.

An important aspect of the programme is the understanding of and the ability to predict the behaviour of multiphase flow in production pipelines. Multiphase flow is a complex phenomenon. The presence of gas and water will affect the transport of oil in the sense that the multiphase mixture will behave differently from the single-

phase flow. From a mathematical point of view, it can be considered as a field which is subdivided into single-phase regions with moving boundaries separating the phases. The difficulties encountered in deriving a physical formulation arise from the presence of a wavy interface and the interaction between the deformed interface and the flow structure in all phases.

In practical engineering problems, most multiphase flow systems have extremely complicated interfacial geometries and motions; consequently, it is still not possible to numerically resolve all details in the flow. Instead, various averaging techniques are used to simplify the global aspects of the flow. In particular, several *closure relations* must be specified in order to include terms like wall and interfacial friction. These closure relations represent the main difficulties in formulating appropriate engineering models. However, the steadily development of more sophisticated numerical methods will eventually give better tools for predicting the flow, without the dependency on empirical closure relations.

1.2 Objective of this study

A great deal of research has been carried out to investigate stratified multiphase flow behaviour. These studies may be classified in the following three categories:

Experimental studies Controlled experiments are carried out in laboratories. Early studies focused mostly on global properties such as pressure drop and in situ phase fractions, leading to simple empirical correlations. Later, more attention has been given to mechanisms and details of the flow field, improving the physical understanding of multiphase flows.

Phenomenological models A mechanistic approach based on simplified physical models is used to determine the frictional pressure drop and in situ phase fractions. This semi-analytical method treats all phases as one-dimensional bulk flows, neglecting the detailed velocity profiles over the cross sections. Empirical correlations based on the average velocities are used to calculate frictional terms.

Detailed flow field analysis The computations are extended to include details of the flow field such as velocity profiles, turbulent intensity and shear stress distribution. Appropriate turbulence models are used to mimic turbulent stresses, and interfacial waves are accounted for through the boundary conditions at the interface.

The focus of this thesis is on detailed flow field analysis with particular emphasis on the numerical aspects.

Although experimentation continues to be important, the use of computational fluid dynamics (CFD) in engineering applications have increased extensively in the past decade. There are basically two reasons for this: a tremendous increase of available computing resources has reduced the cost of using numerical approaches, and the numerical models and algorithms have become more advanced and reliable.

Various techniques for multipurpose use have been successfully employed in modelling evolving surfaces. But these methods have their practical limitations since transient problems are still extremely computationally expensive to solve in multiple spatial dimensions. Instead, it is necessary to introduce some means of simplification to the mathematical formulation. For stratified flow in pipes, the flow is commonly assumed to be fully developed so that it is sufficient to only consider a cross section of the pipe.

Following a classical approach, the equations governing the flow are then discretized and solved on a body-fitted bipolar grid, where the interface is aligned along a grid line. But this numerical procedure is confined to only two-phase flow with simple interface configurations. For typical gas-liquid flow, the assumption of a flat interface is realistic in most practical cases, but for low liquid loads, or liquid-liquid flow, the interface may take a complex curved shape. One of the major disadvantages of using body-fitted grids is the difficulty in representing a complex shaped interface, or even multiple interfaces, without putting too much effort into the grid generation.

The main objective of this study is to investigate the possibilities of using advanced numerical methods to predict stratified multiphase flow in pipes. Particular attention is given to the numerical treatment of the interface. One goal is to construct a numerical model which is more flexible than seen in previous attempts, i.e. capable of solving both two- and three-phase flow with arbitrary shaped interfaces. Towards this aim, ideas originally developed by Leveque & Li (1994) are refined and adapted for this problem. To validate the methods, numerical simulations are compared with analytical and experimental results provided in the literature.

Chapter 2

A Brief Review on Stratified Flow Models

2.1 Introduction

Multiphase pipe flow in different forms occurs in many major industries such as the petroleum, nuclear and chemical industries. In this context, the term multiphase flow refers to both two-phase flow (gas-liquid or liquid-liquid) and three-phase flow (gas-liquid-liquid). For the petroleum industry, a gas phase is usually gaseous hydrocarbons (natural gas), and a liquid phase is either liquid hydrocarbons (oil) or water or a combination of both. The occurrence of multiphase mixtures may arise from production and transportation of hydrocarbons where the gas and the liquid phase initially are separated or a change in pressure and temperature initiate a separation of unprocessed reservoir fluids. Water may arise naturally in the reservoir or be injected for enhanced recovery of hydrocarbons.

Through several years researchers have contributed to the understanding of multiphase flow behaviour. This knowledge is important for many reasons, especially for design and operational purposes. Several different flow patterns can be encountered in two- and three-phase pipe flow. For instance, the different flow regimes in horizontal and near-horizontal gas-liquid flow are usually classified as follows (see Figure 2.1):

Stratified flow The liquid flows along the bottom of the pipe. The interface is either smooth (stratified smooth) or wavy (stratified wavy).

Annular flow The liquid flows as an annular film on the wall. The film may be wavy and droplets are usually dispersed in the gas phase. The film at the bottom is usually thicker than the film at the top for horizontal and near-horizontal flow.

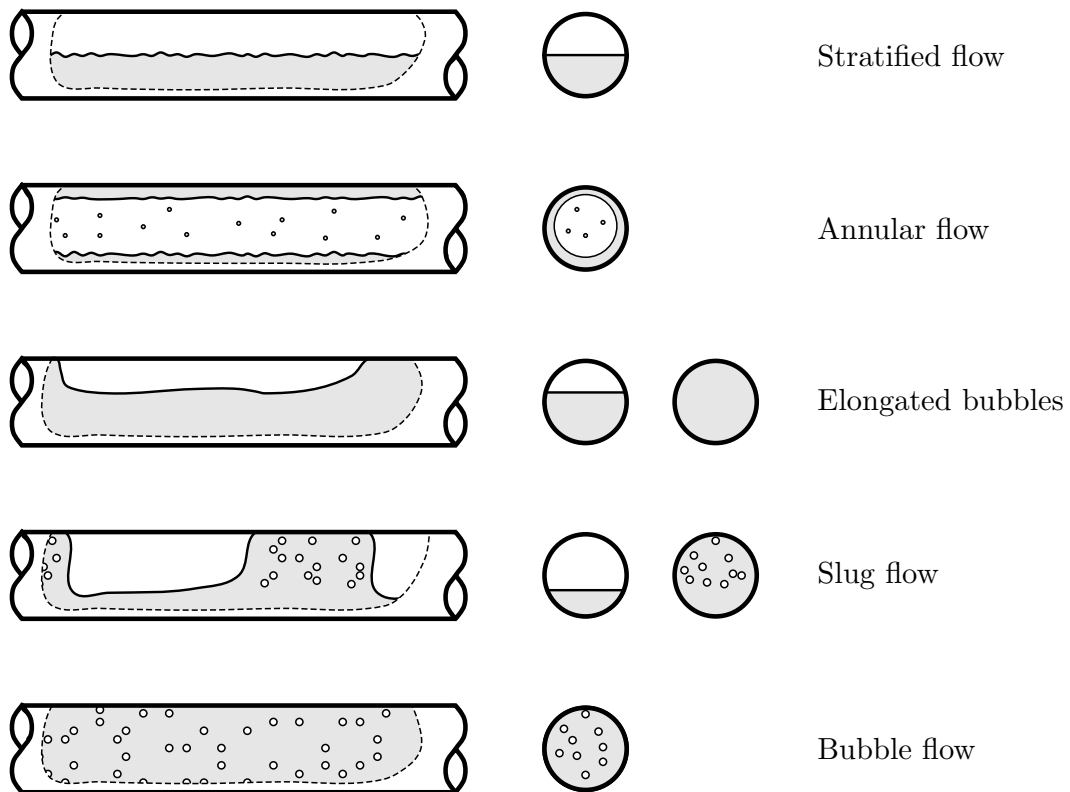


Fig. 2.1: Flow patterns in gas-liquid flow.

Intermittent flow Liquid plugs, free of entrained gas bubbles, are separated by elongated gas bubbles (elongated bubbles) or the liquid phase contains small gas bubbles creating a more chaotic flow pattern (slug flow).

Bubble flow Bubbles are dispersed in the continuous liquid phase.

Stratified flow is the most well-behaved and desirable flow regime in general. Although the nature of stratified flow is much simpler than other flow regimes and probably the best understood one, it is still given a lot of attention. One reason for this is that information about stratified flow can be used as a starting point for analysing transitions to other flow patterns.

The remaining part of this chapter will focus on the stratified flow regime. Only a brief review will be made here, which is limited to the modelling of steady-state two-phase flow, introducing the most common expressions and concepts. A more detailed review of other regimes in two- and three-phase flow can be found in the thesis of Valle (2000), among others.

2.2 One-dimensional models

2.2.1 The Lockhart-Martinelli parameter

Early methods describing two-phase flow have been mainly empirical, such as the parameters proposed by Lockhart & Martinelli (1949). They showed correlations between the pressure drop, represented by the multipliers φ_G and φ_L , and the parameter χ defined as the square root of the ratio of the pressure drop if the liquid flowed alone in the pipe to the pressure drop if the gas flowed alone, e.g.

$$\chi^2 = \frac{|dp/dz|_{Ls}}{|dp/dz|_{Gs}},$$

where the subscript Ls denotes single phase liquid and Gs denotes single phase gas. The pressure gradient multipliers φ_G and φ_L are defined as

$$\varphi_G^2 = \frac{|dp/dz|_{tp}}{|dp/dz|_{Gs}} \quad \text{and} \quad \varphi_L^2 = \frac{|dp/dz|_{tp}}{|dp/dz|_{Ls}},$$

where tp denotes the two-phase system. They also correlated the phase fractions with the parameter χ .

2.2.2 Mechanistic approach

A more physical approach is based on a mechanistic model for the frictional pressure gradient and in situ phase fractions (e.g. Govier & Aziz, 1972; Agrawal et al., 1973; Taitel & Dukler, 1976). For stratified flow, assuming fully developed flow conditions with no hydraulic gradient, the steady-state momentum conservation equations can be expressed as

$$-\alpha_G A \frac{dp}{dz} - \tau_G S_G - \tau_i S_i - \rho_G \alpha_G A g \sin \theta = 0$$

in the gas phase and

$$-\alpha_L A \frac{dp}{dz} - \tau_L S_L + \tau_i S_i - \rho_L \alpha_L A g \sin \theta = 0$$

in the liquid phase, where the subscripts G and L denote the gas and liquid phase, respectively, α is the phase fraction, dp/dz is the pressure gradient, ρ is the phase density, A is the pipe cross sectional area, θ is the pipe inclination angle and S_G , S_L and S_i are the wetted perimeters along the wall and the interface.

The shear stresses are commonly evaluated from

$$\tau_G = f_G \frac{\rho_G \bar{u}_G^2}{2}, \quad \tau_L = f_L \frac{\rho_L \bar{u}_L^2}{2} \quad \text{and} \quad \tau_i = f_i \frac{\rho_G (\bar{u}_G - \bar{u}_L)^2}{2},$$

where \bar{u}_G and \bar{u}_L are the area-averaged bulk velocities in the gas phase and the liquid phase, respectively. Several models exist for the friction factors f_G , f_L and f_i . The gas wall and liquid wall friction factors are almost always calculated using correlations developed for smooth or rough wall single-phase pipe flow. These models are usually Reynolds number dependent where the Reynolds number is based on an equivalent hydraulic diameter for two-phase flow. For instance, Taitel & Dukler (1976) used a modified form of the Blasius formula for the friction factors, i.e.

$$f_G = C_G \text{Re}_G^{-n} \quad \text{and} \quad f_L = C_L \text{Re}_L^{-n},$$

where $C_G = C_L = 0.046$, $n = 0.2$ for turbulent flow and $C_G = C_L = 16$, $n = 1$ for laminar flow. The phase Reynolds numbers are given as

$$\text{Re}_G = \frac{\rho_G D_G \bar{u}_G}{\mu_G} \quad \text{and} \quad \text{Re}_L = \frac{\rho_L D_L \bar{u}_L}{\mu_L},$$

where the hydraulic diameters D_G and D_L are used as suggested by Agrawal et al. (1973),

$$D_G = \frac{4\alpha_G A}{S_G + S_i} \quad \text{and} \quad D_L = \frac{4\alpha_L A}{S_L}.$$

This definition of the hydraulic diameters implies that the wall friction of the liquid phase is similar to that for open-channel flow and of the gas phase is similar to that of closed-duct flow.

In evaluating the interfacial shear stress, Taitel & Dukler (1976) used $f_i = f_G$ and assumed $\bar{u}_G \gg \bar{u}_L$; thus, reducing the interfacial shear stress to be equal to the gas phase wall shear stress. The assumption that f_i equals to f_G gives an acceptable approximation for stratified smooth flow; however, for stratified wavy flow this is acknowledged to give too low estimates of the interfacial shear stress.

It has also been questioned whether the single-phase approximation gives acceptable results in estimating the wall shear stress in two-phase flow (Espedal, 1998). Later studies in mechanistic modelling have mostly been focused on finding better empirical correlations for the wall and interfacial friction terms. The effect of interfacial waves plays an important role in these investigations. Espedal (1998) performed an extensive review of different friction models, which will not be repeated here. He compared the models with his own experimental data and found large deviations among the results, indicating a possible shortcoming in the empirical approach.

The discussion above has been restricted to gas-liquid flow. However, similar mechanistic approaches are used for modelling steady-state liquid-liquid (Brauner & Maron, 1989) and gas-liquid-liquid (Taitel et al., 1995; Khor et al., 1997) flows, where the main difference lies in the definition of the hydraulic diameters.

2.3 Two-dimensional models

Most studies on stratified flow in pipes have been carried out using phenomenological models where various averaging techniques are used to achieve more practical models. Many mechanistic models are applied with reasonable assumption, but these models only predict the integral flow characteristics such as the axial pressure drop and the in situ phase fractions. The only way to obtain the velocity profiles, shear stress distribution and other local flow properties is from a more rigorous treatment of the Navier-Stokes equation. Many researchers have followed this more exact approach, both analytically and numerically.

2.3.1 Laminar flow

Analytical solutions have been obtained for laminar two-phase flow based on simpler or approximated forms of the interface geometry. Derived from the Navier-Stokes equation, the axial velocity profile, u , in both fluids can be described by the Poisson equation

$$\mu \left(\frac{\partial^2 u}{\partial x^2} + \frac{\partial^2 u}{\partial y^2} \right) = \frac{dp}{dz} + \rho g \sin \theta,$$

assuming steady and fully developed flow conditions. In particular, the solution can be expressed in terms of Fourier series or Fourier integrals using a bipolar coordinate system (e.g. Bentwich, 1964; Brauner et al., 1996; Biberg & Halvorsen, 2000), where the interface is commonly aligned along one of the constant curvature lines. Both Brauner et al. (1996) and Biberg & Halvorsen (2000) gave a thorough analysis of the flow, improving the understanding of laminar two-phase flow.

For more complex shaped interfaces, accurate solutions for laminar flow can be obtained numerically. In flow systems with low density difference, the surface-forces may become important, which may lead to a curved interface (Gorelik & Brauner, 1999; Ng et al., 2001). A curved interface affects the fluids' contact area with the pipe wall, and it may have a crucial effect on the pressure drop, particularly for systems with high viscosity ratios. Recently, Ng et al. (2002) used a boundary element method to solve for laminar stratified pipe flow with arbitrary shaped interfaces. They used the Young-Laplace equation, expressing the balance of hydrostatic and surface tension effects, to determine the interface shape (Ng et al., 2001).

2.3.2 Turbulent flow

Yet no rigorous analytical solution exists for turbulent two-phase flow in pipes; therefore, it is necessary to resort to numerical techniques. Among the first few successful attempts to resolve the turbulent flow field numerically in two phase flow are those presented by Akai et al. (1980, 1981) for rectangular channels. For

pipe flow, Shoham & Taitel (1984) discretized and solved the steady-state axial momentum equation in the liquid region using a mixing-length turbulence model. The computations were done in a bipolar coordinate system for convenient mapping of the irregular physical domain. The gas region was treated as a bulk flow, and an empirical correlation was used to couple the two phases through the interfacial shear stress. The spatial dependency of the turbulent viscosity was ignored in their axial momentum equation, casting some doubts about their results.

Based on the work of Akai et al. (1981) and Shoham & Taitel (1984), Issa (1988) included the gas region in the analysis and used a two-equation $k - \varepsilon$ turbulence model with wall functions to calculate stratified smooth two-phase flow in pipes. His results were compared with Shoham & Taitel (1984), and major differences in the computed flow fields were observed. Issa (1988) explained these discrepancies by the importance of resolving the turbulent gas phase in order to provide for correct estimates of the interfacial shear stress.

Newton & Behnia (2000) extended the approach of Issa (1988) by applying a low Reynolds number $k - \varepsilon$ turbulence model to solve stratified smooth gas-liquid flow in pipes. Their model did not rely on empirical wall functions and could therefore predict the wall and interfacial shear stress distributions directly. Later, Newton & Behnia (2001) extended their two-dimensional model for stratified smooth two-phase flow to allow for interfacial waves. A simple empirical shear stress distribution was imposed on the interface in order to modify their model for stratified wavy flow. Although they observed over-predicted turbulence level in the gas phase, their calculations were found to compare favourably with experimental measurements provided that the interfacial conditions remain steady or quasi-steady.

Meknassi et al. (2000) extended the work of Liné et al. (1996) to circular pipes using a bipolar grid. They used the concept of interfacial roughness to account for the wavy gas-liquid interface. The interfacial roughness was estimated from experimental data, and a rough wall function was used to calculate the interfacial shear stress. The effect of secondary flow was considered using an anisotropic turbulence model. The calculated velocity profiles in both phases were compared with the experimental data provided by Lopez (1994) and Strand (1993), and the agreement with the measurements were satisfactory if secondary flows were taken into account.

A slightly different approach than any of the above is given by Mouza et al. (2001). They used a commercial CFD code to calculate the velocity profiles and shear stress distributions in gas-liquid flow for pipe and channel geometries. The objective of their work was to explore the potential of a general purpose CFD code for computing detailed characteristics of stratified flow. The gas and liquid phases were treated separately and coupled through the basic condition of continuity of velocity and shear stress. Calculated values were found to be in good agreement with experimental data.

The various models described above have proven that there is a potential for using

advanced CFD-technology in order to compute detailed characteristics of stratified two-phase flow. But, there is still a need for much more work in this area.

Chapter 3

Mathematical Formulation

A two-dimensional formulation of the stratified flow problem is presented in this chapter. Mathematically, flow of completely separated fluids can be considered by dividing the flow field into single-phase regions where appropriate interfacial boundary conditions couple the phases. A level set function is used to determine the location of the interface.

For brevity, only gas-liquid flow is considered here, but, as shown in Paper III, extension to three-phase flow can also be done by introducing a second level set function.

3.1 Momentum equation

For fully developed, incompressible and stratified two-phase flow in pipes, the time-averaged steady-state axial momentum equation for each phase can be written as (see Appendix A)

$$\frac{\partial}{\partial x} \left(\mu_e \frac{\partial u}{\partial x} \right) + \frac{\partial}{\partial y} \left(\mu_e \frac{\partial u}{\partial y} \right) - \frac{dp}{dz} - \rho g \sin \theta = 0, \quad (3.1)$$

where u is the time-averaged axial velocity, ρ is the density, g is the gravitational acceleration, θ is the pipe inclination angle and dp/dz is the mean pressure gradient in the axial direction.

Assuming isotropic turbulence, the effective viscosity, μ_e , is defined as

$$\mu_e = \mu + \mu_t,$$

where μ is the molecular viscosity and μ_t is the turbulent viscosity. The turbulent viscosity vanishes for the laminar flow, reducing the effective viscosity to the molecular viscosity.

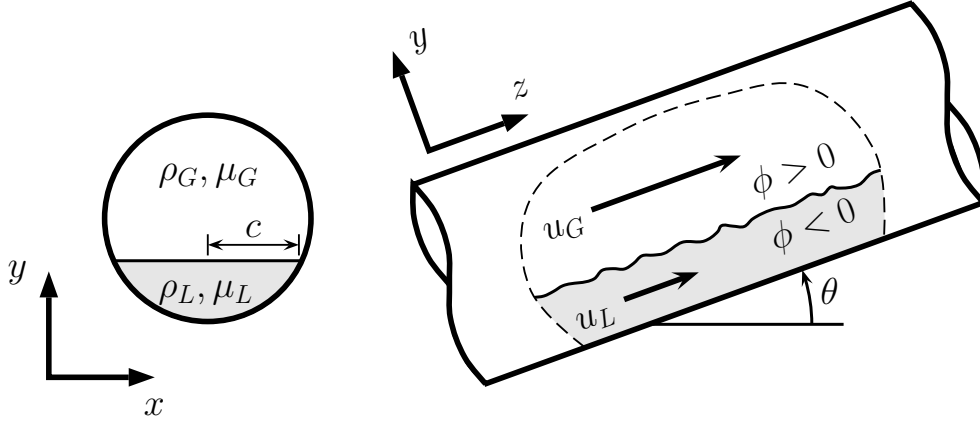


Fig. 3.1: Stratified wavy gas-liquid flow in an inclined pipe.

3.2 Level set formulation

The interface between the two phases, Γ_ϕ , is represented by the zero level of a smooth function ϕ (Osher & Sethian, 1988),

$$\Gamma_\phi = \{(x, y) \in \mathbb{R}^2 \mid \phi(x, y) = 0\}.$$

This auxiliary function is defined as the signed distance to the interface,

$$\phi(x, y) = \pm d_\phi,$$

where d_ϕ is the normal distance to the interface and the sign of ϕ indicates on which side of the interface the point (x, y) is located. The fluid properties can be defined directly from the level set function as (see Fig. 3.1)

$$\rho(\phi) = \begin{cases} \rho_L & \text{if } \phi < 0, \\ \rho_G & \text{if } \phi \geq 0, \end{cases} \quad \text{and} \quad \mu(\phi) = \begin{cases} \mu_L & \text{if } \phi < 0, \\ \mu_G & \text{if } \phi \geq 0, \end{cases}$$

assuming the interface to be infinitely thin. The subscripts L and G denote the liquid phase and the gas phase, respectively.

One advantage using the level set formulation is that for any given point (x, y) the exact distance to the interface is known. This becomes beneficial when evaluating the turbulent length scales in the turbulence model described below.

3.3 Turbulence model

3.3.1 The two-layer model

In this turbulence model, the whole domain is subdivided into a near-surface, viscous-affected inner region and a outer region away from the boundaries. The separation of the two regions is determined by a wall-distance based Reynolds number defined as

$$R_k = \frac{\rho\sqrt{k}d_{\text{eff}}}{\mu},$$

where the effective distance, d_{eff} , for smooth surfaces is given as the shortest distance, d , to a surface, either the wall or the interface. The standard two-equation $k - \varepsilon$ model is used only in the outer region, while the inner region is resolved with a simpler one-equation $k - \ell$ model.

The two models should be matched in a region where viscous effects become negligible. Chen & Patel (1988) found that their results were insensitive to the matching criterion as long as R_k was greater than 200, and they suggested $R_k = 250$ as a suitable matching criterion.

Generally, the eddy viscosity relation can be written as

$$\mu_t = C_\mu \rho \sqrt{k} \ell_\mu, \quad (3.2)$$

where the dimensionless constant C_μ is equal to 0.09, and ℓ_μ is the turbulence length scale. The turbulent kinetic energy (TKE), k , is determined by the model equation

$$\frac{\partial}{\partial x} \left(\mu_k \frac{\partial k}{\partial x} \right) + \frac{\partial}{\partial y} \left(\mu_k \frac{\partial k}{\partial y} \right) + \mu_t \left[\left(\frac{\partial u}{\partial x} \right)^2 + \left(\frac{\partial u}{\partial y} \right)^2 \right] - \rho \varepsilon = 0, \quad (3.3)$$

where $\mu_k = \mu + \mu_t/\sigma_k$, for $\sigma_k = 1.0$.

The length scale ℓ_μ is in the outer region given by

$$\ell_\mu = \frac{k^{3/2}}{\varepsilon}, \quad (3.4)$$

and the dissipation rate, ε , is found from the model equation

$$\frac{\partial}{\partial x} \left(\mu_\varepsilon \frac{\partial \varepsilon}{\partial x} \right) + \frac{\partial}{\partial y} \left(\mu_\varepsilon \frac{\partial \varepsilon}{\partial y} \right) + C_{1\varepsilon} \frac{\varepsilon}{k} \mu_t \left[\left(\frac{\partial u}{\partial x} \right)^2 + \left(\frac{\partial u}{\partial y} \right)^2 \right] - C_{2\varepsilon} \rho \frac{\varepsilon^2}{k} = 0, \quad (3.5)$$

where $\mu_\varepsilon = \mu + \mu_t/\sigma_\varepsilon$, with the constants $\sigma_\varepsilon = 1.3$, $C_{1\varepsilon} = 1.44$ and $C_{2\varepsilon} = 1.92$.

In the viscous-affected inner region, the turbulence length scale takes the form as proposed by Wolfshtein (1969),

$$\ell_\mu = C_\ell d_{\text{eff}} \left(1 - e^{-R_k/A_\mu} \right), \quad (3.6)$$

where the constant C_ℓ is chosen as $\kappa/C_\mu^{3/4}$ to match the log-layer solution, and $\kappa = 0.418$ is the von Karman constant. The model coefficient $A_\mu = 70.0$ is selected so that the model recovers the additive constant in the logarithmic law.

The dissipation rate is represented by

$$\varepsilon = \frac{k^{3/2}}{\ell_\varepsilon} \quad (3.7)$$

in the inner region, where the length scale ℓ_ε is given as

$$\ell_\varepsilon = C_\ell d_{\text{eff}} (1 - e^{-R_k/A_\varepsilon}).$$

The requirement that $\varepsilon \rightarrow 2k\mu/\rho d^2$ as $d \rightarrow 0$ gives $A_\varepsilon = 2C_\ell = 5.08$.

To summarize, the two-layer formulation consists simply of using Eqs. (3.6) and (3.7) near physical boundaries, and switching abruptly to Eqs. (3.4) and (3.5) at the matching point $R_k = 250$.

3.3.2 The modified two-layer model

The interactions between the wave field and the flow in both phases are quite complex. For simplifications, the wavy interface can be treated by an equivalent interfacial roughness. The concept of representing the interfacial waves as surface roughness requires modifications to the turbulence model described above.

Roughness has the effect of increasing the drag force exerted by the rough surface on the flow. This increased flow resistance can be modelled by displacing the effective position of the surface by the height Δd (Rotta, 1962; Jackson, 1981); hence, the shear stress near the rough surface is artificially increased by this shift of origin.

Patel & Yoon (1995) adopted this modification to their two-layer turbulence model and defined the effective distance to a rough surface as

$$d_{\text{eff}} = d + \Delta d.$$

The displacement height can be normalised as follows:

$$\Delta d^+ = \frac{\rho \Delta d u_\tau}{\mu}, \quad (3.8)$$

where Δd^+ is expressed as a function of the normalised roughness height R_s^+ (Cebeci & Smith, 1974; Cebeci & Chang, 1978),

$$\Delta d^+ = 0.9 \left(\sqrt{R_s^+} - R_s^+ e^{-R_s^+/6} \right). \quad (3.9)$$

This relation is a curve fit to the correlation of Rotta (1962), and it is valid for $4.535 < R_s^+ < 2000$. The lower bound corresponds to hydraulically smooth surfaces,

where $\Delta d^+ \cong 0$. The local friction velocity, $u_\tau = \sqrt{\tau/\rho}$, is based on the rough surface shear stress,

$$\tau = (\mu + \mu_t) \frac{\partial u}{\partial n},$$

where $\partial/\partial n$ denotes the derivative in the normal direction of the surface.

The normalised roughness height, $R_s^+ = \rho R_s u_\tau / \mu$, is given from the equivalent sand-grain roughness height, R_s , and it is introduced as a means of converting roughness data obtained from other roughness types and other flow configurations into a roughness measure equivalent to the sand-grain measurements of Nikuradse (1933). Based on this measure, the rough-surface turbulent flow is divided into the following three regimes (Ligrani & Moffat, 1986):

$$\begin{aligned} R_s^+ < 2.25 &: && \text{Hydraulically smooth.} \\ 2.25 \leq R_s^+ \leq 90 &: && \text{Transitional-roughness.} \\ R_s^+ > 90 &: && \text{Fully rough.} \end{aligned}$$

In order to take into account the effects of a wavy interface, the effective distance in the turbulence model described in the previous section can be defined as

$$d_{\text{eff}} = \min(d_w, d_\phi + \Delta d_\phi),$$

where d_w is the normal distance to the wall and Δd_ϕ is defined by Eq. (3.9) for a given equivalent roughness height estimated from the interfacial waves (see Section 3.3.3). The interfacial friction velocity used in Eq. (3.8), $\bar{u}_{\tau,i} = \sqrt{\bar{\tau}_i/\rho}$, is based on the average interfacial shear stress,

$$\bar{\tau}_i = \frac{1}{2c} \int_{-c}^c (\mu + \mu_{t,i}) \frac{\partial u_i}{\partial n} ds, \quad (3.10)$$

where c is half the width of the interface, as indicated in Fig 3.1, and the subscript i denotes the interface. The displacement height, Δd_ϕ , takes different values in the gas and the liquid phase due to the difference in density and viscosity. It should be noted that for a smooth interface, $R_s^+ \rightarrow 0$ and $\Delta d_\phi^+ \rightarrow 0$, the turbulent viscosity, μ_t , is fully damped towards the interface.

Durbin et al. (2001) found it necessary to also delete the damping of the turbulent viscosity to accommodate the fully rough conditions. They suggested the simple linear interpolation

$$A_\mu = \max [A_\mu^{\min}, A_\mu^0 (1 - R_s^+/90)],$$

where A_μ^0 is the value for the smooth case ($A_\mu^0=70$) and A_μ^{\min} was set equal to one. A similar approach for the wavy gas-liquid flow was found to introduce too much turbulent diffusion in both phases. Instead, the turbulence damping near the interface was reduced in the liquid phase only. The expression above was used, where A_μ^{\min} was conveniently chosen as 20.

3.3.3 Equivalent interfacial roughness

It remains to provide a link between the equivalent interfacial roughness and the interfacial waves. Several investigators have proposed different models for estimating the interfacial roughness (e.g. Charnock, 1955; Oliemans, 1987; Hamersma & Hart, 1987; Srichai, 1994). The discussion below is limited to the approach presented in Paper IV, but more details is given in the thesis of Espedal (1998) and the references therein.

The influence of the interfacial roughness on the interfacial momentum transfer has been devoted considerable attention in environmental engineering. Charnock (1955) linked the surface roughness to the frictional velocity by the following expression:

$$R_s = \beta \frac{u_{\tau,i}^2}{g},$$

where the Charnock parameter, β , is between 0.36 and 1.05 for deep water waves. Rosant (1983) proposed to modify β for pipe flow as follows:

$$\beta = 1238 \left(\frac{\rho_G}{\rho_L} \right) \min(\alpha_L, 0.1),$$

where α_L is the liquid phase area fraction.

Meknassi et al. (2000) estimated the Charnock parameter from a large data bank (Strand, 1993; Lopez, 1994) and found a close relation to the formulation given by Rosant (1983). The equivalent roughness height of the interface was approximated for a given experimental estimation of the friction factor using a classical relationship between friction factor and roughness in turbulent flow. This method of obtaining the roughness was then compared with the value determined from the experimental profile of longitudinal velocity above the waves using the experimental data of Strand (1993). They concluded that the values were very close.

Following Meknassi et al. (2000), the equivalent roughness can be estimated from Espedal's (1998) data using Colebrook's (1933) equation,

$$\frac{1}{2\sqrt{f_i}} = -2 \log \left(\frac{2.51}{2\text{Re}_G\sqrt{f_i}} + \frac{R_s}{3.7D_G} \right),$$

where f_i is the interfacial friction factor, Re_G is the gas Reynolds number, and D_G is the hydraulic diameter in the gas phase. The data presented in Paper IV gave a wide scattered result for the Charnock parameter, ranging from 0.1 to 0.2, and Rosant's (1983) correlation gave in most cases lower values for β . According to Liné et al. (1996) the order of magnitude of β should be consistent, but the Charnock parameter cannot be constant for various flow conditions. A sensitivity analysis showed that the choice of Charnock parameter, within the range 0.1–0.2, had an effect on the calculations, but not to dramatic as large changes in the Charnock parameter only led to small changes in the calculations.

3.4 Boundary conditions

At the pipe wall, the boundary conditions for the velocity, u , and the TKE, k , are given by

$$u_w = 0 \quad \text{and} \quad k_w = 0,$$

where the subscript w denotes the boundary value at the wall. The turbulent viscosity and the dissipation rate is given explicitly by Eqs. (3.2) and (3.7), where the limiting values for $d_{\text{eff}} = d \rightarrow 0$ are

$$\mu_{t,w} = 0 \quad \text{and} \quad \varepsilon_w = \lim_{d \rightarrow 0} \frac{2\mu k}{\rho d^2}.$$

To model the wavy interface, more complex boundary conditions are required. The steady nature of the present model rules out the use of an unsteady interface. Instead, the wavy interface must be accounted for by using approximate methods. Since the wavy interface is already treated as a rough interface it is reasonable to continue this approach when determining the interfacial boundary conditions.

It is customary to use empirical wall functions for rough surfaces to calculate the interfacial velocity and shear stress (e.g. Akai et al., 1981; Issa, 1988; Meknassi et al., 2000). However, the two-layer model resolves the turbulence in the vicinity of the interface, allowing for a direct calculation of the interfacial shear stress. Therefore, assuming a nonzero, finite value for the TKE, the turbulent viscosity, μ_t , takes a nonzero value at the interface for the non-smooth case. The requirement of continuity in velocity and shear stress yields the following interfacial boundary condition for the velocity field

$$u_{i,L} = u_{i,G},$$

and

$$(\mu + \mu_{t,i})_L \frac{\partial u_{i,L}}{\partial n} = (\mu + \mu_{t,i})_G \frac{\partial u_{i,G}}{\partial n},$$

where $\partial/\partial n$ denotes the derivative normal to the boundary and the subscript i denotes the interfacial boundary value.

In the early work of Akai et al. (1981) it is suggested that the continuity condition for the TKE is not always necessary. They explained this by the large scale eddies containing a large amount of energy produced by the flow separation in the gas phase. This is considered not to be a concern in the liquid phase. The boundary condition on k for a fully rough surface is $u_\tau^2/\sqrt{C_\mu}$. Similar expression was proposed by Rodi (1993) for wind-induced shear stress at a free surface, and adopted by Newton & Behnia (2001) for both the gas and the liquid sides of the interface. In this case, since the interfacial shear stress is equal in both phases, the level of the TKE at the interface will differ by the ratio of the fluid densities. Meknassi et al. (2000) used

this boundary condition only on the gas side, and assumed that k takes a maximum value on the liquid side of the interface, i.e. $\partial k/\partial n = 0$.

The present model uses a similar boundary condition on k as proposed by Newton & Behnia (2001) for a fully rough interface. On a smooth surface, k is equal to zero, and Durbin et al. (2001) suggested a simple quadratic interpolation for the transitional regime. Therefore, the boundary condition used on the TKE at the interface, k_i , takes the form

$$k_i = \frac{u_{\tau,i}^2}{\sqrt{C_\mu}} \min [1, (R_s^+/90)^2],$$

on both sides of the interface. The local interfacial friction velocity, $u_{\tau,i} = \sqrt{\hat{\tau}_i/\rho}$, is approximated by a power law distribution of the interfacial shear stress (Newton & Behnia, 2001),

$$\hat{\tau}_i = \left(1 + \frac{1}{m}\right) \bar{\tau}_i \left(1 - \frac{s}{c}\right)^{1/m},$$

where $m = 6.6$, c is half the width of the interface, and s is the distance from the vertical centerline along the interface. The average interfacial shear stress, $\bar{\tau}_i$, is estimated from the flow field by Eq. (3.10). This empirical distribution gives maximum value for the interfacial TKE at the vertical center line of the pipe, and the level of turbulence will be reduced close to the wall.

Chapter 4

The Grid Structure

The governing equations presented in Chapter 3 are discretized and solved using a finite difference scheme on a composite, overlapping grid (Chesshire & Henshaw, 1990; Henshaw & Schwendeman, 2003) with local grid refinements (Martin & Cartwright, 1996; Martin, 1998) near the interface and the wall. This chapter describes the grid structure used for the multiphase pipe flow calculations.

4.1 Composite, overlapping grid

Most practical flow problems involve complex geometries which are not easily fit with Cartesian grids. The idea behind a composite grid framework is to divide a complex computational domain into simpler subdomains, so that every subdomain can be covered with a component grid. Each component grid is logically rectangular, and it has its own coordinate transformation, or mapping function, defined as

$$(x, y) = \Phi(\xi, \eta),$$

from the computational space (ξ, η) to the physical space (x, y) . The component grids may overlap to cover the entire computational domain.

Every point on a component grid are classified as one of the following:

- *Discretization point.* A point is a discretization point if it can be discretized in terms of points on the same component grid which are discretization points or interpolation points.
- *Interpolation point.* An interpolation point is a point that can be interpolated from discretization or interpolation points on another component grid.
- *Exterior or unused point.* If the point is not classified as any of the above, then it is an exterior or unused point.

In addition, the computational boundaries on each component grid are classified as a physical boundary, a periodic boundary or an interpolation boundary.

The partial differential equations are discretized and solved in computational space on each component grid separately. Grid function values at interpolation points (interior or boundary) of a component grid are obtained by interpolation from *interpolee* points on another component grid at every iteration step. The interpolation is either *explicit* (the interpolee points are all discretization points) or *implicit* (some of the interpolee points are interpolation points). The interpolation is done in computational space using standard interpolation techniques where the interpolation point, (x, y) , is given in computational space coordinates using the inverse mapping $(\xi, \eta) = \Phi^{-1}(x, y)$.

The overlapping grid framework used for solving stratified flow in pipes consists of two base component grids describing half the cross section of a pipe: a rectangular and a circular grid. The grid nodes are cell centered, and the grid function values are obtained by an explicit, two-dimensional Lagrange interpolation of degree two at interpolation points. This quadratic interpolation is used in order to obtain second order accuracy when solving second order elliptic equations (see Chesshire & Henshaw, 1990, for further details).

4.1.1 Discretization in computational space

The discretized equations are solved in the computational space (ξ, η) . It is therefore convenient to rewrite the governing equations using a general orthogonal, curvilinear coordinate system which represents the computational domain.

Let the general orthogonal, curvilinear system (ξ, η) be related to a Cartesian system (x, y) so that the element of arc length ds is given by

$$(ds)^2 = (dx)^2 + (dy)^2 = (l_\xi d\xi)^2 + (l_\eta d\eta)^2.$$

The metric stretching factors l_ξ and l_η defines the arc length along the curvilinear ξ - and η -coordinate lines, and they are given as

$$l_\xi = \sqrt{\left(\frac{\partial x}{\partial \xi}\right)^2 + \left(\frac{\partial y}{\partial \xi}\right)^2} \quad \text{and} \quad l_\eta = \sqrt{\left(\frac{\partial x}{\partial \eta}\right)^2 + \left(\frac{\partial y}{\partial \eta}\right)^2}.$$

The gradient of a scalar grid function v is in the curvilinear system given as

$$\nabla v = \left(\frac{1}{l_\xi} \frac{\partial v}{\partial \xi}, \frac{1}{l_\eta} \frac{\partial v}{\partial \eta} \right),$$

and the divergence of any vector $\mathbf{A} = (A_1, A_2)$ is

$$\nabla \cdot \mathbf{A} = \frac{1}{l_\xi l_\eta} \left[\frac{\partial}{\partial \xi} (l_\eta A_1) + \frac{\partial}{\partial \eta} (l_\xi A_2) \right].$$

Then any of the elliptic equations in Chapter 3, given in the general Cartesian form

$$(\beta v_x)_x + (\beta v_y)_y = f(x, y),$$

can be rewritten as

$$(\beta^\xi v_\xi)_\xi + (\beta^\eta v_\eta)_\eta = l_\xi l_\eta f(\xi, \eta) \quad (4.1)$$

for a component grid in computational space, where v denotes any of the flow variables, and

$$\beta^\xi = \frac{l_\eta}{l_\xi} \beta \quad \text{and} \quad \beta^\eta = \frac{l_\xi}{l_\eta} \beta,$$

for the diffusion coefficient β .

Further, let the logically rectangular and uniform grid $[a, b] \times [c, d]$ describe the component grid. The grid nodes are cell centered and equally spaced,

$$h = (b - a)/M = (d - c)/N,$$

where M and N are the number of gridpoints in the ξ - and η -direction, respectively. The grid coordinates are defined as

$$\xi_i = a + ih, \quad \eta_j = c + jh \quad \text{for } 0 \leq i \leq M, \quad 0 \leq j \leq N,$$

and the numerical approximation of $v(\xi_i, \eta_j)$ is written as $V_{i,j}$. Then the left-hand-side of Eq. (4.1) can be approximated with the following discretization in the computational domain:

$$\begin{aligned} \mathcal{L}_h^\beta V_{i,j} = & \frac{\beta_{i+1/2,j}^\xi (V_{i+1,j} - V_{i,j}) - \beta_{i-1/2,j}^\xi (V_{i,j} - V_{i-1,j})}{h^2} \\ & + \frac{\beta_{i,j+1/2}^\eta (V_{i,j+1} - V_{i,j}) - \beta_{i,j-1/2}^\eta (V_{i,j} - V_{i,j-1})}{h^2}, \end{aligned} \quad (4.2)$$

where

$$\beta_{i+1/2,j}^\xi = \beta^\xi(\xi_{i+1/2}, \eta_j) \quad \text{and} \quad \beta_{i,j+1/2}^\eta = \beta^\eta(\xi_i, \eta_{j+1/2}).$$

It should be noticed that the finite difference stencil in Eq. (4.2) is not well-defined across physical interfaces where the solution may not be smooth and continuous. For those grid cells adjacent to an interface, a modified discretization is used. The numerical issues related to this modification are fully discussed in Chapter 5.

4.2 Local grid refinement

A major characteristic of all turbulent flows is the large variety in length scales. Although large scales of turbulent motions are the most energy containing motions,

small scale motions play a crucial role in transferring and dissipating the energy. Therefore these small scale motions need to be sufficiently resolved, i.e. very high grid resolution is needed at the regions where these motions are likely to occur, such as near the solid walls and the interface.

The choice of grid resolution is a compromise between the numerical accuracy wanted and the computational resources available. Since small scale effects occur only in small parts of the domain the grid is refined locally only where it is needed. For turbulence models applied to the viscous sublayer, such as two-layer models and low Reynolds number models, it is very important that the region below approximately $y^+ = 30$ is sufficiently resolved, where y^+ is the local wall unit distance. A goal for this work has been to obtain adequate resolution of the viscous sublayer. This has been achieved by using a grid cell spacing of approximately 2–3 y^+ -units at the finest level.

4.2.1 Block-structured subgrids

The local grid refinement approach adds new refinement grids where the variations of the turbulent quantities are estimated to be large. The grid cells that are tagged for refinement are grouped together using the point clustering algorithm of Berger & Rigoutsos (1991) to form efficient block structured patches which cover the tagged regions. In this way, areas that need higher resolution can be covered with a relatively small number of refined subgrids.

The point clustering algorithm is as follows (see Fig. 4.1):

- 1) The smallest box possible is placed around the tagged cells. Check if this box satisfy the grid efficiency requirement,

$$n_{\text{eff}} = \frac{\text{number of tagged cells}}{\text{total number of cells refined}} \geq n_{\text{min}} (= 0.8 \text{ in this work}).$$

If $n_{\text{eff}} < n_{\text{min}}$ and the box is sufficiently large, then proceed to the next step.

- 2) Split the box in two. The position of the split, the cut point, is found by using a histogram formed from the number of tagged cells in each plane normal to both coordinate directions. Use the following prioritized order to determine the cut point:
 - i) Look for gaps in the tagged cells (the histogram, Σ , goes to zero).
 - ii) Look for inflection points (places where the sign of the second derivative, Δ , of the histogram changes). The cut point is located at the biggest inflection point.
 - iii) Bisect the box.

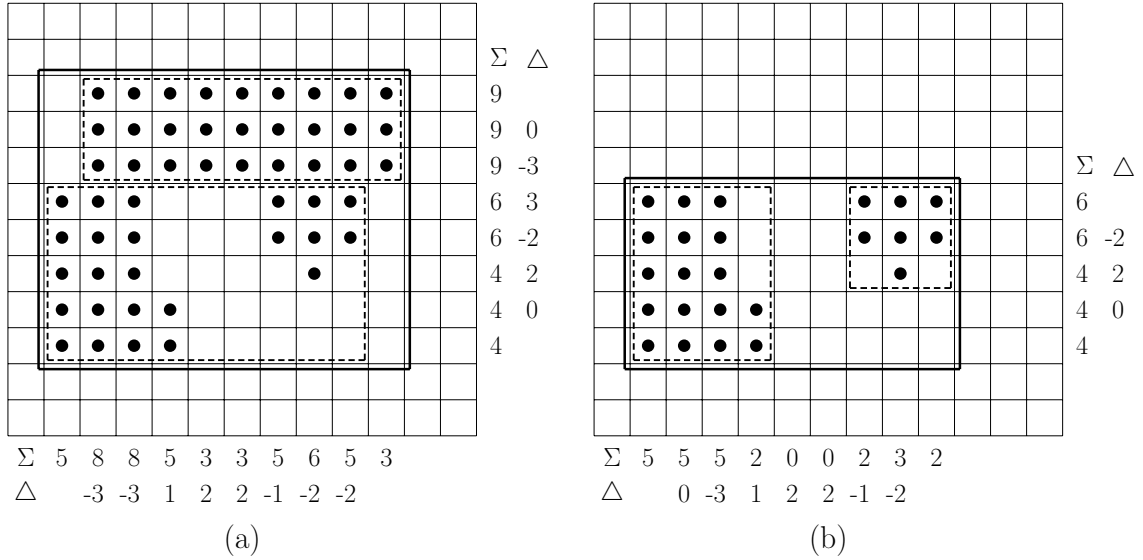


Fig. 4.1: Box splitting of tagged cells (\bullet) where solid lines denote the old box boundary and the dashed lines denote the new sub-boxes boundaries. (a) The box is split in two sub-boxes at the biggest inflection point (change of sign of Δ with largest difference); (b) The box is split at gaps in tagged cells ($\Sigma = 0$).

- 3) After the box is split in two, step 1 is repeated for each one of the two new sub-boxes.

Then, after the box splitting, the new subgrids are refined and, until adequate resolution is obtained, tagged for further point clustering and refinement.

The refinement is done in computational space, and the refined subgrids are aligned with the underlying base component grids, arranged in a hierarchy with the base grids belonging to level $l = 0$, the next finer grids are added to $l = 1$, and so on. The subgrids are properly nested, meaning that any refined grid is bordered by either a physical boundary, another grid at the same refinement level l , or grids with only one refinement level lower, $l - 1$.

4.2.2 The coarse/fine grid interface

Special attention must be given to the coarse/fine grid interface in order to get the expected increase of accuracy. The communication between the grid levels are done in a similar manner as explained by Martin & Cartwright (1996). The coarse grid passes information to the fine grid in the form of a Dirichlet boundary condition. The fine grid solution uses this Dirichlet boundary condition and changes the slope of the solution along the coarse/fine grid interface. This way, the grid function itself

is continuous across the coarse/fine interface, but its normal derivative, or flux, is only continuous if this change of the solution is passed back to the coarse grid in a proper way. This is what Martin & Cartwright (1996) referred to as the elliptic matching condition.

Consider a refined grid with only one level of refinement ($l_{\max} = 1$). Let Ω^c and Ω^f represent the coarse and the fine computational domain, respectively, where $\partial\Omega^f$ denotes the boundary between the domains. Rewrite the elliptic operator \mathcal{L}_h^β in Eq. (4.2) as a flux difference operator, i.e.

$$\mathcal{L}_h^\beta V_{i,j} = \frac{F_{i+1/2,j}^\xi - F_{i-1/2,j}^\xi + F_{i,j+1/2}^\eta - F_{i,j-1/2}^\eta}{h},$$

where the fluxes are given as

$$F_{i+1/2,j}^\xi = \beta_{i+1/2,j}^\xi \frac{(V_{i+1,j} - V_{i,j})}{h} \quad \text{and} \quad F_{i,j+1/2}^\eta = \beta_{i,j+1/2}^\eta \frac{(V_{i,j+1} - V_{i,j})}{h}$$

in both coordinate directions.

For the region away from $\partial\Omega^f$, in both Ω^c and Ω^f , the operator \mathcal{L}_h^β is simply the standard five point stencil given by Eq. (4.2). If the cell is bordering the interface, then special care must be taken. On the coarse side of the interface, the flux passing through $\partial\Omega^f$ is replaced by an average flux calculated on the fine grid level. Summing the fluxes passing in and out of a coarse cell located above the boundary gives

$$\mathcal{L}_h^\beta V_{i,j} = \frac{F_{i+1/2,j}^\xi - F_{i-1/2,j}^\xi + F_{i,j+1/2}^\eta - F_{i,j-1/2}^{\eta,\text{ave}}}{h^c},$$

where

$$F_{i,j-1/2}^{\eta,\text{ave}} = \frac{1}{2} \left(F_{\text{left}}^{\eta,f} + F_{\text{right}}^{\eta,f} \right) \quad (4.3)$$

and

$$F_{\text{left/right}}^{\eta,f} = \frac{\beta^\eta}{h^f} (V^g - V^f).$$

The superscripts c and f denote the value on the coarse and the fine level, respectively.

The interpolated value V^g is obtained by first a quadratic interpolation parallel to the boundary to get the intermediate points on both sides of the coarse grid node location, as shown in Fig. 4.2. Then a quadratic interpolation is used normal to the coarse/fine interface to get the "ghost cell" value, V^g , for the fine grid. For fine cells adjacent to the boundary, \mathcal{L}_h^β is the standard stencil using these "ghost cell" values, since this will be equivalent to enforcing the elliptic matching condition at $\partial\Omega^f$.

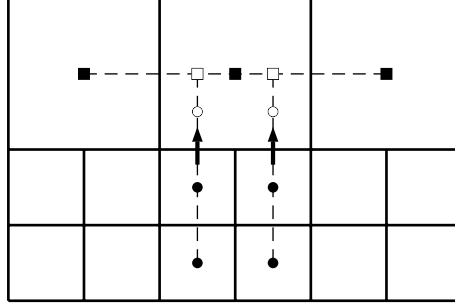


Fig. 4.2: Interpolation stencil on the fine/coarse interface. Coarse cells (■); intermediate values on coarse grid (□); fine cells (●); "ghost cells" (○) for computing of coarse/fine fluxes (arrows) .

The average flux given in Eq. (4.3) was found to produce numerical instabilities in some occasions. To overcome this problem, a weighted flux at the coarse/fine interface is introduced: the average refined flux is weighted with a coarse flux,

$$F_{i,j-1/2}^{\eta,\text{ave}} = \frac{\omega}{2} \left(F_{\text{left}}^{\eta,\text{f}} + F_{\text{right}}^{\eta,\text{f}} \right) + (1 - \omega) F_{i,j-1/2}^{\eta,\text{c}}.$$

This approach enhance numerical stability, even for poor initial guesses of the solution. The accuracy is lowered (but not significantly) using $\omega = 0.5$. The weighting parameter ω can then be increased upto 1 as the iterative solution converge. The coarse flux $F_{i,j-1/2}^{\eta,\text{c}}$ is calculated using a coarse "ghost cell" value obtained from a quadratic interpolation on the fine grid.

4.3 Grid coupling

The grid structure is static, or fixed, since the stratified flow is assumed to be in steady-state with no moving interfaces. The governing equations are solved separately on each component grid, which are coupled in between every iteration step. To make sure that interpolation points are updated with the correct values due to overlapping regions, it is crucial that the communication between the component grids are in correct order.

The information about the grid nodes is stored in integer tables. These integer tables are used to identify whether the cell is active or not, meaning that an active cell is a discretization point. A non-active cell is either a grid node in the overlapping region, a boundary cell or a grid point hidden by a refinement grid, and its value is determined by quadratic interpolation from another subgrid. The C++ library

BoxLib developed by the Center of Computational Science and Engineering¹ is used to manage the hierarchy of subgrids.

The algorithm to couple the grids is as follows (see Fig. 4.3):

- 1) Information is passed down from level $l + 1$ to coarser level l on the same base grid, starting from the finest level all the way down to $l = 0$.
- 2) The overlapping region of the base composite grids on the coarsest level, $l = 0$, is coupled.
- 3) Starting from $l = 1$, boundary nodes on level l is updated from same base grid on coarser level $l - 1$. Then bordering subgrids at level l share boundary information. Those subgrids at level l bordering with a different base grid are coupled with the other base grid on the same refinement level l in the overlapping region. This step is repeated until the finest level is updated.

Refined subgrids bordering to a different base composite grid share information in the overlapping region at the same refinement level only. Subgrids on level l never interpolate from finer grids than level $l + 1$.

¹<http://seesar.lbl.gov/ccse/>

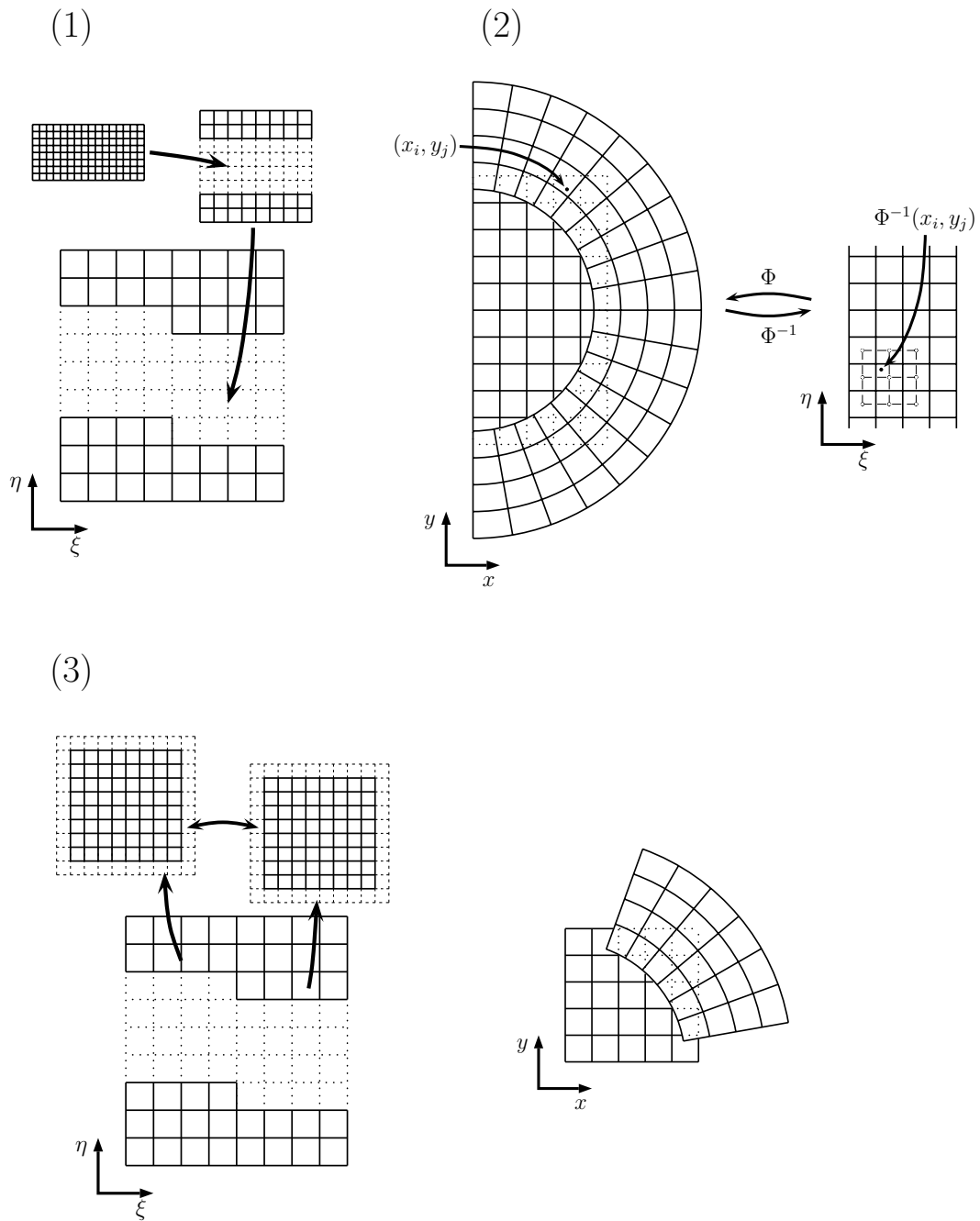


Fig. 4.3: The three basic steps in coupling the subgrids and overlapping regions: (1) Pass information from fine level to coarse level; (2) Couple base grids; (3) Boundary cells on fine grids are updated from coarser levels, then coupled with neighbouring/overlapping subgrids at the same refinement level.

Chapter 5

The Immersed Interface Method

The immersed interface method is a numerical technique formulated to solve partial differential equations in the presence of interfaces where the solution and its derivatives may be discontinuous and non-smooth. These interface problems are often encountered in fluid dynamics where two or more fluids with different properties interact. It is well-known that traditional Cartesian finite difference methods work poorly for these problems since the numerical discretization is not well-defined across the interface.

5.1 Introduction

A simple solution to the interface problem is to adopt the immersed boundary (IB) method (Peskin, 1977) where a δ -function formulation is used to smear out discontinuous coefficients and singular sources. This idea has been applied to solve a number of interface-related problems, such as in the level set method (Sussman et al., 1994; Chang et al., 1996) where material properties are smeared out across the interface. Another example is the continuum surface force (CSF) model by Brackbill et al. (1992) where the singular surface tension effect is introduced as a new, smooth forcing term in the momentum equation. A similar approach as the CSF model has been adopted in many commonly used multiphase methods (e.g. Unverdi & Tryggvason, 1992; Sussman et al., 1994; Chang et al., 1996; Scardovelli & Zaleski, 1999). Although the IB method is very robust and easy to use, it is not very accurate and unable to reproduce discontinuities.

Instead, several techniques, classified as sharp interface methods, have been developed in order to solve interface problems properly. In the immersed interface method (IIM) by Leveque & Li (1994), the interfacial boundary conditions are incorporated into the finite difference stencil in a non-trivial way that preserves the jumps in both the function and its derivatives. This method is fairly complex, and

Liu et al. (2000) tried to simplify the IIM and still obtain a sharp solution at the interface. Their concept was based on the ghost fluid method (GFM) by Fedkiw et al. (1999), and it is among the simpler sharp interface methods. The method decomposes the jumps in each axis direction treating the problem dimension by dimension. However, Liu et al.'s (2000) approach provides only first order accuracy, and their approximations of the jump conditions is not very rigorous.

The basic idea of sharp interface techniques has been extended and applied to solve a number of general interface-related problems (Wiegmann & Bube, 2000; Li & Lai, 2001; Kang et al., 2000; Li, 2003), but in most cases it has been limited to problems with piecewise constant coefficients.

5.2 One-dimensional formulation

5.2.1 The Poisson equation

Among the simplest interface problems is the one given by the one-dimensional Poisson equation

$$v_{xx} = f(x), \quad x \in \Omega,$$

on the unit domain $\Omega = [0, 1]$ for a non-smooth and discontinuous function $v(x)$ with fixed Dirichlet boundary conditions,

$$v(0) = g_1 \quad \text{and} \quad v(1) = g_2,$$

at the exterior boundary $\partial\Omega$.

The interface is a single point Γ located at x^* somewhere inside Ω . The set of all points where $x < x^*$ and the set of all points where $x > x^*$ represent the disjoint subdomains Ω^- and Ω^+ , respectively, for all $x \in \Omega$.

The jump conditions, or interfacial boundary conditions, are specified at the interface as

$$\begin{aligned} [v] &= w_1, & x &= x^*, \\ [v_x] &= w_2, & x &= x^*, \\ [v_{xx}] &= w_3, & x &= x^*, \end{aligned}$$

where the jumps are defined as the limiting values

$$\begin{aligned} [v] &= \lim_{x \rightarrow \Gamma^+} v(x) - \lim_{x \rightarrow \Gamma^-} v(x) = v^+ - v^-, \\ [v_x] &= \lim_{x \rightarrow \Gamma^+} v_x(x) - \lim_{x \rightarrow \Gamma^-} v_x(x) = v_x^+ - v_x^-, \\ [v_{xx}] &= \lim_{x \rightarrow \Gamma^+} v_{xx}(x) - \lim_{x \rightarrow \Gamma^-} v_{xx}(x) = v_{xx}^+ - v_{xx}^-. \end{aligned}$$

Here $x \rightarrow \Gamma^+$ means approaching the interface from the Ω^+ side and $x \rightarrow \Gamma^-$ from the Ω^- side.

The computational domain is discretized into equally spaced cells of size h where the cell centers are referred to as grid nodes, with the i th node located at x_i . A grid node x_i is defined as regular if both neighbouring nodes are on the same side of the interface. On the contrary, a grid node x_i is irregular if one adjacent node is on the other side of the interface.

If x_i is a regular node, then Taylor expansion for $v(x_{i+1})$ at x_i gives

$$v(x_{i+1}) = v(x_i) + v_x(x_i)h + \frac{1}{2}v_{xx}(x_i)h^2 + \frac{1}{6}v_{xxx}(x_i)h^3 + \mathcal{O}(h^4), \quad (5.1)$$

and for $v(x_{i-1})$ at x_i gives

$$v(x_{i-1}) = v(x_i) - v_x(x_i)h + \frac{1}{2}v_{xx}(x_i)h^2 - \frac{1}{6}v_{xxx}(x_i)h^3 + \mathcal{O}(h^4). \quad (5.2)$$

Adding Eqs. (5.1) and (5.2), and with some manipulations, gives the standard second order approximation to $v_{xx}(x_i)$,

$$v_{xx}(x_i) = \frac{v(x_{i+1}) - 2v(x_i) + v(x_{i-1}))}{h^2} + \mathcal{O}(h^2). \quad (5.3)$$

On the other hand, if x_i is an irregular node, Eq. (5.3) cannot be used since the Taylor expansion is not valid across the interface. Instead, a correction to the expression above is necessary in order to have a well-defined approximation. Assume that the interface Γ is located between the nodes x_i and x_{i+1} at $x^* = x_i + ah$ for $0 \leq a \leq 1$. Taylor expansion for $v(x_{i+1})$ at x^* yields

$$\begin{aligned} v(x_{i+1}) &= v(x^* + (1-a)h) \\ &= v^+ + v_x^+(1-a)h + \frac{1}{2}v_{xx}^+(1-a)^2h^2 + \mathcal{O}(h^3). \end{aligned} \quad (5.4)$$

Using the definitions of the jumps, Eq. (5.4) can be rewritten as

$$v(x_{i+1}) = v^- + v_x^-(1-a)h + \frac{1}{2}v_{xx}^-(1-a)^2h^2 + \bar{C}(x, a) + \mathcal{O}(h^3), \quad (5.5)$$

where

$$\bar{C}(x, a) = [v] + [v_x](1-a)h + \frac{1}{2}[v_{xx}](1-a)^2h^2. \quad (5.6)$$

Now, v^- , v_x^- and v_{xx}^- can themselves be obtained by Taylor expansion at x_i , which inserted into Eq. (5.5) gives

$$\begin{aligned} v(x_{i+1}) &= v(x_i) + v_x(x_i)h + \frac{1}{2}v_{xx}(x_i)h^2 + v_x(x_i)(1-a)h \\ &\quad + v_{xx}(x_i)(1-a)ah^2 + \frac{1}{2}v_{xx}(x_i)(1-a)^2h^2 + \bar{C}(x, a) + \mathcal{O}(h^3) \\ &= v(x_i) + v_x(x_i)h + \frac{1}{2}v_{xx}(x_i)h^2 + \bar{C}(x, a) + \mathcal{O}(h^3). \end{aligned} \quad (5.7)$$

The Taylor expansion for $v(x_{i-1})$ is

$$v(x_{i-1}) = v(x_i) - v_x(x_i)h + \frac{1}{2}v_{xx}(x_i)h^2 + \mathcal{O}(h^3). \quad (5.8)$$

Adding Eq. (5.7) to (5.8), and rearranging, gives a valid approximation to $v_{xx}(x_i)$ at an irregular node,

$$v_{xx}(x_i) = \frac{v(x_{i+1}) - 2v(x_i) + v(x_{i-1}))}{h^2} - \frac{\bar{C}(x, a)}{h^2} + \mathcal{O}(h),$$

where the correction term $\bar{C}(x, a)$ is given by Eq. (5.6).

5.2.2 A variable coefficient linear equation

A more general problem is described by the linear differential equation

$$(\beta v_x)_x + \alpha v_x = f(x), \quad x \in \Omega, \quad (5.9)$$

where α , β and f are continuous and smooth on each subdomain, but may have jumps across the interface,

$$\alpha(x) = \begin{cases} \alpha^-(x), & x \in \Omega^-, \\ \alpha^+(x), & x \in \Omega^+, \end{cases}$$

$$\beta(x) = \begin{cases} \beta^-(x), & x \in \Omega^-, \\ \beta^+(x), & x \in \Omega^+, \end{cases}$$

and

$$f(x) = \begin{cases} f^-(x), & x \in \Omega^-, \\ f^+(x), & x \in \Omega^+. \end{cases}$$

The jumps, or the interfacial boundary conditions, are now given on the form

$$[v] = w_1, \quad x = x^*,$$

$$[\beta v_x] = w_2, \quad x = x^*.$$

Also, it is convenient to introduce the level set function $\phi(x)$ defined in Chapter 3 in order to determine the location of the interface. Since ϕ is a signed distance function, the problem domain can be defined as

$$\Omega = \begin{cases} \Omega^-, & \phi < 0, \\ \Omega^+, & \phi \geq 0, \end{cases}$$

assuming the interface to be infinitely thin. The distance property of ϕ makes it easy to locate the exact position of Γ_ϕ . For instance, if the interface is located at $x^* = x_i + ah$ ($0 \leq a \leq 1$), then

$$a = \frac{\phi_i}{\phi_i - \phi_{i+1}},$$

where ϕ_i denotes $\phi(x_i)$.

Further, let V_i be the numerical approximation of $v(x_i)$ and $\beta_{i+1/2}$ denote $\beta(x_i + 1/2h)$. Then, assuming that the jump conditions $[v]$, $[v_x]$, $[v_{xx}]$, $[\beta v_x]$ and $[(\beta v_x)_x]$ are all known, the following numerical approximations of the differential terms in Eq. (5.9) can be established:

$$v_x(x_i) = \frac{V_{i+1} - V_{i-1}}{2h} - C_i^1 + \mathcal{O}(h^2) \quad (5.10)$$

and

$$(\beta v_x)_x(x_i) = \frac{\beta_{i+1/2}(V_{i+1} - V_i) - \beta_{i-1/2}(V_i - V_{i-1})}{h^2} + C_i^2 + \mathcal{O}(h) \quad (5.11)$$

where $h = x_{i+1} - x_i = x_i - x_{i-1}$.

The correction terms are given as

$$C_i^1 = S_\phi \lambda \frac{C(x, a)}{2h} \quad \text{and} \quad C_i^2 = S_\phi \bar{\beta} \frac{C_1(x, a)}{h^2} + S_\phi \frac{C_2(x, a)}{h}, \quad (5.12)$$

where

$$S_\phi = \begin{cases} -1, & \phi_i < 0, \\ 1, & \phi_i \geq 0, \end{cases}$$

and

$$C(x, a) = [v] - \lambda[v_x](1-a)h + \frac{1}{2}[v_{xx}](1-a)^2h^2,$$

$$C_1(x, a) = \begin{cases} [v] - \lambda[v_x]ah + \frac{1}{2}[v_{xx}]a^2h^2, & \text{if } (\phi_i \geq 0 \text{ and } 0 \leq a < 1/2) \\ & \text{or } (\phi_i < 0 \text{ and } 0 < a \leq 1/2), \\ [v] + \lambda[v_x](1-a)h & \text{if } (\phi_i \geq 0 \text{ and } 0 \leq a < 1/2) \\ + \frac{1}{2}[v_{xx}](1-a)^2h^2, & \text{or } (\phi_i < 0 \text{ and } 0 < a \leq 1, /2), \end{cases}$$

$$C_2(x, a) = \begin{cases} \lambda[\beta v_x] + \frac{1}{2}[(\beta v_x)_x](1-2a)h, & \text{if } (\phi_i \geq 0 \text{ and } 0 \leq a < 1/2) \\ & \text{or } (\phi_i < 0 \text{ and } 0 < a \leq 1/2), \\ 0, & \text{otherwise.} \end{cases}$$

The parameters λ , a and $\bar{\beta}$ are defined as follows:

- If the interface is between x_i and x_{i+1}
(i.e. $\phi_i \cdot \phi_{i+1} < 0$, or $\phi_i = 0$ and $\phi_{i+1} < 0$, or $\phi_i < 0$ and $\phi_{i+1} = 0$)

$$\lambda = 1, \quad a = \frac{\phi_i}{\phi_i - \phi_{i+1}} \quad \text{and} \quad \bar{\beta} = \beta_{i+1/2}.$$

- If the interface is between x_{i-1} and x_i
(i.e. $\phi_i \cdot \phi_{i-1} < 0$, or $\phi_i = 0$ and $\phi_{i-1} < 0$, or $\phi_i < 0$ and $\phi_{i-1} = 0$)

$$\lambda = -1, \quad a = \frac{\phi_i}{\phi_i - \phi_{i-1}} \quad \text{and} \quad \bar{\beta} = \beta_{i-1/2}.$$

The jump of a general function $g(x)$ is defined as

$$[g] = \lim_{\phi^+ \rightarrow 0} g(x) - \lim_{\phi^- \rightarrow 0} g(x) = g^+ - g^-.$$

The derivation of (5.11) is given in Paper I and will not be repeated here. Equation (5.10) can be obtained by subtracting (5.8) from (5.7).

Remark 1 *If the solution is smooth and continuous (regular nodes), the jumps become zero and the correction terms vanish.*

Remark 2 *The local truncation error in Eq. (5.11) is of first order only, but as shown in Paper I it is still expected that the global accuracy approach second order since the interface is of one dimension lower than the problem.*

5.3 Two-dimensional formulation

5.3.1 Decomposing the jump conditions

In two dimensions, the jump conditions are usually given as physical boundary conditions defined in the normal and tangential directions to the interface. If the theory established in the previous section is to be used, it would be more convenient to decompose these jump conditions into jumps in the coordinate directions.

A local coordinate system aligned with the interface at (x^*, y^*) is defined as

$$\begin{aligned} x_n &= (x - x^*) \cos \theta + (y - y^*) \sin \theta, \\ x_t &= -(x - x^*) \sin \theta + (y - y^*) \cos \theta, \end{aligned}$$

where θ is the angle between the x - and x_n -axis. The x_n -axis is normal to the interface while the x_t -axis is tangential. The local coordinate transformation can

be determined from the level set function $\phi(x, y)$, since the normal vector $\mathbf{n} = (\cos \theta, \sin \theta)$ is given as

$$\mathbf{n} = \frac{\nabla \phi}{|\nabla \phi|}.$$

Transforming the normal and tangential jump conditions into Cartesian coordinates yields

$$\begin{aligned} [\beta v_x] &= [\beta v_n] \cos \theta - [\beta v_t] \sin \theta, \\ [\beta v_y] &= [\beta v_n] \sin \theta + [\beta v_t] \cos \theta, \end{aligned}$$

and differentiation using the chain rule gives

$$\begin{aligned} [(\beta v_x)_x] &= [(\beta v_n)_n] \cos^2 \theta - ([(\beta v_n)_t] + [(\beta v_t)_n]) \cos \theta \sin \theta + [(\beta v_t)_t] \sin^2 \theta, \\ [(\beta v_y)_y] &= [(\beta v_n)_n] \sin^2 \theta + ([(\beta v_n)_t] + [(\beta v_t)_n]) \cos \theta \sin \theta + [(\beta v_t)_t] \cos^2 \theta. \end{aligned}$$

Similarly, differentiation of the jump $[v]$ gives

$$\begin{aligned} [v_x] &= [v_n] \cos \theta - [v_t] \sin \theta, \\ [v_y] &= [v_n] \sin \theta + [v_t] \cos \theta, \end{aligned}$$

and

$$\begin{aligned} [v_{xx}] &= [v_{nn}] \cos^2 \theta - 2[v_{nt}] \cos \theta \sin \theta + [v_{tt}] \sin^2 \theta, \\ [v_{yy}] &= [v_{nn}] \sin^2 \theta + 2[v_{nt}] \cos \theta \sin \theta + [v_{tt}] \cos^2 \theta. \end{aligned}$$

Finally, assuming that $[v]$, $[v_n]$, $[v_{nn}]$, $[v_t]$, $[v_{tt}]$, $[\beta v_n]$, $[(\beta v_n)_n]$, $[\beta v_t]$, $[(\beta v_t)_t]$, $[(\beta v_n)_t]$ and $[(\beta v_t)_n]$ are all known, then the jumps can be decomposed into jump conditions in the coordinate directions. This enables for a dimension by dimension approach of the numerical method.

5.3.2 Approximate correction terms

In most cases, the known jump conditions are limited to only a few of those needed for closure of the correction terms. The remaining jumps are usually solution-dependent and must be obtained as part of the solution. For elliptic problems in higher dimensions, it is common to use some iterative methods to solve the discretized equations. The idea is therefore to obtain the correction terms iteratively as well. Using the given interfacial boundary conditions together with an appropriate interpolation scheme, the interfacial values on both sides of the interface can be estimated from the solution at the previous iteration step (or initial guess). Then the decomposed correction terms can be approximated by using one-sided difference stencils on both sides of the interface to estimate the jumps in the first and second derivatives. The correction terms are updated and given explicitly at every iteration step, as they converge to the correct solutions.

5.3.3 Curvilinear coordinates

The finite difference stencil in Eq. (4.2) can be modified using the decomposed immersed interface method in order to make the discretization well-defined across the interface. Although the present formulation is given in Cartesian coordinates, it is possible to show that this method can be generalized to any orthogonal, curvilinear coordinate system. This is simply done by treating the differential terms in Eq. (4.1) dimension by dimension, introducing the componentwise correction terms in the computational space.

The elliptic equation (4.1) is discretized in the computational space forming the following set of algebraic equations:

$$\mathcal{L}_h^\beta V_{i,j} = l_\xi l_\eta f_{i,j} - C_{i,j},$$

where the difference operator \mathcal{L}_h^β is defined by Eq. (4.2). The correction term $C_{i,j}$ consists of a component in the ξ -direction and one in the η -direction, i.e.

$$C_{i,j} = C_{i,j}^\xi + C_{i,j}^\eta.$$

Each one of these terms are given by Eq. (5.12) in their respective coordinate directions, where the interfacial jumps can be determined by the approximation method described previously.

At the end, the decomposed immersed interface method can be adopted to calculate stratified multiphase flow in pipes. The governing equations in Chapter 3 can be discretized and solved in the computational space using a composite, overlapping grid framework where componentwise correction terms are added to the finite difference scheme at irregular grid nodes.

Chapter 6

Comments on the Papers

6.1 Paper I

A decomposed immersed interface method for variable coefficient elliptic equations with non-smooth and discontinuous solutions

Paper I, which constitutes the basis of this doctoral thesis, is based on the ideas of Leveque & Li (1994), Li & Lai (2001), Wiegmann & Bube (2000), and Liu et al. (2000). A sharp interface formulation capable of solving two-dimensional elliptic interface problems with piecewise smooth coefficients on Cartesian grids was derived. The method introduced componentwise correction terms for the grid nodes adjacent to the interface, where ordinary finite difference schemes are not generally well-defined. The adjustment of the numerical stencil was given in terms of interfacial jump conditions. An iterative method that approximated the necessary jump conditions was also proposed. This approach used a numerical approximation of the normal jump condition in order to estimate the interfacial boundary values. One-sided difference stencils were then used on both sides of the interface to approximate the componentwise jump conditions.

Concluding remarks

Numerical test cases showed acceptable agreements with analytical solutions, and the order of accuracy was found to be comparable with other immersed interface methods. The accuracy was not influenced noticeably when the interfacial jump conditions in the correction terms were approximated numerically. But for a few cases the finite difference representation of the derivatives normal to the interface became too inaccurate, which resulted in a poor approximation of the interfacial boundary values.

The main advantage of the presented method is that it is relatively simple to implement it in existing codes, since it does not require construction of complex coefficient matrices, as it is in many other immersed interface methods. However, the right-hand-side of the system must be adjusted iteratively, where a sufficient under-relaxation is necessary.

6.2 Paper II

Stratified smooth two-phase flow using the immersed interface method

In Paper II, the immersed interface method was used to derive a two-dimensional numerical method for solving fully developed, stratified smooth two-phase flow in pipes.

The purpose of this paper was to investigate the possibilities of using the immersed interface method to predict stratified two-phase flow in pipes. For turbulent flow, a low Reynolds number $k - \varepsilon$ model (Lam & Bremhorst, 1981) was used to mimic turbulent stresses. This turbulence model resolved the flow in the immediate vicinity of the wall and the interface. A level set function was used to determine the location of the interface. The principal difference with the presented approach compared to the body-fitted grid techniques (e.g. Issa, 1988; Newton & Behnia, 2000) is the way in which the interfacial boundary conditions are incorporated into the numerical scheme.

Concluding remarks

The present method was found to be accurate for laminar flow with a flat interface. Moreover, the integral properties for laminar two-phase flow with a curved interface were determined by the Bond number, the contact angle and the phase area fractions.

Numerical predictions of pressure gradient, liquid phase area fraction and shear stresses for turbulent gas-liquid flow compared well with the experimental results of Espedal (1998) in an inclined pipe. The gas-liquid interface was rather smooth in the experimental data used for comparison.

For turbulent liquid-liquid flow, the calculated pressure gradient and phase area fractions showed acceptable agreement with the experimental data of Elseth (2001) for low mixture velocities and intermediate water cuts. At lower and higher water cuts, the numerical results deviated more from the measured data due to the increased interfacial disturbances occurring for these flow conditions. In these cases, the assumption of having a smooth interface was questionable. Further, numerical

simulations showed that variation of the interface curvature influenced the slip ratio between the two liquid phases even though the viscosity difference is small.

6.3 Paper III

Numerical modelling of stratified turbulent two- and three-phase pipe flow with arbitrary shaped interfaces

Paper III is an extension of Paper II to three-phase flow calculations. An additional interface was included and the same numerical method was used. This was simply done by introducing a second level set function which described the new interface. A two-layer $k - \varepsilon$ model (Chen & Patel, 1988) was used to account for the effects of turbulence. A parametric study for horizontal three-phase flow was presented, and, in particular, the effect of varying the shape of the liquid-liquid interface was considered.

Concluding remarks

From the simulations, it was very clear that increasing the wall contact area for the oil phase increased the flow resistance and reduced the total liquid flow rate for a given pressure gradient and phase fractions. In the meantime, the water-to-liquid flow rate ratio increased since most of the reduction in the total liquid flow rate was done by the oil phase. To our knowledge, similar two-dimensional analysis on three-phase pipe flow has not been previously carried out. The application of this model is yet confined to smooth interfaces; however, such calculations still give new and valuable information about stratified smooth three-phase flow.

6.4 Paper IV

Calculations of stratified wavy two-phase flow in pipes

The primary purpose of Paper IV was to include the effect of interfacial waves.

Stratified smooth flow conditions occur rarely in industrial problems; therefore, a model in which stratified wavy flows can be predicted will have far more practical value. The wavy interface has been commonly treated as a rough wall in previous studies. The shear stress on a rough interface has been calculated either by means of a wall function (Meknassi et al., 2000) or an interfacial friction factor implemented directly in the numerical scheme (Shoham & Taitel, 1984; Newton & Behnia, 2001).

In the current paper, the wavy interface was represented by an equivalent interfacial roughness height. Turbulent stresses were modelled using a two-layer turbulence

model, which was modified to account for the roughness introduced at the interface (Patel & Yoon, 1995; Durbin et al., 2001). This turbulence model allowed for direct calculation of the wavy interfacial shear stress without using a wall function.

Concluding remarks

Numerical predictions of stratified wavy gas-liquid flow compared satisfactorily with experimental data given by Espedal (1998). The interfacial roughness, represented by the Charnock parameter, was estimated from the experiments. The results were found to be sensitive to the choice of Charnock parameter, but this effect was not too striking in appearance as doubling the Charnock parameter from $\beta = 0.1$ to $\beta = 0.2$ only led to approximately 10% change in the calculated liquid phase area fractions and axial pressure gradients for the presented test cases.

The momentum transfer from the gas phase to the liquid phase was found to be slightly under-estimated. It was therefore expected that the predicted gas flow rate would exceed the measured value; however, it was not observed for the lowest flow rates. This observation suggested that the calculated level of turbulence in the gas phase was too high, although the turbulent viscosity at the interface was not sufficiently large to correctly predict the interfacial shear stress.

6.5 Further work

For the decomposed immersed interface method presented in Paper I, the following issues can be considered to be of relevance for further work:

- Other techniques, such as the multigrid method, can be employed to achieve increased computational efficiency, rather than the Successive Overrelaxation Gauss Seidel method that have been used in this work for elliptic equations.
- Extension to three-dimensional elliptic problems should be considered.
- The possibility of using the approximated jump conditions in conjunction with the work presented by Li & Lai (2001) should be explored in order to derive a full Navier-Stokes solver in which the density and viscosity are also discontinuous across an interface.

Based on the numerical method presented in this thesis for solving stratified multi-phase flow in pipes, the following areas need more investigations:

- The boundary conditions for the turbulence quantities need to be refined at the gas-liquid interface for wavy flow in order to improve the accuracy.

- The concept of equivalent interfacial roughness can be extended to liquid-liquid interface in order to improve calculations of stratified liquid-liquid flow.
- The present method can be used for more physically realistic three-phase flow simulations where the gas-liquid interface is considered to be wavy. The treatment of the liquid-liquid interface also needs modifications, either as a wavy interface (see the point above) or as a mixed interface, where flow properties are smeared across the boundary.
- Using more sophisticated turbulence models which are capable of predicting the secondary flow effects is important.

Appendix A

The Mean Flow Equation

The governing equations of the mean turbulent flow are obtained by performing a time averaging of the Navier-Stokes equations. Details about the averaging procedure can be found in many textbooks in fluid dynamics and CFD (e.g. White, 1991; Versteeg & Malalasekera, 1995), so only a brief summary is given in this appendix. The notation in this appendix may differ from what is actually used in previous chapters.

A.1 The Reynolds equations

An ordinary Cartesian coordinate system, x_i , is defined using the index notation ($i = 1, 2, 3$). Let $u_i(t)$ and $p(t)$ be the instantaneous velocity and pressure field, respectively, in an incompressible flow. The instantaneous variables can be decomposed into a mean and a fluctuating quantity,

$$u_i(t) = \frac{1}{\Delta t} \int_0^{\Delta t} u_i(t) dt + u'_i(t) = \bar{u}_i + u'_i(t),$$
$$p(t) = \frac{1}{\Delta t} \int_0^{\Delta t} p(t) dt + p'(t) = \bar{p} + p'(t),$$

where the overhead bar denotes the time-averaged value and the prime denotes the fluctuations. For shortness, the time dependence will from now on be omitted in the notation. By definition, the time-average of the fluctuating components are zero:

$$\bar{u}'_i = \frac{1}{\Delta t} \int_0^{\Delta t} u'_i dt = 0 \quad \text{and} \quad \bar{p}' = \frac{1}{\Delta t} \int_0^{\Delta t} p' dt = 0.$$

Applying the time-averaging to each term in the Navier-Stokes equations yields

$$\frac{\partial \bar{u}_j}{\partial x_j} = 0 \tag{A.1}$$

and

$$\frac{\partial \bar{\rho} \bar{u}_i}{\partial t} + \frac{\partial \bar{\rho} \bar{u}_i \bar{u}_j}{\partial x_j} = -\frac{\partial \bar{p}}{\partial x_i} + \mu \frac{\partial^2 \bar{u}_i}{\partial x_j \partial x_j} + \bar{f}_i - \frac{\partial}{\partial x_j} (\overline{\rho u'_i u'_j}), \quad (\text{A.2})$$

using the convention of summation of repeated indices, where \bar{f}_i is the time averaged body force, such as gravity. Equation (A.2) is also known as the Reynolds' averaged equation, where $\overline{\rho u'_i u'_j}$ are called turbulent stresses or Reynolds stresses. The turbulent stresses are usually very large compared to the viscous stresses in a turbulent flow.

A.2 Mean turbulent flow in a duct

The time-averaged equation above can, for some particular flows, be reduced to a simpler form. For instance, consider a stationary ($\partial/\partial t = 0$) flow in a straight duct where the axial centerline is aligned with the x_1 -axis. The flow is assumed to be fully developed and uni-directional, except for the fluctuating components in the cross-stream directions, meaning that $\bar{u}_2 = \bar{u}_3 = 0$; thus, Eq. (A.1) simplifies to

$$\frac{\partial \bar{u}_1}{\partial x_1} = 0.$$

Substitution into Eq. (A.2) reduces the governing equations describing the mean flow to one momentum equation for the mean axial velocity component,

$$0 = -\frac{\partial \bar{p}}{\partial x_1} + \mu \left(\frac{\partial^2 \bar{u}_1}{\partial x_2^2} + \frac{\partial^2 \bar{u}_1}{\partial x_3^2} \right) + \bar{f}_1 - \frac{\partial}{\partial x_2} (\overline{\rho u'_1 u'_2}) - \frac{\partial}{\partial x_3} (\overline{\rho u'_1 u'_3}). \quad (\text{A.3})$$

Further, the turbulent stresses, $\overline{\rho u'_1 u'_2}$ and $\overline{\rho u'_1 u'_3}$, can be modelled by means of turbulence modelling. Assuming there exist an analogy between the action of viscous stresses and the Reynolds stresses on the mean flow, the Reynolds stresses can be linked to mean rates of deformation. Following Boussinesq (1877), the turbulent stresses can be modelled as

$$-\overline{\rho u'_i u'_j} = \mu_t \left(\frac{\partial \bar{u}_i}{\partial x_j} + \frac{\partial \bar{u}_j}{\partial x_i} \right),$$

where μ_t is the turbulent viscosity. The underlying assumption of this approach is that the turbulent viscosity is isotropic: the ratio between Reynolds stress and mean rate of deformation is the same in all directions.

Adopting this formulation and rearranging Eq. (A.3) gives the following equation for the mean turbulent flow in axial direction:

$$\frac{\partial}{\partial x_2} \left(\mu_e \frac{\partial \bar{u}_1}{\partial x_2} \right) + \frac{\partial}{\partial x_3} \left(\mu_e \frac{\partial \bar{u}_1}{\partial x_3} \right) - \frac{\partial \bar{p}}{\partial x_1} + \bar{f}_1 = 0,$$

where $\mu_e = \mu + \mu_t$. It remains to find a closure for the turbulent viscosity μ_t .

References

- Agrawal, S. S., Gregory, G. A. & Govier, G. W. (1973), An analysis of horizontal stratified two phase flow in pipes, *The Canadian Journal of Chemical Engineering* **51**, 280–286.
- Akai, M., Inoue, A. & Aoki, S. (1981), The prediction of stratified two-phase flow with a two-equation model of turbulence, *International Journal of Multiphase Flow* **7**(1), 21–39.
- Akai, M., Inoue, A., Aoki, S. & Endo, K. (1980), A co-current stratified air-mercury flow with wavy interface, *International Journal of Multiphase Flow* **6**(3), 173–190.
- Bentwich, M. (1964), Two-phase viscous axial flow in a pipe, *Transaction of the ASME, Journal of Basic Engineering* pp. 669–672.
- Berger, M. & Rigoutsos, I. (1991), An algorithm for point clustering and grid generation, *IEEE Transaction on System, Man and Cybernetics* **21**(5), 1278–1286.
- Biberg, D. & Halvorsen, G. (2000), Wall and interfacial shear stress in pressure driven two-phase laminar stratified pipe flow, *International Journal of Multiphase Flow* **26**(10), 1645–1673.
- Boussinesq, J. (1877), Theorie de l'écoulement tourbillant, *Mémoires présentés par divers savants à l'Académie des Sciences* **23**, 46–50.
- Brackbill, J. U., Kothe, D. B. & Zemach, C. (1992), A continuum method for modeling surface tension, *Journal of Computational Physics* **100**(2), 335–354.
- Brauner, N. & Maron, D. M. (1989), Two phase liquid-liquid stratified flow, *PhysicoChemical Hydrodynamics* **11**(4), 487–506.
- Brauner, N., Rovinsky, J. & Maron, D. M. (1996), Analytical solution for laminar-laminar two-phase stratified flow in circular conduits, *Chemical Engineering Communication* **141–142**, 102–143.

- Cebeci, T. & Chang, K. C. (1978), Calculation of incompressible rough-wall boundary-layer flows, *AIAA Journal* **16**(7), 730–735.
- Cebeci, T. & Smith, A. M. O. (1974), *Analysis of turbulent boundary layers*, Academic Press, New York, USA.
- Chang, Y. C., Hou, T. Y., Merriman, B. & Osher, S. (1996), A level set formulation of Eulerian interface capturing methods for incompressible fluid flows, *Journal of Computational Physics* **124**, 449–464.
- Charnock, H. (1955), Wind stress on a water surface, *Quarterly Journal of the Royal Meteorological Society* **81**, 639–640.
- Chen, H. C. & Patel, V. C. (1988), Near-wall turbulence models for complex flows including separation, *AIAA Journal* **26**(6), 641–648.
- Chesshire, G. & Henshaw, W. D. (1990), Composite overlapping meshes for the solution of partial differential equations, *Journal of Computational Physics* **90**(1), 1–64.
- Colebrook, C. F. (1933), Turbulent flow in pipes, with particular reference to the transition region between the smooth and rough pipe laws, *Journal of the Institution of Civil Engineers* **11**, 133–156.
- Durbin, P. A., Medic, G., Seo, J.-M., Eaton, J. K. & Song, S. (2001), Rough wall modification of two-layer $k - \varepsilon$, *ASME Journal of Fluids Engineering* **123**(1), 16–21.
- Elseth, G. (2001), An experimental study of oil/water flow in horizontal pipes, Dr.ing. thesis, Telemark University College/Norwegian University of Science and Technology, Norway.
- Espedal, M. (1998), An experimental investigation of stratified two-phase pipe flow at small inclinations, Dr.ing. thesis, Norwegian University of Science and Technology, Department of Applied Mechanics, Thermo- and Fluid Dynamics, Trondheim, Norway.
- Fedkiw, R. P., Aslam, T., Merriman, B. & Osher, S. (1999), A non-oscillatory Eulerian approach to interfaces in multimaterial flows (the ghost fluid method), *Journal of Computational Physics* **152**(2), 457–492.
- Gorelik, D. & Brauner, N. (1999), The interface configuration in two-phase stratified pipe flows, *International Journal of Multiphase Flow* **25**(6–7), 977–1007.

- Govier, G. W. & Aziz, K. (1972), *The flow of complex mixtures in pipes*, Van Nostrand-Reinhold Company, New York, USA.
- Hamersma, P. J. & Hart, J. (1987), A pressure drop correlation for gas/liquid pipe flow with a small liquid holdup, *Chemical Engineering Science* **42**, 1187–1196.
- Henshaw, W. D. & Schwendeman, D. W. (2003), An adaptive numerical scheme for high-speed reactive flow on overlapping grids, *Journal of Computational Physics* **191**(2), 420–447.
- Issa, R. I. (1988), Prediction of turbulent, stratified, two-phase flow in inclined pipes and channels, *International Journal of Multiphase Flow* **14**(2), 141–154.
- Jackson, P. S. (1981), On the displacement height in the logarithmic velocity profile, *Journal of Fluid Mechanics* **111**, 15–25.
- Kang, M., Fedkiw, R. P. & Liu, X.-D. (2000), A boundary condition capturing method for multiphase incompressible flow, *Journal of Scientific computing* **15**(3), 323–360.
- Khor, S. H., Mendes-Tatsis, M. A. & Hewitt, G. F. (1997), One-dimensional modelling of phase holdups in three-phase stratified flow, *International Journal of Multiphase Flow* **23**(5), 885–897.
- Lam, C. K. G. & Bremhorst, K. (1981), A modified form of the $k - \epsilon$ model for predicting wall turbulence, *ASME Journal of Fluids Engineering* **103**, 456–460.
- Leveque, R. J. & Li, Z. (1994), The immersed interface method for elliptic equations with discontinuous coefficients and singular sources, *SIAM Journal of Numerical Analysis* **31**(4), 1019–1044.
- Li, Z. (2003), An overview of the immersed interface method and its applications, *Taiwanese Journal of Mathematics* **7**(1), 1–49.
URL: <http://www.math.nthu.edu.tw/tjm/>
- Li, Z. & Lai, M.-C. (2001), The immersed interface method for the Navier-Stokes equations with singular forces, *Journal of Computational Physics* **171**(2), 822–842.
- Ligrani, P. M. & Moffat, R. J. (1986), Structure of transitional rough and fully rough turbulent boundary layers, *Journal of Fluid Mechanics* **162**, 69–98.
- Liné, A., Masbernat, L. & Soualmia, A. (1996), Interfacial interaction and secondary flows in stratified two-phase flow, *Chemical Engineering Communication* **141–142**, 303–329.

- Liu, X.-D., Fedkiw, R. P. & Kang, M. (2000), A boundary condition capturing method for Poisson's equation on irregular domains, *Journal of Computational Physics* **160**(1), 151–178.
- Lockhart, R. W. & Martinelli, R. C. (1949), Proposed correlation of data for isothermal two-phase, two-component flow in pipes, *Chemical Engineering Progress* **45**, 139–48.
- Lopez, D. (1994), Ecoulements diphasiques à phases séparées à faible contenu de liquide, Thèse de doctorat, I.N.P., Toulouse, France.
- Martin, D. F. (1998), An adaptive cell-centered projection method for the incompressible Euler equations, PhD thesis, Mechanical Engineering, University of California at Berkeley, USA.
- Martin, D. F. & Cartwright, K. (1996), Solving Poisson's equation using adaptive mesh refinement, Technical Report UCB/ERI M96/66, University of California at Berkeley, USA.
URL: <http://seesar.lbl.gov/ANAG/staff/martin/AMRPoisson/>
- Meknassi, F., Benkirane, R., Line, A. & Masbernat, L. (2000), Numerical modeling of wavy stratified two-phase flow in pipes, *Chemical Engineering Science* **55**, 4682–4697.
- Mouza, A. A., Paras, S. V. & Karabelas, A. J. (2001), CFD code application to wavy stratified gas-liquid flow, *Trans IChemE* **79**(Part A), 561–568.
- Newton, C. H. & Behnia, M. (2000), Numerical calculation of turbulent stratified gas-liquid pipe flows, *International Journal of Multiphase Flow* **26**(2), 327–337.
- Newton, C. H. & Behnia, M. (2001), A numerical model of stratified wavy gas-liquid pipe flow, *Chemical Engineering Science* **56**, 6851–6861.
- Ng, T. S., Lawrence, C. J. & Hewitt, G. F. (2001), Interface shapes for two-phase laminar stratified flow in a circular pipe, *International Journal of Multiphase Flow* **27**(7), 1301–1311.
- Ng, T. S., Lawrence, C. J. & Hewitt, G. F. (2002), Laminar stratified pipe flow, *International Journal of Multiphase Flow* **28**(6), 963–996.
- Nikuradse, J. (1933), Strömungsgesetze in rauhen röhren, Forschungsheft 361, VDI Verlag Berlin. English translation, NACA Technical Memorandum 1921, 1950.
- Oliemans, R. V. A. (1987), Modelling of gas-condensate flow in horizontal and inclined pipes, in 'ASME Pipeline Engineering Symposium - ETCE', Dallas, Texas.

- Osher, S. & Sethian, J. A. (1988), Fronts propagating with curvature-dependent speed: Algorithms based on Hamilton-Jacobi formulations, *Journal of Computational Physics* **79**(1), 12–49.
- Patel, V. C. & Yoon, J. Y. (1995), Application of turbulence models to separated flow over rough surfaces, *ASME Journal of Fluids Engineering* **117**, 235–241.
- Peskin, C. S. (1977), Numerical analysis of blood flow in heart, *Journal of Computational Physics* **25**(3), 220–252.
- Rodi, W. (1993), *Turbulence models and their application in hydraulics; A state-of-the-art review*, IAHR Monograph series, 3rd edn, Balkema, Rotterdam, Netherlands.
- Rosant, J. M. (1983), Ecoulements diphasiques liquide-gaz en conduite. Etude de la configuration stratifiée au voisinage de l’horizontale, Thèse de docteur ès sciences, Ecole Nationale Supérieure de Mécanique de Nantes, France.
- Rotta, J. (1962), Turbulent boundary layers in incompressible flow, *Progress in Aerospace Science* **2**, 1–219.
- Scardovelli, R. & Zaleski, S. (1999), Direct numerical simulation of free-surface and interfacial flow, *Annual Review of Fluid Mechanics* **31**, 567–603.
- Shoham, O. & Taitel, Y. (1984), Stratified turbulent-turbulent gas-liquid flow in horizontal and inclined pipes, *AIChE Journal* **30**(3), 377–385.
- Srichai, S. (1994), High pressure separated two-phase flow, PhD thesis, Imperial College of Science, Technology and Medicine, London, UK.
- Strand, Ø. (1993), An experimental investigation of stratified two-phase flow in horizontal pipes, Dr.scient. thesis, University of Oslo, Department of Mathematics, Mechanics Division, Oslo, Norway.
- Sussman, M., Smereka, P. & Osher, S. (1994), A level set approach for computing solutions to incompressible two-phase flow, *Journal of Computational Physics* **114**(1), 146–159.
- Taitel, Y., Barnea, D. & Brill, J. P. (1995), Stratified three phase flow in pipes, *International Journal of Multiphase Flow* **21**(1), 53–60.
- Taitel, Y. & Dukler, A. E. (1976), A model for predicting flow regime transitions in horizontal and near horizontal gas-liquid flow, *AIChE Journal* **22**(1), 47–55.

- Unverdi, S. O. & Tryggvason, G. (1992), A front-tracking method for viscous, incompressible multi-fluid flows, *Journal of Computational Physics* **100**(1), 25–37.
- Valle, A. (2000), Three phase gas-oil-water pipe flow, Phd thesis, Imperial College, Department of Chemical Engineering and Chemical Technology, London, England.
- Versteeg, H. K. & Malalasekera, W. (1995), *An introduction to computational fluid dynamics*, Longman Ltd, London, UK.
- White, F. M. (1991), *Viscous fluid flow*, Mechanical Engineering Series, 2nd edn, McGraw-Hill, Inc, New York, USA.
- Wiegmann, A. & Bube, K. P. (2000), The explicit-jump immersed interface method: finite difference methods for PDEs with piecewise smooth solutions, *SIAM Journal of Numerical Analysis* **37**(3), 827–862.
- Wolfshtein, M. (1969), The velocity and temperature distribution in one-dimensional flow with turbulence augmentation and pressure gradient, *International Journal of Heat and Mass Transfer* **14**, 301–318.

Paper I

A decomposed immersed interface method for
variable coefficient elliptic equations with
non-smooth and discontinuous solutions

P. A. Berthelsen

Journal of Computational Physics

Vol. 197(1), 2004, pp. 364–386



A decomposed immersed interface method for variable coefficient elliptic equations with non-smooth and discontinuous solutions

Petter Andreas Berthelsen *

The Fluids Engineering Group, Department of Energy and Process Engineering, Norwegian University of Science and Technology, Kolbjørn Hejes vei 2, N-7491 Trondheim, Norway

Received 16 September 2003; received in revised form 3 December 2003; accepted 3 December 2003
Available online 22 January 2004

Abstract

A second order accurate finite difference method is presented for solving two-dimensional variable coefficient elliptic equations on Cartesian grids, in which the coefficients, the source term, the solution and its derivatives may be non-smooth or discontinuous across an interface. A correction term is introduced to the standard central difference stencil so that the numerical discretization is well-defined across the interface. We also propose a new method to approximate the correction term as part of the iterative procedure. The method is easy to implement since the correction term only needs to be added to the right-hand-side of the system. Therefore, the coefficient matrix remains symmetric and diagonally dominant, allowing for most standard solvers to be used. Numerical examples show good agreements with exact solutions, and the order of accuracy is comparable with other immersed interface methods.

© 2003 Elsevier Inc. All rights reserved.

PACS: 02.70.Bf; 02.60.Cb; 02.60.Lj

AMS: 65N06; 76T05; 35J05

Keywords: Immersed interface method; Discontinuous coefficients; Irregular domain; Elliptic interface problem; Finite difference method; Cartesian grid; Level set method

1. Introduction

Elliptic problems with discontinuous coefficients and singular sources are often encountered in fluid dynamics and material science. These interface problems usually lead to non-smooth or discontinuous

* Tel.: +4773595348; fax: +4773593491.

E-mail address: petterab@mtf.ntnu.no (P.A. Berthelsen).

solutions across an interface. Traditional Cartesian finite difference methods work poorly for these problems since the numerical discretization is not well-defined across the interface.

In Peskin's [15] immersed boundary method (IB), originally developed to model blood flow in the heart, singular forces are smeared out by a discrete delta function. The idea has been extended and applied to solve a number of interface-related problems. For example, in [3,4,16,17] the surface tension effect was introduced as a new, smooth forcing term in the momentum equation leading to continuity in pressure. Material properties may also be smeared out (e.g. using a level set function [4,16]) removing discontinuities across the interface, making the solution continuous, smooth and suitable for standard finite difference schemes. The IB is widely used because of its robustness, and it can easily be implemented into existing CFD codes, even in multiple spatial dimensions. However, the numerical smearing makes the method not very accurate and unable to properly produce discontinuities.

With the weakness of IB in mind, several new techniques classified as sharp interface methods have been developed. The immersed interface method (IIM), as presented in [8,9], handles two- and three-dimensional interface problems based on the analysis of [2]. The IIM is second order accurate and includes the interfacial boundary conditions into the finite difference discretization in such a way that it preserves the jumps in the solution and its derivatives. In the original IIM this was done by adding additional nodes to the numerical stencil, leading to a non-symmetric coefficient matrix. This non-symmetric matrix reduces the numbers of efficient numerical solvers to be used and convergence is not always guaranteed. In fact, the method has only been shown to be stable for one-dimensional problems and for two-dimensional problems with piecewise constant coefficients [6].

To avoid this convergence problem, a new version of the IIM was proposed in [12]. A maximum principle preserving method is enforced to obtain a diagonally dominant linear system. This way, some iterative methods are guaranteed to converge. The maximum principle approach was successfully implemented with a specially designed multigrid method in [1].

Another sharp interface technique is the ghost fluid method (GFM) introduced in [5] to treat two-phase contact discontinuities in the Euler equations. The basic principle behind GFM is to extend values across the interface into an artificial fluid (ghost fluid) inducing the proper conditions at the interface.

The GFM concept was extended in [13] to solve elliptic equations with variable coefficients. One of the main objectives with their approach was to simplify the IIM and still obtain a sharp solution at the interface. In contrast to IIM, the jump conditions are incorporated into the numerical discretization such that the symmetry of the finite difference stencil is kept. This allows for most standard solvers to be used. The method decomposes the flux jumps in each axis direction treating the problem dimension by dimension. This extended GFM is only first order accurate. The method has been applied to multiphase incompressible flow in [7].

Decomposing the jump conditions into each axis direction was also done in [11,18] using the IIM where the coefficients are piecewise constant. The approach in [18] produces a symmetric problem. Instead of focusing on finding new coefficients for the finite difference scheme they focus on the jumps in the solution and its derivatives. If the jumps $[u]$, $[u_x]$, $[u_{xx}]$, $[u_y]$ and $[u_{yy}]$ are all known, then the standard finite difference discretization can be used with some correction terms to adjust for the discontinuities. They also consider variable coefficients by rewriting the partial differential equation into a more convenient form for their method. The method shows to be second order accurate.

The intention of this paper is to extend the ideas of [11,13,18] to derive a second order sharp interface method capable of solving elliptic interface problems with variable coefficients in two dimensions. The primary objective is to keep the standard finite difference stencil, making only corrections to the right-hand side of the problem. This way we will keep the linear system symmetric and diagonally dominant. We give a more formal derivation of the finite difference scheme than found in [13], and the order of accuracy is improved by including more jump conditions. The main difference from [11,18] is that we also consider the case with variable coefficients when deriving the correction term. We also propose a simple technique for

approximating the solution-dependent jump conditions as part of the iterative method. A level set function [14] is used to represent the interface because of its simplicity and strength in describing fairly complex shapes.

The rest of the paper is organized as follows: In Section 2 we present the mathematical equations to be solved, introduce the level set function and decompose the jump conditions. Then, in Section 3 we describe the numerical discretization for our sharp interface method and suggest an approach to estimate the interfacial jumps. Numerical examples are presented in Section 4 before we conclude with a summary in Section 5.

2. Mathematical formulation

2.1. The elliptic equation

Consider a domain Ω divided into two (or more) separate subdomains Ω^+ and Ω^- by a lower dimensional interface Γ . The two dimensional variable coefficient elliptic equation is given as

$$(\beta u_x)_x + (\beta u_y)_y = f(x, y), \quad (x, y) \in \Omega, \quad (1)$$

with Dirichlet boundary conditions

$$u(x, y) = g(x, y), \quad (x, y) \in \delta\Omega,$$

where $\delta\Omega$ is the exterior boundary and (x, y) are the spatial coordinates. The coefficient $\beta(x, y)$ and source term $f(x, y)$ are continuous and smooth on each subdomain, but may have jumps across the interface, i.e.

$$\beta(x, y) = \begin{cases} \beta^+(x, y), & (x, y) \in \Omega^+, \\ \beta^-(x, y), & (x, y) \in \Omega^-, \end{cases}$$

and

$$f(x, y) = \begin{cases} f^+(x, y), & (x, y) \in \Omega^+, \\ f^-(x, y), & (x, y) \in \Omega^-. \end{cases}$$

Discontinuities in the coefficient $\beta(x, y)$ and the source term $f(x, y)$ may make the solution and its derivatives discontinuous and non-smooth at the interface. These jumps in solution and its derivatives can be specified as jump conditions along the interface, i.e.

$$[u] = w(x, y), \quad (x, y) \in \Gamma, \quad (2)$$

$$[\beta u_n] = v(x, y), \quad (x, y) \in \Gamma, \quad (3)$$

where $u_n = \partial u / \partial n = \nabla u \cdot \vec{n}$ is the normal derivative of u , \vec{n} is the local unit normal vector to the interface pointing towards the Ω^+ -region, and the jumps are defined as the limiting values

$$[u] = \lim_{(x,y) \rightarrow \Gamma^+} u(x, y) - \lim_{(x,y) \rightarrow \Gamma^-} u(x, y) = u^+ - u^-,$$

$$[\beta u_n] = \lim_{(x,y) \rightarrow \Gamma^+} \beta(x, y) u_n(x, y) - \lim_{(x,y) \rightarrow \Gamma^-} \beta(x, y) u_n(x, y) = \beta^+ u_n^+ - \beta^- u_n^-.$$

Here $(x, y) \rightarrow \Gamma^+$ means approaching the interface from the Ω^+ side and $(x, y) \rightarrow \Gamma^-$ from the Ω^- side.

2.2. Level set representation

The main idea of the level set method is to introduce a smooth auxiliary function $\phi(x, y)$ defined as

$$\phi(x, y) = \pm d,$$

where d is the shortest distance to the interface. The sign of ϕ indicates whether (x, y) is in the Ω^+ -region (positive) or in the Ω^- -region (negative). It will be evident from the definition above that the interface Γ is given by the zero level set of the function ϕ ,

$$\Gamma = \{(x, y) \in \mathbb{R}^2 \mid \phi(x, y) = 0\}.$$

The normal vector can easily be deduced from ϕ and at any point is given as $\vec{n} = \nabla\phi/|\nabla\phi|$.

The interface appears as a closed curve in two dimensions. We assume the interface to be infinitely thin so that our problem domain can be defined as (see Fig. 1)

$$\Omega = \begin{cases} \Omega^-, & \phi < 0, \\ \Omega^+, & \phi \geq 0. \end{cases} \tag{4}$$

2.3. Decomposing the jump conditions

Since the jump conditions usually are defined in normal or tangential direction of the interface we define a local coordinate system aligned with the interface at (x^*, y^*) ,

$$\xi = (x - x^*) \cos \theta + (y - y^*) \sin \theta,$$

$$\eta = -(x - x^*) \sin \theta + (y - y^*) \cos \theta,$$

where θ is the angle between the x - and ξ -axis. The ξ -axis is normal to the interface while the η -axis is tangential.

Transforming these jump conditions into Cartesian coordinates yields

$$[\beta u_x] = [\beta u_\xi] \cos \theta - [\beta u_\eta] \sin \theta,$$

$$[\beta u_y] = [\beta u_\xi] \sin \theta + [\beta u_\eta] \cos \theta,$$

and differentiating using the chain rule gives

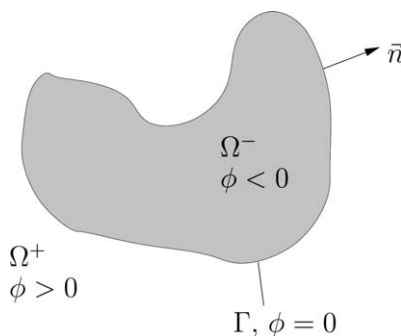


Fig. 1. An irregular interface Γ dividing the domain Ω into two subdomains Ω^+ and Ω^- with normal vector \vec{n} pointing towards the Ω^+ -region.

$$\begin{aligned}
 [(\beta u_x)_x] &= [(\beta u_\xi)_\xi] \cos^2 \theta - ([(\beta u_\xi)_\eta] + [(\beta u_\eta)_\xi]) \cos \theta \sin \theta + [(\beta u_\eta)_\eta] \sin^2 \theta, \\
 [(\beta u_y)_y] &= [(\beta u_\xi)_\xi] \sin^2 \theta + ([(\beta u_\xi)_\eta] + [(\beta u_\eta)_\xi]) \cos \theta \sin \theta + [(\beta u_\eta)_\eta] \cos^2 \theta.
 \end{aligned}$$

Similarly, differentiation of the jump $[u]$ gives

$$\begin{aligned}
 [u_x] &= [u_\xi] \cos \theta - [u_\eta] \sin \theta, \\
 [u_y] &= [u_\xi] \sin \theta + [u_\eta] \cos \theta,
 \end{aligned}$$

and

$$\begin{aligned}
 [u_{xx}] &= [u_{\xi\xi}] \cos^2 \theta - 2[u_{\xi\eta}] \cos \theta \sin \theta + [u_{\eta\eta}] \sin^2 \theta, \\
 [u_{yy}] &= [u_{\xi\xi}] \sin^2 \theta + 2[u_{\xi\eta}] \cos \theta \sin \theta + [u_{\eta\eta}] \cos^2 \theta.
 \end{aligned}$$

For now we will assume that the jumps $[u]$, $[u_\xi]$, $[u_{\xi\xi}]$, $[u_\eta]$, $[u_{\eta\eta}]$, $[\beta u_\xi]$, $[(\beta u_\xi)_\xi]$, $[\beta u_\eta]$, $[(\beta u_\eta)_\eta]$, $[(\beta u_\xi)_\eta]$ and $[(\beta u_\eta)_\xi]$ are all known. In this way, we can apply a dimension by dimension approach of the numerical method.

3. Numerical method

3.1. Discretization

For simplicity, we use a uniform, rectangular grid, $[a, b] \times [c, d]$, describing the computational domain Ω . The grid nodes are equally spaced, $h = (b - a)/M = (d - c)/N$, where M and N are the number of grid points in x - and y -direction, respectively. The grid coordinates are defined as

$$x_i = a + ih, \quad y_j = c + jh \quad \text{for } 0 \leq i \leq M, \quad 0 \leq j \leq N,$$

and the numerical approximation of u at (x_i, y_j) is written as $U_{i,j}$.

We define a grid node (x_i, y_j) as regular if all neighbouring nodes are on the same side of the interface. On the contrary, a grid node (x_i, y_j) is irregular if at least one adjacent node is on the other side of the interface, i.e. the interface cuts one of the grid lines between the nodes.

The elliptic equation (1) is approximated with the following discretization

$$\mathcal{L}_h^\beta U_{i,j} = f_{i,j} - C_{i,j}, \tag{5}$$

where $\mathcal{L}_h^\beta U_{i,j}$ is the standard five point variable coefficient central difference scheme

$$\mathcal{L}_h^\beta U_{i,j} = \frac{\beta_{i+1/2,j}(U_{i+1,j} - U_{i,j}) - \beta_{i-1/2,j}(U_{i,j} - U_{i-1,j})}{h^2} + \frac{\beta_{i,j+1/2}(U_{i,j+1} - U_{i,j}) - \beta_{i,j-1/2}(U_{i,j} - U_{i,j-1})}{h^2}$$

and $\beta_{i+1/2,j}$ denotes $\beta(x_{i+1/2,j}, y_j)$, and so on. At regular nodes, $\mathcal{L}_h^\beta U_{i,j}$ yields a second order accurate approximation of the second derivatives, i.e.

$$(\beta u_x)_x + (\beta u_y)_y = \mathcal{L}_h^\beta U_{i,j} + \mathcal{O}(h^2).$$

The correction term $C_{i,j}$ is introduced to make the numerical discretization (5) well-defined at irregular nodes and should vanish at regular nodes. In the remaining part of this section we will discuss how to find this correction term.

3.2. Determining the correction term

As shown in Section 2.3, the jump conditions can be decomposed into jumps in the x - and y -directions allowing for a dimension by dimension approach. This way, the correction term $C_{i,j}$ is made up by a component in x -direction and one in y -direction, i.e.

$$C_{i,j} = C_{i,j}^x + C_{i,j}^y \tag{6}$$

The procedure for obtaining the componentwise correction term is equivalent whether we consider the x -direction or y -direction. Therefore, we shall only discuss how to find the correction in x -direction. For simpler notation, we will neglect the subscript j in the notation below, reducing the derivations to a one-dimensional problem.

We wish to find a correction term so that the standard finite difference approximation of $(\beta u_x)_x$ is valid even at the interface. We consider an irregular grid node x_i where the interface is located at $x^* = x_i + ah$, $0 \leq a \leq 1$ and $a = \phi_i / (\phi_i - \phi_{i+1})$. The correction can be derived in two steps. First, we need to correct the numerical discretization of u_x , then, if necessary, the approximation of the second derivative $(\beta u_x)_x$ also needs to be corrected.

The first derivative is estimated at the centre between x_i and x_{i+1} . The correction of this approximation depends on what side of $x_{i+1/2}$ the interface is located. In other words, using the definitions of Eq. (4), if $\phi_i < 0$ and $0 < a \leq 1/2$ then the interface is to the left of $x_{i+1/2}$, i.e. $\{x_{i+1/2}, x_{i+1}\} \in \Omega^+$. Else if $1/2 < a \leq 1$ then $\{x_i, x_{i+1/2}\} \in \Omega^-$. Otherwise, if $\phi_i \geq 0$, the subregions switches and instead we have if $0 \leq a < 1/2$ then $\{x_{i+1/2}, x_{i+1}\} \in \Omega^-$ or if $1/2 \leq a < 1$ then $\{x_i, x_{i+1/2}\} \in \Omega^+$.

Following the same approach as [11] using Taylor expansion for $u(x_{i+1})$ at $x^* = x_i + ah$ for the case $\phi_i < 0$ and $1/2 < a \leq 1$ yields

$$\begin{aligned} u(x_{i+1}) &= u(x^* + (1 - a)h) = u^+ + u_x^+(1 - a)h + \frac{1}{2}u_{xx}^+(1 - a)^2h^2 + \mathcal{O}(h^3) \\ &= u^- + u_x^-(1 - a)h + \frac{1}{2}u_{xx}^-(1 - a)^2h^2 + C_1(x, a) + \mathcal{O}(h^3) \\ &= u(x_{i+1/2}) + u_x(x_{i+1/2})(a - \frac{1}{2})h + \frac{1}{2}u_{xx}(x_{i+1/2})(a - \frac{1}{2})^2h^2 + u_x(x_{i+1/2})(1 - a)h \\ &\quad + \frac{1}{2}u_{xx}(x_{i+1/2})(2a - 1)(1 - a)h^2 + \frac{1}{2}u_{xx}(x_{i+1/2})(1 - a)^2h^2 + C_1(x, a) + \mathcal{O}(h^3) \\ &= u(x_{i+1/2}) + u_x(x_{i+1/2})\frac{h}{2} + \frac{1}{2}u_{xx}(x_{i+1/2})\left(\frac{h}{2}\right)^2 + C_1(x, a) + \mathcal{O}(h^3), \end{aligned} \tag{7}$$

and Taylor expansion for $u(x_i)$ at $x_{i+1/2}$ becomes

$$u(x_i) = u(x_{i+1/2}) - u_x(x_{i+1/2})\frac{h}{2} + \frac{1}{2}u_{xx}(x_{i+1/2})\left(\frac{h}{2}\right)^2 + \mathcal{O}(h^3), \tag{8}$$

where the correction term is given as

$$C_1(x, a) = [u] + [u_x](1 - a)h + \frac{1}{2}[u_{xx}](1 - a)^2h^2.$$

Subtracting Eq. (8) from (7) and rearranging gives

$$u_x(x_{i+1/2}) = \frac{u(x_{i+1}) - u(x_i)}{h} - \frac{C_1(x, a)}{h} + \mathcal{O}(h^2).$$

Or, if $0 < a \leq 1/2$, we Taylor expand $u(x_i)$ at $x^* = x_i + ah$:

$$\begin{aligned}
u(x_i) &= u(x^* - ah) = u^- - u_x^- ah + \frac{1}{2}u_{xx}^- a^2 h^2 + \mathcal{O}(h^3) \\
&= u^+ - u_x^+ ah + \frac{1}{2}u_{xx}^+ a^2 h^2 - C_1(x, a) + \mathcal{O}(h^3) = u(x_{i+1/2}) - u_x(x_{i+1/2})(\frac{1}{2} - a)h \\
&\quad + \frac{1}{2}u_{xx}(x_{i+1/2})(\frac{1}{2} - a)^2 h^2 - u_x(x_{i+1/2})ah + \frac{1}{2}u_{xx}(x_{i+1/2})(1 - 2a)ah^2 \\
&\quad + \frac{1}{2}u_{xx}(x_{i+1/2})a^2 h^2 - C_1(x, a) + \mathcal{O}(h^3) \\
&= u(x_{i+1/2}) - u_x(x_{i+1/2})\frac{h}{2} + \frac{1}{2}u_{xx}(x_{i+1/2})\left(\frac{h}{2}\right)^2 - C_1(x, a) + \mathcal{O}(h^3)
\end{aligned} \tag{9}$$

and the Taylor expansion for $u(x_{i+1})$ at $x_{i+1/2}$ will be

$$u(x_{i+1}) = u(x_{i+1/2}) + u_x(x_{i+1/2})\frac{h}{2} + \frac{1}{2}u_{xx}(x_{i+1/2})\left(\frac{h}{2}\right)^2 + \mathcal{O}(h^3), \tag{10}$$

where

$$C_1(x, a) = [u] - [u_x]ah + \frac{1}{2}[u_{xx}]a^2 h^2.$$

Again, subtracting Eq. (9) from (10) and rearranging gives

$$u_x(x_{i+1/2}) = \frac{u(x_{i+1}) - u(x_i)}{h} - \frac{C_1(x, a)}{h} + \mathcal{O}(h^2).$$

In the second step, if the flux βu_x is non-smooth or discontinuous at the interface and $0 < a \leq 1/2$, then we need a second correction term, C_2 , for the second derivative. Expanding gives

$$\begin{aligned}
\beta u_x(x_{i+1/2}) &= \beta u_x(x^* + (\frac{1}{2} - a)h) = (\beta u_x)^+ + (\beta u_x)_x^+(\frac{1}{2} - a)h + \mathcal{O}(h^2) \\
&= (\beta u_x)^- + (\beta u_x)_x^-(\frac{1}{2} - a)h + C_2(x, a) + \mathcal{O}(h^2) \\
&= \beta u_x(x_i) + (\beta u_x)_x(x_i)ah + (\beta u_x)_x(x_i)(\frac{1}{2} - a)h^2 + C_2(x, a) + \mathcal{O}(h^2) \\
&= \beta u_x(x_i) + (\beta u_x)_x(x_i)\frac{h}{2} + C_2(x, a) + \mathcal{O}(h^2)
\end{aligned} \tag{11}$$

and similarly at $x_{i-1/2}$

$$\beta u_x(x_{i-1/2}) = \beta u_x(x_i) - (\beta u_x)_x(x_i)\frac{h}{2} + \mathcal{O}(h^2), \tag{12}$$

where

$$C_2(x, a) = [\beta u_x] + \frac{1}{2}[(\beta u_x)_x](1 - 2a)h.$$

Subtracting Eq. (12) from (11) and rearranging gives

$$(\beta u_x)_x(x_i) = \frac{\beta u_x(x_{i+1/2}) - \beta u_x(x_{i-1/2})}{h} - \frac{C_2(x, a)}{h} + \mathcal{O}(h).$$

To summarize, if we extend this approach to consider the case when the interface is located anywhere between x_{i-1} and x_{i+1} , and we replace u with the numerical approximation U , then we can write

$$(\beta u_x)_x(x_i) = \frac{\beta_{i+1/2}(U_{i+1} - U_i) - \beta_{i-1/2}(U_i - U_{i-1})}{h^2} + C_i + \mathcal{O}(h), \tag{13}$$

with the correction term

$$C_i = S_\phi \bar{\beta} \frac{C_1(x, a)}{h^2} + S_\phi \frac{C_2(x, a)}{h}, \tag{14}$$

where

$$S_\phi = \begin{cases} -1, & \phi_i < 0, \\ 1, & \phi_i \geq 0, \end{cases}$$

and

$$C_1(x, a) = \begin{cases} [u] - \lambda[u_x]ah + \frac{1}{2}[u_{xx}]a^2h^2, & \text{if } (\phi_i \geq 0 \text{ and } 0 \leq a < 1/2) \\ & \text{or } (\phi_i < 0 \text{ and } 0 < a \leq 1/2), \\ [u] + \lambda[u_x](1-a)h + \frac{1}{2}[u_{xx}](1-a)^2h^2, & \text{if } (\phi_i \geq 0 \text{ and } 0 \leq a < 1/2) \\ & \text{or } (\phi_i < 0 \text{ and } 0 < a \leq 1, /2), \end{cases}$$

$$C_2(x, a) = \begin{cases} \lambda[\beta u_x] + \frac{1}{2}[(\beta u_x)_x](1-2a)h, & \text{if } (\phi_i \geq 0 \text{ and } 0 \leq a < 1/2) \\ & \text{or } (\phi_i < 0 \text{ and } 0 < a \leq 1/2), \\ 0, & \text{otherwise.} \end{cases}$$

The parameters λ , a and $\bar{\beta}$ are defined as follows:

- If the interface is between x_i and x_{i+1}
(i.e. $\phi_i \cdot \phi_{i+1} < 0$, or $\phi_i = 0$ and $\phi_{i+1} < 0$, or $\phi_i < 0$ and $\phi_{i+1} = 0$)
 $\lambda = 1, a = \phi_i / (\phi_i - \phi_{i+1})$ and $\bar{\beta} = \beta_{i+1/2}$.
- If the interface is between x_{i-1} and x_i
(i.e. $\phi_i \cdot \phi_{i-1} < 0$, or $\phi_i = 0$ and $\phi_{i-1} < 0$, or $\phi_i < 0$ and $\phi_{i-1} = 0$)
 $\lambda = -1, a = \phi_i / (\phi_i - \phi_{i-1})$ and $\bar{\beta} = \beta_{i-1/2}$.

For both cases, we can define the jump of a function f as

$$[f] = \lim_{\phi^+ \rightarrow 0} f(x) - \lim_{\phi^- \rightarrow 0} f(x) = f^+ - f^-.$$

Remark 1. If the solution is smooth and continuous (regular nodes), the jumps become zero and the correction term vanish.

Remark 2. The local truncation error in Eq. (13) is of first order only, but we can still expect the global accuracy to approach second order since the interface is of one dimension lower than the problem.

Returning to the two-dimensional case, the x -component in Eq. (6) can be replaced by Eq. (14) and a similar expression can be found for $C_{i,j}^y$ making Eq. (5) well-defined at all nodes.

3.3. Approximating the jump conditions

So far we have assumed the interface jump conditions to be known. Unfortunately, that is rarely the case as they are usually solution-dependent and must be obtained as part of the solution. This is probably the most difficult task when using sharp interface methods, as it is crucial for both solving the discrete equations efficiently and maintaining a certain accuracy.

In higher dimensional problems it is common to use some iterative methods to solve the discretized equations. The idea is therefore to obtain the correction term iteratively as well. We can approximate the solution at the interface using Eqs. (2) and (3) by interpolating the result from the previous iteration step (or initial guess). Then using one-sided difference stencils on both sides of the interface we can approximate the jump conditions. The correction term is updated and given explicitly at every iteration step, as it converges to the correct solution.

Using low-order interpolation schemes to approximate the jumps may increase the local truncation error. To keep the local first order accuracy at irregular nodes we see from Eq. (14) that it is necessary to use at least a third order accurate interpolation technique when guessing the interfacial values. To provide a sufficient approximation of the jumps in first and second derivatives, second and first order methods are needed, respectively. We found the Lagrange polynomial of degree two,

$$P(x) = \sum_{i=0}^2 \left(\prod_{\substack{j=0 \\ j \neq i}}^2 \frac{(x - x_j)}{(x_i - x_j)} f_i \right), \quad (15)$$

to be sufficient to meet our required accuracy.

The first step in finding the correction term is approximating the solution at the interface. Consider an irregular grid node (x_i, y_j) where the interface crosses the horizontal grid line at (x^*, y^*) , i.e. $y^* = y_j$. Using a set of interpolated values on both sides of the interface, we can reconstruct the boundary conditions (2) and (3) to solve for the interfacial values at (x^*, y^*) . The procedure is as follows (see Fig. 2):

- (1) Construct a line which is normal to the interface at (x^*, y^*) using the level set function, e.g. find the normal vector $\vec{n} = \nabla \phi / |\nabla \phi|$ in the neighbour gridpoints of (x^*, y^*) , and use linear interpolation to estimate \vec{n} at (x^*, y^*) .
- (2) Chose two points along the normal line on both sides of the interface, e.g. P_1^+, P_2^+, P_1^- and P_2^- , with the distances a_1, a_2, b_1 and b_2 from the interface.
- (3) Use the nodes surrounding P_1^+ and the Lagrange polynomial to find a new value U_1^+ in P_1^+ . Repeat for U_2^+, U_1^- and U_2^- in P_2^+, P_1^- and P_2^- . The points, P_1^+, P_2^+, P_1^- and P_2^- , must be chosen carefully so that all surrounding nodes lie on the same side of the interface, e.g. let $a_1 = \sqrt{2}h$ and $a_2 = 2\sqrt{2}h$, likewise on the other side of the interface.
- (4) Differentiate Eq. (15) to estimate the normal fluxes at the interface as

$$\begin{aligned} \beta^+ u_n^+ &= \beta^+ \left(-\frac{a_1 + a_2}{a_1 a_2} U_0^+ + \frac{a_2}{a_1(a_2 - a_1)} U_1^+ - \frac{a_1}{a_2(a_2 - a_1)} U_2^+ \right), \\ \beta^- u_n^- &= \beta^- \left(\frac{b_1 + b_2}{b_1 b_2} U_0^- - \frac{b_2}{b_1(b_2 - b_1)} U_1^- + \frac{b_1}{b_2(b_2 - b_1)} U_2^- \right). \end{aligned}$$

Combine this with Eqs. (2) and (3) to obtain the interfacial values as

$$\begin{aligned} U_0^- &= \frac{\beta^- \frac{a_1 a_2}{b_2 - b_1} (b_2^2 U_1^- - b_1^2 U_2^-) + \beta^+ \frac{b_1 b_2}{a_2 - a_1} (a_2^2 U_1^+ - a_1^2 U_2^+)}{\beta^- a_1 a_2 (b_1 + b_2) + \beta^+ b_1 b_2 (a_1 + a_2)} \\ &\quad - \frac{a_1 a_2 b_1 b_2 v(x^*, y^*) + \beta^+ b_1 b_2 (a_1 + a_2) w(x^*, y^*)}{\beta^- a_1 a_2 (b_1 + b_2) + \beta^+ b_1 b_2 (a_1 + a_2)} \end{aligned} \quad (16)$$

and

$$U_0^+ = U_0^- + w(x^*, y^*). \quad (17)$$

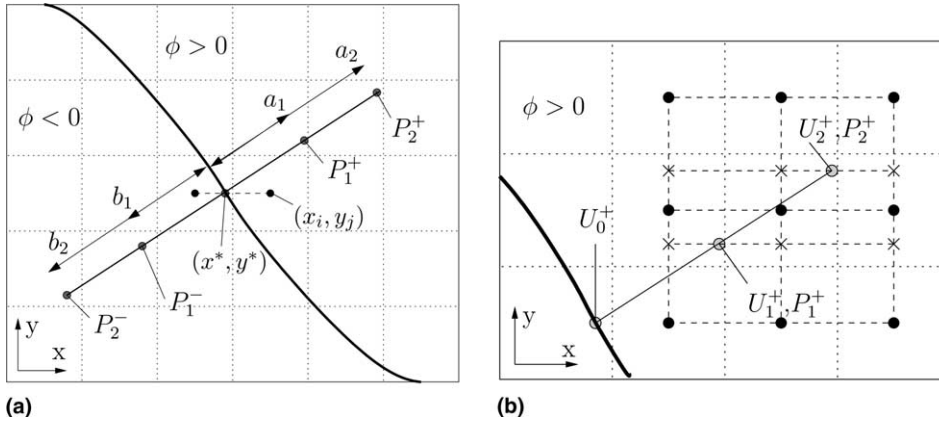


Fig. 2. (a) The interpolation stencil for finding the values at the interface when $y^* = y_j$. (b) The surrounding nodes for the Lagrange polynomial interpolation. First, interpolate in y -direction, then in x -direction to find U_1^+ and U_2^+ .

Next, we use the interfacial values to approximate the jumps in Eq. (6) along the x -direction where $a = \phi_{i,j}/(\phi_{i,j} - \phi_{i-1,j})$ and $b = 1 - a$,

$$u_x^+ = \frac{1}{h} \left(-\frac{2a+1}{a(a+1)} U_0^+ + \frac{a+1}{a} U_{i,j} - \frac{a}{a+1} U_{i+1,j} \right),$$

$$u_x^- = \frac{1}{h} \left(\frac{2b+1}{b(b+1)} U_0^- - \frac{b+1}{b} U_{i-1,j} + \frac{b}{b+1} U_{i-2,j} \right),$$

$$u_{xx}^+ = \frac{1}{h^2} \left(\frac{2}{a(a+1)} U_0^+ - \frac{2}{a} U_{i,j} + \frac{2}{a+1} U_{i+1,j} \right),$$

$$u_{xx}^- = \frac{1}{h^2} \left(\frac{2}{b(b+1)} U_0^- - \frac{2}{b} U_{i-1,j} + \frac{2}{b+1} U_{i-2,j} \right),$$

$$\beta^+ u_x^+ = \frac{\beta^+}{h} \left(-\frac{2a+1}{a(a+1)} U_0^+ + \frac{a+1}{a} U_{i,j} - \frac{a}{a+1} U_{i+1,j} \right),$$

$$\beta^- u_x^- = \frac{\beta^-}{h} \left(\frac{2b+1}{b(b+1)} U_0^- - \frac{b+1}{b} U_{i-1,j} + \frac{b}{b+1} U_{i-2,j} \right),$$

$$\begin{aligned}
 (\beta^+ u_x^+)_x &= \frac{1}{a^2(a+1)^2 h^2} \left\{ \left(\beta^+ (2a+1)^2 - \beta_{i,j} (a+1)^2 - \beta_{i+1,j} a^2 \right) U_0^+ \right. \\
 &\quad - \left(\beta^+ (a+1)^2 (2a+1) - \beta_{i,j} (1-a^2) (a+1)^2 - \beta_{i+1,j} a^2 (a+1)^2 \right) U_{i,j} \\
 &\quad \left. + \left(\beta^+ a^2 (2a+1) + \beta_{i,j} a^2 (a+1)^2 - \beta_{i+1,j} a^3 (2+a) \right) U_{i+1,j} \right\},
 \end{aligned}$$

and finally

$$\begin{aligned}
 (\beta^- u_x^-)_x = & \frac{1}{b^2(b+1)^2 h^2} \left\{ \left(\beta^- (2b+1)^2 - \beta_{i-1,j}(b+1)^2 - \beta_{i-2,j}b^2 \right) U_0^- \right. \\
 & - \left(\beta^- (b+1)^2 (2b+1) - \beta_{i-1,j}(1-b^2)(b+1)^2 - \beta_{i-2,j}b^2(b+1)^2 \right) U_{i-1,j} \\
 & \left. + \left(\beta^- b^2(2b+1) + \beta_{i-1,j}b^2(b+1)^2 - \beta_{i-2,j}b^3(2+b) \right) U_{i-2,j} \right\}.
 \end{aligned}$$

Similar expressions can be found for the jumps in y -direction. This procedure is repeated for every irregular node at every iteration step until convergence is reached in solving Eq. (5).

3.4. Solving the discrete equations

The system of linear discretized equations (5) is a symmetric and diagonally dominant matrix problem which can be solved with most standard linear solvers. Implementation into already existing codes is straightforward, as all correction applies to the right-hand side of the linear system only. We have successfully implemented the method using a Successive Overrelaxation Red–Black Gauss Seidel method.

In each iteration we need to modify the right-hand-side to adjust the discretization at irregular nodes. To ensure numerical stability and convergence, we found it necessary to underrelax the approximation of the correction term $C_{i,j}$, i.e.

$$C_{i,j}^l = C_{i,j}^{l-1} - \alpha(C_{i,j}^{l-1} - C_{i,j}^{\text{new}}),$$

where $C_{i,j}^{\text{new}}$ is the correction term approximated from the l th iteration step and α is the underrelaxation parameter.

The initial guess, normally set equal to zero, for the solution and for the first approximated correction term, $C_{i,j}^0$, deviates of course largely from the correct values, and consequently the term $(C_{i,j}^0 - C_{i,j}^{\text{new}})$ will be large. Such large adjustments in the right-hand-side of the discretized system will lead to numerical instabilities. To suppress these instabilities the underrelaxation parameter α was introduced. This effect was enhanced for finer grids, thereby requiring a smaller α . As the numerical solution was iterated towards the correct solution, the underrelaxation parameter could slowly be increased and the system would still be stable. We did not seek for any optimal value, but for the examples below it was sufficient to set α somewhere between 0.05 and 0.01 in most cases.

4. Numerical examples

We have performed a number of numerical experiments to test our method. From these experiments we are particularly interested in the accuracy of the computed solution and how well it performs when we estimate the jumps according to Section 3.3 compared to using the exact jumps. We also compare some of our results with other authors' work.

All examples below are computed on a square domain Ω , $[-1, 1] \times [-1, 1]$, with equally spaced nodes, so that $\Delta x = \Delta y = h$ and $N = M = n$. The accuracy of the scheme is found from a grid refinement analysis. The order of the scheme is given as

$$\text{order} = \left| \frac{\log(\|E_n\|_\infty / \|E_{2n}\|_\infty)}{\log(2)} \right|,$$

where we use the maximum norm

$$\|E_n\|_\infty = \max_{i,j} |u(x_i, y_j) - U_{i,j}|$$

to estimate the error using an $n \times n$ grid.

We are also interested in finding the error when we mimic the correction term. Let $\bar{C}_{i,j}$ represent the approximate correction, then the relative error in the correction term is defined as

$$\|CE_n\|_\infty = \frac{\max_{i,j} |C_{i,j} - \bar{C}_{i,j}|}{\max_{i,j} |C_{i,j}|}.$$

4.1. Example 1

In the first example we consider a case studied in [8,18]. We solve Laplace’s equation, $\nabla^2 u = 0$ and the interface is defined by the circle $x^2 + y^2 = 1/4$ with the jump conditions $[u] = 0$ and $[u_n] = 2$. This can be considered as a problem where there is a singular source term along the interface, and the exact solution is given as

$$u(x, y) = \begin{cases} 1, & x^2 + y^2 < 1/4, \\ 1 + \log(2\sqrt{x^2 + y^2}), & x^2 + y^2 \geq 1/4. \end{cases}$$

The exterior boundary conditions are given from the exact solution.

Table 1 (top) shows the result of the grid refinement analysis. The first column shows the mesh size. The next two columns give the maximum error and order of convergence when we use the exact correction term calculated from the true solution. The last four columns give the result when we approximate the correction term according to Section 3.3. We notice the absolute error increases when we approximate the correction term, but both cases show that the convergence approaches second order as the grid is refined.

To explain the discrepancy in error between the two approaches, we replaced Eqs. (16) and (17) with the exact values given by the solution at the interface. These fixed values were then used to approximate the one-sided differences at the interface according to Section 3.3. The results are summarized in Table 2. We

Table 1
Grid refinement analysis in example 1

n	Exact correction term		Approximate correction term			
	$\ E_n\ _\infty$	Order	$\ E_n\ _\infty$	Order	$\ CE_n\ _\infty$	Order
20	1.048×10^{-3}		2.049×10^{-2}		2.519×10^{-2}	
40	2.403×10^{-4}	2.12	6.366×10^{-3}	1.69	8.204×10^{-3}	1.61
80	6.436×10^{-5}	1.90	1.760×10^{-3}	1.85	2.890×10^{-3}	1.51
160	1.565×10^{-5}	2.04	4.747×10^{-4}	1.89	7.550×10^{-4}	1.94
320	3.185×10^{-6}	2.30	1.206×10^{-4}	1.98	1.983×10^{-4}	1.93
n	IIM in [8]		EJIIM in [18]			
	$\ E_n\ _\infty$	Order	$\ E_n\ _\infty$	Order		
20	2.391×10^{-3}		1.4×10^{-3}			
40	8.346×10^{-4}	1.52	1.8×10^{-4}	2.94		
80	2.445×10^{-4}	1.77	6.6×10^{-5}	1.43		
160	6.686×10^{-5}	1.87	1.9×10^{-5}	1.77		
320	1.567×10^{-5}	2.09	3.4×10^{-6}	2.51		

Top: results obtained in this study. Bottom: results obtained in [8] and [18].

Table 2
Grid refinement analysis with fixed interface in example 1

n	Approximate correction term (fixed interface)			
	$\ E_n\ _\infty$	Order	$\ CE_n\ _\infty$	Order
20	7.883×10^{-4}		5.635×10^{-3}	
40	2.011×10^{-4}	1.97	1.383×10^{-3}	2.03
80	5.032×10^{-5}	2.00	4.430×10^{-4}	1.64
160	1.267×10^{-5}	1.99	1.181×10^{-4}	1.91
320	3.187×10^{-6}	1.99	2.651×10^{-5}	2.16

notice the maximum error decreases significantly and becomes nearly identical to the error obtained when using the exact correction terms. This is illustrated in Fig. 3 where we plot the error for all three cases together with the numerical solution on a 40×40 mesh.

The order of convergence compares well with the results reported in [8,18] for all three cases (see Table 1, bottom), but an equivalent or better accuracy is only achieved for the case with exact correction term or with a fixed interface. When we approximate the correction term, the maximum error is worse than obtained in [8,18]. We realize a possible weakness in using Eqs. (16) and (17), though we still find the performance satisfactorily. Alternatively, using even higher order differences complicates the implementation by involving more grid nodes. More nodes may require higher grid resolution to allow for one-sided differences at the interface.

If we look at the accuracy of the approximate correction term, we notice that the relative error, $\|CE_n\|_\infty$, decreases almost with a rate of second order. This is better than what we expected and clearly satisfies our

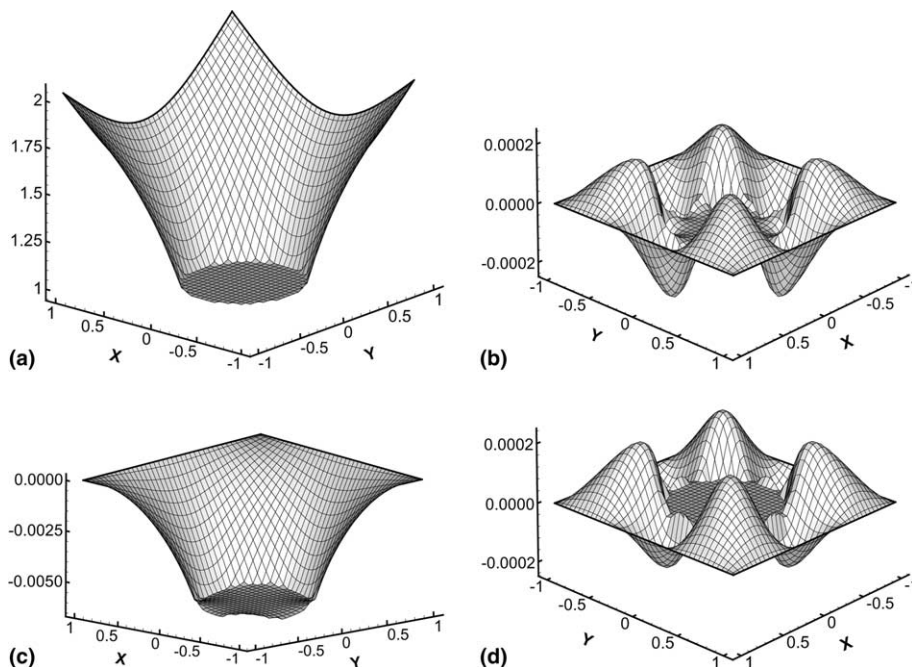


Fig. 3. Example 1. (a) The numerical solution on a 40×40 mesh. (b) The error when using the exact correction term. (c) The error when using approximate correction term. (d) The error when using approximate correction term with fixed interface.

requirements of at least local first order accuracy. Using exact values at the interface improves the error for the correction term.

4.2. Example 2

Now we consider an example with discontinuous coefficients. The problem is also given by [8,12,18] and is defined by the variable coefficient elliptic equation

$$(\beta u_x)_x + (\beta u_y)_y = f(x, y)$$

with

$$\beta(x, y) = \begin{cases} r^2 + 1, & r < 1/2, \\ b, & r \geq 1/2, \end{cases}$$

and

$$f(x, y) = 8r^2 + 4,$$

for jumps $[u] = 0$ and $[\beta u_n] = C/r$, where $r = \sqrt{x^2 + y^2}$ and C and b are arbitrary constants. The boundary values are found from the analytical solution,

$$u(x, y) = \begin{cases} r^2, & r < 1/2, \\ (1 - \frac{1}{8b} - \frac{1}{b})/4 + (\frac{r^4}{2} + r^2) + C \log(2r), & r \geq 1/2. \end{cases}$$

The results are summarized in Table 3 for $b = 10$ and $C = 0.1$. The maximum error does not show a significant difference whether we approximate the correction term or not. The decrease in error is second order as the grid resolution increases. We obtain better accuracy than [8], but their approach converges slightly faster as the grid is refined. In [18], the convergence is slower than obtained here, however, their maximum norm is very close to our results when we approximate the correction term. Again, the relative error, $\|CE_n\|_\infty$, in approximating the correction term converges quadratically as the grid is refined.

Table 3
Grid refinement analysis in example 2 with $b = 10$ and $C = 0.1$

n	Exact correction term		Approximate correction term			
	$\ E_n\ _\infty$	Order	$\ E_n\ _\infty$	Order	$\ CE_n\ _\infty$	Order
20	9.643×10^{-4}		1.394×10^{-3}		1.479×10^{-2}	
40	2.490×10^{-4}	1.95	3.228×10^{-4}	2.11	3.479×10^{-3}	2.09
80	6.315×10^{-5}	1.98	7.857×10^{-5}	2.04	9.863×10^{-4}	1.82
160	1.589×10^{-5}	1.99	1.925×10^{-5}	2.03	2.143×10^{-4}	2.20
320	3.922×10^{-6}	2.02	4.774×10^{-6}	2.01	5.782×10^{-5}	1.89
n	IIM in [8]		EJIIM in [18]			
	$\ E_n\ _\infty$	Order	$\ E_n\ _\infty$	Order		
20	3.520×10^{-3}		7.6×10^{-4}			
40	7.561×10^{-4}	2.22	2.4×10^{-4}	1.7		
80	1.651×10^{-4}	2.20	7.9×10^{-5}	1.6		
160	3.600×10^{-5}	2.20	2.2×10^{-5}	1.8		
320	8.441×10^{-6}	2.09	5.3×10^{-6}	2.1		

Top: results obtained in this study. Bottom: results obtained in [8] and [18].

Table 4

Grid refinement analysis with fixed interface in example 2 with $b = 10$ and $C = 0.1$

n	Approximate correction term (fixed interface)			
	$\ E_n\ _\infty$	Order	$\ CE_n\ _\infty$	Order
20	5.378×10^{-4}		4.525×10^{-3}	
40	1.378×10^{-4}	1.96	1.059×10^{-3}	2.10
80	3.470×10^{-5}	1.99	2.732×10^{-4}	1.95
160	8.704×10^{-6}	2.00	5.672×10^{-5}	2.27
320	2.177×10^{-6}	2.00	1.522×10^{-5}	1.90

As in the previous example we want to investigate the effect of replacing Eqs. (16) and (17) with the exact values given by the true solution. Table 4 summarizes the results. As earlier, we notice improvements in accuracy. However, for this problem the improvements are not that significant and we believe that Eqs. (16) and (17) give a fairly good estimate of the values at the interface. Fig. 4 shows the numerical solution and the error for the three cases.

We also consider the same problem with large jumps in the coefficients at the interface. The results are given in Table 5 for $b = 1000$ and $b = 0.001$ when we approximate the correction term. The method still converges with second order and the accuracy is slightly better than obtained in [12]. It should be noted that for small b , the solution in the outer region becomes very large so that the absolute error in Table 5 is actually small compared to the exact solution. We discuss some numerical problems associated with highly discontinuous coefficients in more detail in the next example.

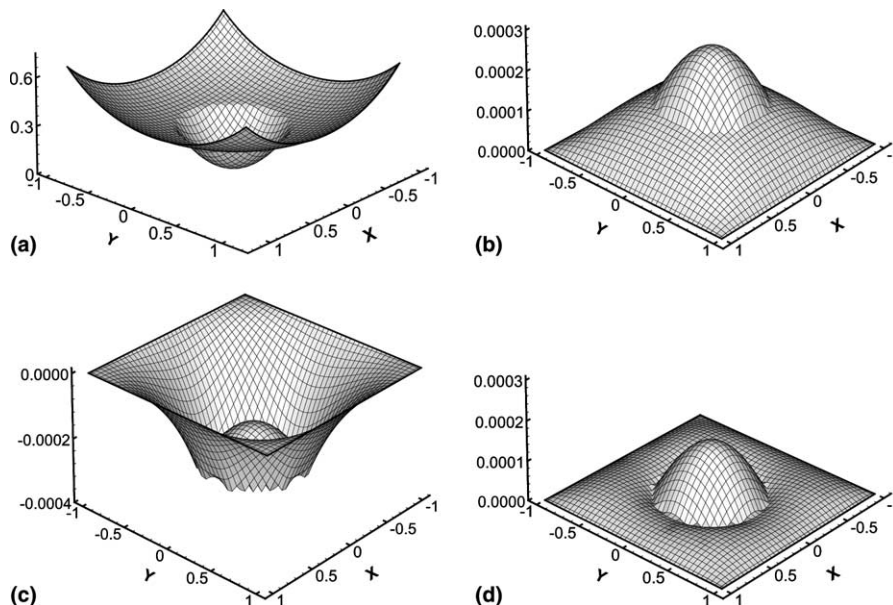


Fig. 4. Example 2. (a) The numerical solution on a 40×40 mesh. (b) The error when using the exact correction term. (c) The error when using approximate correction term. (d) The error when using approximate correction term with fixed interface.

Table 5
Grid refinement analysis in example 2 with large jumps in the coefficients

n	$b = 1000, C = 0.1$				$b = 0.001, C = 0.1$			
	$\ E_n\ _\infty$	Order	$\ CE_n\ _\infty$	Order	$\ E_n\ _\infty$	Order	$\ CE_n\ _\infty$	Order
32	2.083×10^{-4}		7.563×10^{-4}		4.971×10^0		1.285×10^{-2}	
64	5.296×10^{-5}	1.98	1.702×10^{-4}	2.15	1.176×10^0	2.08	3.097×10^{-3}	2.05
128	1.330×10^{-5}	1.99	4.731×10^{-5}	1.85	2.900×10^{-1}	2.02	7.680×10^{-4}	2.01
256	3.330×10^{-6}	2.00	1.234×10^{-5}	1.93	7.086×10^{-2}	2.03	1.903×10^{-4}	2.01
n	$b = 1000, C = 0.1$		$b = 0.001, C = 0.1$					
	$\ E_n\ _\infty$	Order	$\ E_n\ _\infty$	Order				
32	5.136×10^{-4}		9.246×10^0					
64	8.235×10^{-5}	2.76	2.006×10^0	2.32				
128	1.869×10^{-5}	2.19	5.808×10^{-1}	1.83				
256	4.026×10^{-6}	2.24	1.374×10^{-1}	2.10				

Top: results obtained in this study with approximated correction term. Bottom: results obtained in [12].

4.3. Example 3

In this example we consider a composite material problem with piecewise constant coefficients. We are particularly interested in the case with large differences in material properties. Let

$$u(x, y) = \begin{cases} \frac{2x}{\rho + 1 + s^2(\rho - 1)}, & r < s, \\ \frac{x(\rho + 1) - s^2(\rho - 1)x/r^2}{\rho + 1 + s^2(\rho - 1)}, & r \geq s, \end{cases}$$

where $\rho = \beta^- / \beta^+$, $r = \sqrt{x^2 + y^2}$ and s is the radius of the circular interface. This is the solution to $\nabla^2 u = 0$ with $[u] = 0$ and $[\beta u] = 0$ at the interface and exterior boundary as given by the analytical solution.

In fact, this problem is identical to Example 7.3 in [18] where they reported poor performance for the fast iterative IIM [10] (FIIM) and their own explicit-jump IIM (EJIIM) in some cases. In EJIIM the correction term is found from approximating the jumps with one-sided interpolation on one side of the interface only. Choosing the correct side of the interface may be crucial for the results. They explained this with support from their observations that the interior solution is pictured by a circular plane and finite differences on this side represent the normal derivatives exactly, thus the jumps are exact. On the exterior side, the finite difference representation is not that exact, introducing an error in the jump approximation and reducing the accuracy of the scheme.

Tables 6 and 7 summarize the results for $\rho = 5000$, while Tables 8 and 9 summarize the grid refinement analysis for $\rho = 1/5000$. We have chosen $s = 1/2$ for both cases. For $\rho = 5000$ ($\beta^- \gg \beta^+$) we clearly have $u_n^+ \gg u_n^-$ and we may assume that Eq. (16) simplifies into solving $u_n^- = 0$ if u_n^+ is finite and not too large (this is actually not true, but Eq. (16) is mostly influenced by the solution in the interior region as long as u_n^+ is not too large). On the interior side, the finite differences approximate the normal derivatives exactly. Therefore, the interface values are correctly approximated. This explains the good performance of our approach for $\rho = 5000$. There are no remarkable differences in accuracy whether we use exact jumps or approximate them with or without the exact solution at the interface. This is also illustrated in Fig. 5 where the numerical solution is plotted together with the error for all three cases. The differences in error are small and all cases show better accuracy than found in [18].

Table 6
Grid refinement analysis in example 3 with $\rho = 5000$

n	Exact correction term		Approximate correction term			
	$\ E_n\ _\infty$	Order	$\ E_n\ _\infty$	Order	$\ CE_n\ _\infty$	Order
25	9.811×10^{-4}		8.185×10^{-4}		9.441×10^{-3}	
50	2.730×10^{-4}	1.85	3.278×10^{-4}	1.32	4.796×10^{-3}	0.98
100	4.841×10^{-5}	2.50	5.277×10^{-5}	2.64	3.046×10^{-3}	0.65
200	1.260×10^{-5}	1.94	1.371×10^{-5}	1.94	1.802×10^{-3}	0.75
400	3.491×10^{-6}	1.85	3.653×10^{-6}	1.91	9.370×10^{-4}	0.94
n	FIIM		Interior EJIIM		Exterior EJIIM	
	$\ E_n\ _\infty$	Order	$\ E_n\ _\infty$	Order	$\ E_n\ _\infty$	Order
25	1.2×10^{-2}		1.4×10^{-3}		9.1×10^{-2}	
50	9.2×10^{-2}		3.5×10^{-4}	2.0	2.5×10^{-2}	1.9
100	5.9×10^{-2}	0.6	9.0×10^{-5}	2.0	6.8×10^{-3}	1.9
200	7.7×10^{-3}	2.9	2.2×10^{-5}	2.0	2.0×10^{-3}	1.8

Top: results obtained in this study. Bottom: results obtained in [18].

Table 7
Grid refinement analysis with fixed interface in example 3 with $\rho = 5000$

n	Approximate correction term (fixed interface)			
	$\ E_n\ _\infty$	Order	$\ CE_n\ _\infty$	Order
25	8.136×10^{-4}		9.410×10^{-3}	
50	2.249×10^{-4}	1.85	4.611×10^{-3}	1.03
100	5.137×10^{-5}	2.13	3.044×10^{-3}	0.60
200	1.372×10^{-5}	1.90	1.803×10^{-3}	0.76
400	3.423×10^{-6}	2.00	9.368×10^{-4}	0.94

Table 8
Grid refinement analysis in example 3 with $\rho = 1/5000$

n	Exact correction term		Approximate correction term			
	$\ E_n\ _\infty$	Order	$\ E_n\ _\infty$	Order	$\ CE_n\ _\infty$	Order
25	1.635×10^{-3}		2.267×10^{-2}		6.126×10^{-2}	
50	4.549×10^{-4}	1.85	7.038×10^{-3}	1.68	1.843×10^{-2}	1.73
100	8.066×10^{-5}	2.50	1.934×10^{-3}	1.86	7.108×10^{-3}	1.37
200	2.102×10^{-5}	1.94	5.209×10^{-4}	1.89	3.103×10^{-3}	1.20
400	5.823×10^{-6}	1.85	1.346×10^{-4}	1.95	1.280×10^{-3}	1.28
n	FIIM		Interior EJIIM		Exterior EJIIM	
	$\ E_n\ _\infty$	Order	$\ E_n\ _\infty$	Order	$\ E_n\ _\infty$	Order
25	5.2×10^{-3}		1.9×10^{-3}		1.3×10^1	
50	1.6×10^{-3}	1.7	5.5×10^{-4}	1.8	5.6×10^0	1.3
100	2.3×10^{-4}	2.8	1.3×10^{-4}	2.1	6.4×10^{-1}	3.1
200	5.0×10^{-5}	2.2	3.2×10^{-5}	2.0	8.1×10^{-2}	3.0

Top: results obtained in this study. Bottom: results obtained in [18].

For $\rho = 1/5000$ ($\beta^- \ll \beta^+$) we may assume that Eq. (16) simplifies into solving $u_n^+ = 0$ if u_n^- is finite and not too large. In this case, the finite difference approximation of the normal derivative is less accurate on the exterior side, resulting in an inaccurate approximation of the values at the interface. This explains

Table 9
Grid refinement analysis with fixed interface in example 3 with $\rho = 1/5000$

n	Approximate correction term (fixed interface)			
	$\ E_n\ _\infty$	Order	$\ CE_n\ _\infty$	Order
25	1.356×10^{-3}		9.410×10^{-3}	
50	3.748×10^{-4}	1.85	4.611×10^{-3}	1.03
100	8.560×10^{-5}	2.13	3.044×10^{-3}	0.60
200	2.287×10^{-5}	1.90	1.803×10^{-3}	0.76
400	5.703×10^{-6}	2.00	9.368×10^{-4}	0.94

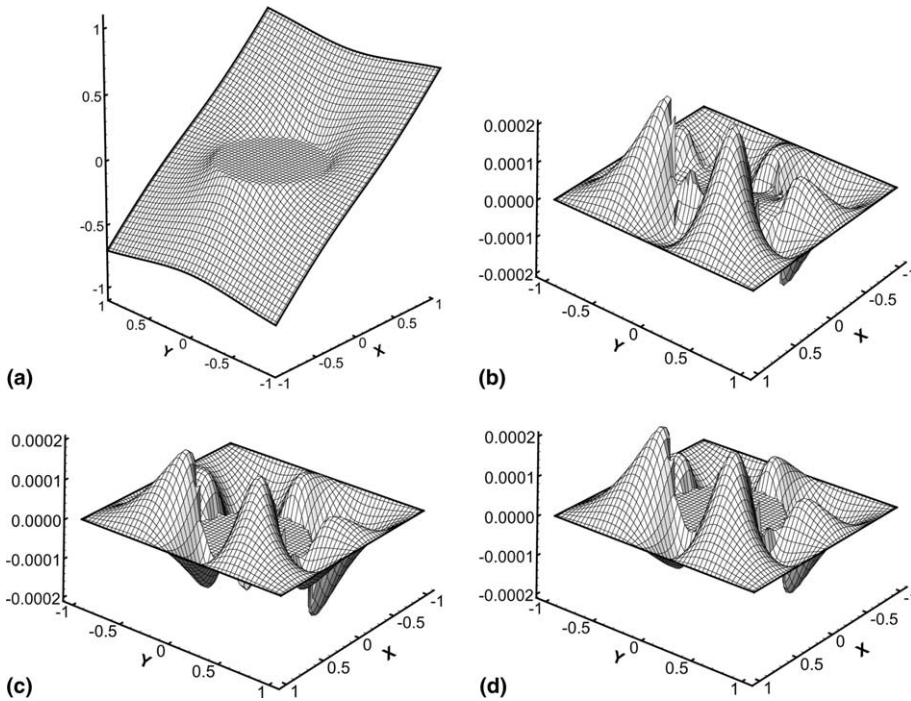


Fig. 5. Example 5, $\rho = 5000$. (a) The numerical solution on a 50×50 mesh. (b) The error when using the exact correction term. (c) The error when using approximate correction term. (d) The error when using approximate correction term with fixed interface.

why the accuracy is lower when we use Eqs. (16) and (17) to approximate the correction terms. If we instead replace Eqs. (16) and (17) with the exact values when approximating the jumps, the accuracy becomes nearly identical with the case where we use exact jumps to find the correction terms. This is also shown in Fig. 6.

Despite the lower accuracy obtained for $\rho = 1/5000$ when we used approximate correction terms, the performance of our method seems acceptable. The result obtained on the coarsest grid for $\rho = 1/5000$ is still better than the best approximation with the exterior EJIIM in [18], but it is worse than the results obtained with the FIIM or interior EJIIM. The rate of convergence is second order for all cases. The relative error, $\|CE_n\|_\infty$, in approximating the correction term converges only with a first order rate here. This is actually what we first expected when we derived the scheme for finding the jumps at the interface.

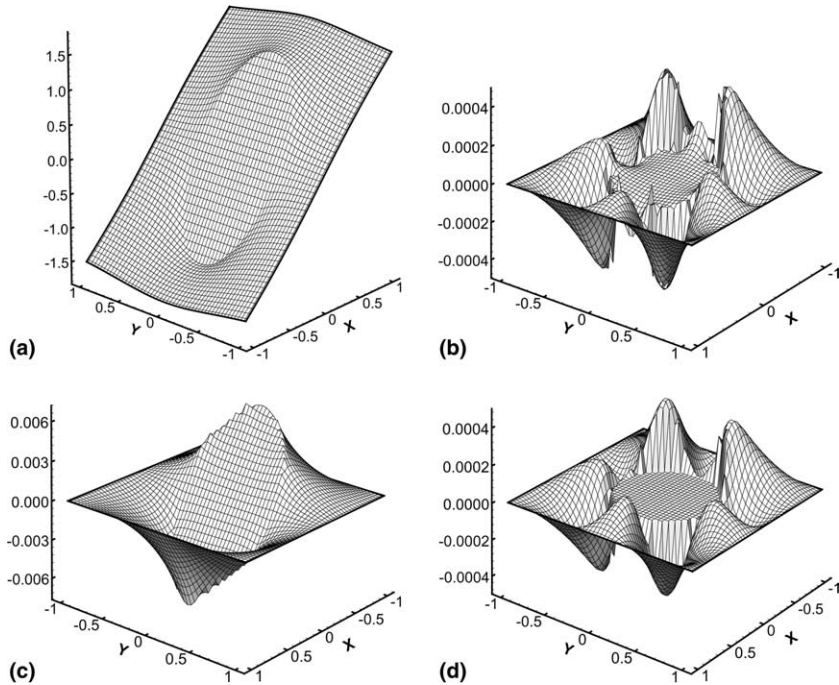


Fig. 6. Example 5, $\rho = 1/5000$. (a) The numerical solution on a 50×50 mesh. (b) The error when using the exact correction term. (c) The error when using approximate correction term. (d) The error when using approximate correction term with fixed interface.

4.4. Example 4

In the two remaining examples we will only focus on the performance of approximating the correction term. We want to compare the performance of the method with constant and variable coefficients by solving two different problems leading to the same exact solution,

$$u(x, y) = \begin{cases} e^x \cos y, & x^2 + y^2 < 1/4, \\ 0, & x^2 + y^2 \geq 1/4, \end{cases}$$

with a discontinuity at the interface.

Case I is defined by $\nabla^2 u = 0$ with jumps $[u] = -e^x \cos y$ and $[u_n] = 2e^x(y \sin y - x \cos y)$ (this example is also found in [8,13]). In Case II, we solve the variable coefficient elliptic equation $(\beta u_x)_x + (\beta u_y)_y = f(x, y)$, where

$$\beta(x, y) = \begin{cases} x^2 + y^2 + 1, & x^2 + y^2 < 1/4, \\ 1, & x^2 + y^2 \geq 1/4, \end{cases}$$

$$f(x, y) = \begin{cases} 2e^x(y \sin y - x \cos y), & x^2 + y^2 < 1/4, \\ 0, & x^2 + y^2 \geq 1/4, \end{cases}$$

and the jumps are $[u] = -e^x \cos y$ and $[\beta u_n] = 2e^x(x^2 + y^2 + 1)(y \sin y - x \cos y)$. The exterior boundary condition is $u = 0$ for both cases.

The results from Case I and II are summarized in Table 10 where we have used approximate correction terms. We can see how the discontinuity is captured sharply in Fig. 7. The accuracy of both numerical

Table 10
Grid refinement analysis in example 4

n	Case I				Case II			
	$\ E_n\ _\infty$	Order	$\ CE_n\ _\infty$	Order	$\ E_n\ _\infty$	Order	$\ CE_n\ _\infty$	Order
20	6.429×10^{-4}		1.964×10^{-4}		7.771×10^{-4}		2.309×10^{-3}	
40	1.895×10^{-4}	1.76	3.026×10^{-5}	2.70	2.302×10^{-4}	1.76	4.947×10^{-4}	2.22
80	5.085×10^{-5}	1.90	6.417×10^{-6}	2.24	6.193×10^{-5}	1.89	1.452×10^{-4}	1.77
160	1.321×10^{-5}	1.94	8.480×10^{-7}	2.92	1.601×10^{-5}	1.95	3.357×10^{-5}	2.11
320	3.342×10^{-6}	1.98	1.047×10^{-7}	3.02	4.051×10^{-6}	1.98	8.689×10^{-6}	1.94
n	Results obtained in [8]							
	$\ E_n\ _\infty$	Order						
20	4.379×10^{-4}							
40	1.079×10^{-4}	2.02						
80	2.778×10^{-5}	1.95						
160	7.499×10^{-6}	1.89						
320	1.740×10^{-6}	2.11						

Top: results obtained in this study. Bottom: results obtained in [8] for Case I.

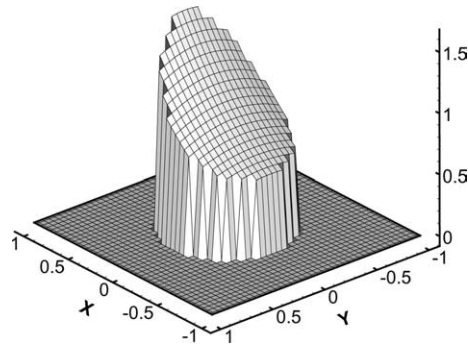


Fig. 7. Example 4. The numerical solution on a 40×40 mesh.

solutions agrees well with each other and both converge quadratically. In Case I, the relative error, $\|CE_n\|_\infty$, in the correction term becomes negligibly small already at coarse grids. The rate of convergence of $\|CE_n\|_\infty$ is close to three. The relative error in the correction term in Case II is also remarkably low compared to previous examples. We have also included the results obtained in [8] for Case I in Table 10. Their results are slightly better than what we achieved, but the differences are not significant.

4.5. Example 5

For this example we solve one problem with different shapes of the interface. Consider the variable coefficient Elliptic equation $(\beta u_x)_x + (\beta u_y)_y = f(x, y)$ with the coefficient

$$\beta(x, y) = \begin{cases} x^2 + y^2 + 1, & \phi(x, y) < 0, \\ x + 2, & \phi(x, y) \geq 0, \end{cases}$$

and source term

Table 11
Grid refinement analysis in example 5

<i>n</i>	Case I				Case II			
	$\ E_n\ _\infty$	Order	$\ CE_n\ _\infty$	Order	$\ E_n\ _\infty$	Order	$\ CE_n\ _\infty$	Order
20	4.141×10^{-4}		1.591×10^{-3}					
40	1.205×10^{-4}	1.78	3.578×10^{-4}	2.15	1.732×10^{-4}		3.935×10^{-4}	
80	3.254×10^{-5}	1.89	1.038×10^{-4}	1.79	4.916×10^{-5}	1.82	1.029×10^{-4}	1.94
160	8.365×10^{-6}	1.96	2.406×10^{-5}	2.11	1.109×10^{-5}	2.15	2.469×10^{-5}	2.06
320	2.130×10^{-6}	1.97	6.141×10^{-6}	1.97	2.933×10^{-6}	1.91	5.468×10^{-6}	2.17

$$f(x, y) = \begin{cases} 2e^x(y \sin y - x \cos y), & \phi(x, y) < 0, \\ -2x - 3, & \phi(x, y) \geq 0. \end{cases}$$

The jumps are given as $[u] = x - y^2 - e^x \cos y$ and $[\beta u_n] = \{x + 2 - (x^2 + y^2 + 1)e^x \cos y\}n_x + \{-2y(x + 2) + (x^2 + y^2 + 1)e^x \sin y\}n_y$, where the normal vector $\vec{n} = (n_x, n_y)$ is given as $\nabla\phi/|\nabla\phi|$.

For Case I, we define the level set function $\phi(x, y)$ as follows:

$$\phi(x, y) = \text{sign}(x^2 + y^2 - 1/4)\sqrt{x^2 + y^2 - 1/4}.$$

For Case II, the level set function is obtained by solving the minimum value problem

$$d = \min \sqrt{(x - X(\theta))^2 + (y - Y(\theta))^2},$$

where the interface is given by the parametrized curve $(X(\theta), Y(\theta))$,

$$\begin{aligned} X(\theta) &= \frac{3}{8} \cos(\theta) - \frac{1}{4} \cos(3\theta), \\ Y(\theta) &= \frac{2}{3} \sin(\theta) - \frac{1}{12} \sin(3\theta) + \frac{1}{15} \sin(7\theta), \end{aligned}$$

for $\theta \in [0, 2\pi)$. Then $\phi(x, y) = \pm d$, where the negative sign corresponds to the inner region enclosed by the curve $(X(\theta), Y(\theta))$, while the plus sign is for the outer region. The exterior boundary conditions are given from the exact solution

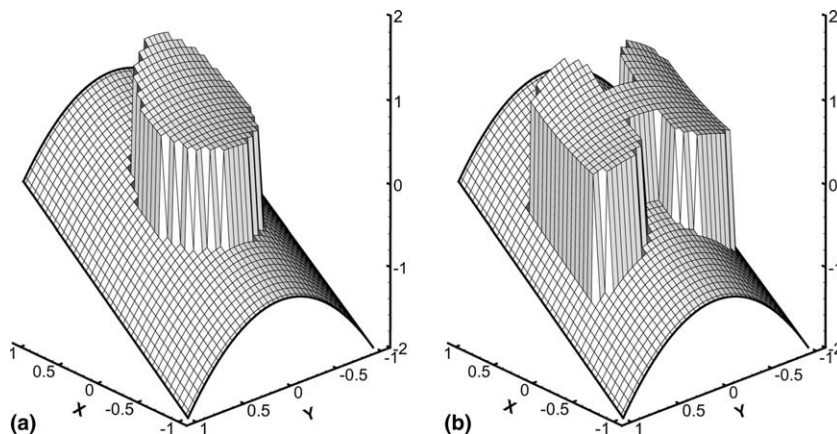


Fig. 8. Example 5. (a) Numerical solution on a 40×40 mesh, Case I. (b) Numerical solution on a 40×40 mesh, Case II.

$$u(x, y) = \begin{cases} e^x \cos y, & \phi(x, y) < 0, \\ x - y^2, & \phi(x, y) \geq 0. \end{cases}$$

The grid refinement analysis is summarized in Table 11, and Fig. 8 shows the numerical results for both interface shapes. We had to omit the coarsest grid for the irregular shaped interface to allow for one-sided differences. For both cases, the accuracy is high and the rate of convergence is second order. The relative error, $\|CE_n\|_\infty$, in correction terms are almost identical, regardless of interface shape. The accuracy does not seem to be affected by the irregular interface as long as the grid resolution is high enough to allow for one-sided differences at the interface.

5. Summary

We have derived a finite difference method for two-dimensional elliptic equations with discontinuous, variable coefficients and source terms. Numerical experiments show good agreement with analytical solutions, and the rate of convergence is found to be of second order. The method decomposes the interface problem and introduces componentwise correction terms at irregular grid nodes to make the difference scheme well-defined across interfaces. These correction terms are derived so that the difference stencil remains symmetric and diagonally dominant, allowing for most standard solvers to be used. The main advantage of the present approach is to preserve the symmetry of the discretized elliptic problem for more general coefficients than in previous methods, i.e. piecewise smooth coefficients, with higher order accuracy.

We have also proposed a new method for estimating the solution-dependent correction terms. The main idea is to obtain the correct correction term iteratively in parallel with the solution. Using sufficient underrelaxation on the approximated correction term gives a converging solution. Optimizing the value of the underrelaxation parameter is crucial for the number of iterations required, and a separate study of this issue could be of interest.

The approximate correction approach does not seem to influence the accuracy noticeably. However, for some cases the values estimated at the interface become too inaccurate, increasing the maximum error of the scheme. Despite this weakness, test cases show second order convergence and the accuracy is found to be acceptable. The only restriction is a sufficient grid resolution to allow for one-sided differencing at the interface.

The present method is very simple to implement in existing codes. It does not require constructions of complex coefficient matrices, as required by many other immersed interface methods. We believe an extension to three dimensions should be straight forward following the same approach as presented here.

Acknowledgements

This work was supported by the Norwegian Research Council through the Petronics programme for doctoral studies. The author would especially like to thank his supervisor Professor Tor Ytremhus for his advice, encouragement and comments on the work presented here. The author is also grateful for the discussions with Associate Professor Reidar Kristoffersen and Tore Flåtten, their suggestions and comments were very helpful while preparing the manuscript.

References

- [1] L. Adams, Z. Li, The immersed interface/multigrid methods for interface problems, *SIAM J. Sci. Comput.* 24 (2) (2002) 463–479.
- [2] R.P. Beyer, R.J. Leveque, Analysis of a one-dimensional model for the immersed boundary method, *SIAM J. Numer. Anal.* 29 (2) (1992) 332–364.

- [3] J.U. Brackbill, D.B. Kothe, C. Zemach, A continuum method for modeling surface tension, *J. Comput. Phys.* 100 (1992) 335–354.
- [4] Y.C. Chang, T.Y. Hou, B. Merriman, S. Osher, A level set formulation of Eulerian interface capturing methods for incompressible fluid flows, *J. Comput. Phys.* 124 (1996) 449–464.
- [5] R.P. Fedkiw, T. Aslam, B. Merriman, S. Osher, A non-oscillatory Eulerian approach to interfaces in multimaterial flows (The Ghost Fluid Method), *J. Comput. Phys.* 152 (1999) 457–492.
- [6] H. Huang, Z. Li, Convergence analysis of the immersed interface method, *IMA J. Numer. Anal.* 19 (1999) 583–608.
- [7] M. Kang, R.P. Fedkiw, X.-D. Liu, A boundary condition capturing method for multiphase incompressible flow, *J. Sci. Comput.* 15 (3) (2000) 323–360.
- [8] R.J. Leveque, Z. Li, The immersed interface method for elliptic equations with discontinuous coefficients and singular sources, *SIAM J. Numer. Anal.* 31 (4) (1994) 1019–1044.
- [9] Z. Li, A note on immersed interface method for three-dimensional elliptic equations, *Comput. Math. Applic* 31 (3) (1996) 9–17.
- [10] Z. Li, A fast iterative algorithm for elliptic interface problems, *SIAM J. Numer. Anal.* 35 (1) (1998) 230–254.
- [11] Z. Li, M.-C. Lai, The immersed interface method for the Navier–Stokes equations with singular forces, *J. Comput. Phys.* 171 (2001) 822–842.
- [12] Z. Li, K. Ito, Maximum principle preserving schemes for interface problems with discontinuous coefficients, *SIAM J. Sci. Comput.* 23 (1) (2001) 330–361.
- [13] X.-D. Liu, R.P. Fedkiw, M. Kang, A boundary condition capturing method for Poisson’s equation on irregular domains, *J. Comput. Phys.* 160 (2000) 151–178.
- [14] S. Osher, J.A. Sethian, Fronts propagating with curvature-dependent speed: algorithms based on Hamilton–Jacobi formulations, *J. Comput. Phys.* 79 (1988) 12–49.
- [15] C.S. Peskin, Numerical analysis of blood flow in heart, *J. Comput. Phys.* 25 (1977) 220–252.
- [16] M. Sussman, P. Smereka, S. Osher, A level set approach for computing solutions to incompressible two-phase flow, *J. Comput. Phys.* 114 (1994) 146–159.
- [17] S.O. Unverdi, G. Tryggvason, A front-tracking method for viscous, incompressible multi-fluid flows, *J. Comput. Phys.* 100 (1992) 25–37.
- [18] A. Wiegmann, K.P. Bube, The explicit-jump immersed interface method: finite difference methods for PDEs with piecewise smooth solutions, *SIAM J. Numer. Anal.* 37 (3) (2000) 827–862.

Paper II

Stratified smooth two-phase flow using the
immersed interface method

P. A. Berthelsen & T. Ytrehus

Submitted to
Computers & Fluids

Paper III

Numerical modelling of stratified turbulent two-
and three-phase pipe flow with arbitrary shaped
interfaces

P. A. Berthelsen & T. Ytrehus

Presented at
The 5th International Conference on Multiphase Flow
Yokohama, Japan, May 30–June 4, 2004

Numerical Modelling of Stratified Turbulent Two- and Three-Phase Pipe Flow with Arbitrary Shaped Interfaces

Petter Andreas Berthelsen¹, Tor Ytrehus²

1: The Fluids Engineering Group, Department of Energy and Process Engineering, Norwegian University of Science and Technology, Trondheim, Norway, petter.a.berthelsen@ntnu.no

2: The Fluids Engineering Group, Department of Energy and Process Engineering, Norwegian University of Science and Technology, Trondheim, Norway, tor.ytrehus@ntnu.no

Abstract A numerical method for the prediction of fully developed, turbulent, stratified smooth two- and three-phase flows in horizontal and inclined pipes is presented. The method solves the two-dimensional steady-state axial momentum equation together with a two-layer $k - \varepsilon$ turbulence model to account for the effect of turbulence. The governing equations are discretized using a finite difference scheme on a composite, overlapping grid with local grid refinement near interfaces and near solid boundaries. The immersed interface method is used to enforce proper boundary conditions at the interface. This sharp interface technique makes the representation of the interfaces independent of the grid structure, and allows for using arbitrary shaped interfaces. The interfaces are represented by level set functions. Predictions of liquid holdup, pressure gradient and friction factors in two-phase flow show acceptable agreement with experimental data. A parametric study for horizontal three-phase flow is presented for calculations of liquid holdup, pressure gradient, friction factors and momentum corrections factors.

1 Introduction

Predictions of correct pressure drop and void fractions in two- and three-phase pipe flows have practical importance, in particular, in the oil and gas industry. The production and transportation of hydrocarbons through long pipelines usually implies unstable flow configurations. These instabilities may cause transitions from stratified flow to other flow regimes, such as slug flow or annular flow. Slug flow is characterized by its large fluctuations in pressure and flow rate. In order to prevent this oscillating flow structure, it is necessary to choke the flow, and therefore the production rate will be dramatically reduced. Consequently, reliable models are of great importance for predicting the correct pressure drop and holdup to obtain optimal and efficient production and transportation of oil and gas.

Most common models for multiphase pipe flows are based on greatly simplified representations of the flow structure. Many mechanistic models are applied with reasonable assumptions. The mechanistic approach treats all phases as one-dimensional bulk flows, neglecting the detailed velocity profiles over the cross sections. Empirical correlations based on the average velocity are used to calculate the shear stresses. For stratified two-phase flow, the most notable model is the one proposed by Taitel and Dukler (1976) which uses a modified Blasius formula to determine the wall and interfacial friction factors. Several attempts have been made to improve the friction factors, particularly for predicting the interfacial shear stress. A large number of two-phase pipe flow experiments have been carried out to incorporate the effect of interfacial waves (e.g. Andritsos and Hanratty 1987, Spedding and Hand 1997, Biberg 1999). These correlations are often restricted to a certain range of flow parameters, and does not always reflect the correct physics of the flow.

Less attention has been devoted to the stratified three-phase pipe flow modelling. Early studies combined water and oil into one liquid phase, which inaccurately simplified the problem into a two-phase flow problem. Following the mechanistic approach, the one-dimensional methodology has been extended to three-phase flow by means of an extra equation to model the third phase (e.g. Taitel et

al. 1995). This approach still requires empirical correlations to determine the friction factors. Khor et al. (1997) studied the performance of several different three-phase models and concluded that considerable errors are present, even when the best combination of friction factors are used.

A few attempts have been made to extend the flow analysis to two-dimensional numerical models. In the early work of Shoham and Taitel (1984), the steady-state axial momentum equation was discretized and solved in the liquid region in a bipolar coordinate system using a mixing-length turbulence model. The gas region was treated as a bulk flow and an empirical correlation was used to couple the two phases through the interfacial shear stress. Issa (1988) included the gas region in the analysis and used a two-equation turbulence model with wall functions to calculate stratified smooth two-phase pipe flow. More recently, Newton and Behnia (2000) extended the approach of Issa (1988) by applying a low Reynolds number $k - \varepsilon$ turbulence model to the problem. This model resolved the flow in the vicinity of the wall and the interface, which permitted the direct calculation of the wall and interfacial shear stress distribution without using empirical wall functions. Later, Newton and Behnia (2001) introduced a simple empirical interfacial shear stress to modify their two-dimensional model for wavy stratified flow. These two-dimensional models brought more details into the analysis, although they confined only to two-phase flow.

Recently, Berthelsen and Ytrehus (2004) developed a new two-dimensional numerical technique to calculate stratified smooth two-phase pipe flow, using the immersed interface method (Berthelsen 2004). In this approach, the representation of the interface is made independent of the grid structure, and allows for using arbitrary shaped interfaces. In the present study, the technique is extended to numerical modelling of stratified smooth three-phase flow. A two-layer turbulence model is used to calculate the time-averaged velocity profile in all phases. The interfaces are represented by level set functions.

The main purpose of this work is to investigate the applicability of the immersed interface method for turbulent, stratified two- and three-phase flow. The model is yet confined to the assumption of having smooth interfaces between the different fluid layers. However, it is believed that the effect of interfacial waves is more related to proper modelling rather than the actual numerical method being used. To this end, similar analysis on three-phase flow has not been previously done.

2 Modelling

2.1 Level set representation

In the level set method, a smooth auxiliary function ϕ is introduced as

$$\phi(x, y) = \pm d_\phi,$$

where d_ϕ is the shortest distance to the interface between two fluids. The sign of ϕ indicates what side of the interface (x, y) is located. From the definition above, the interface Γ_ϕ is given by the zero level set of the function ϕ , i.e.

$$\Gamma_\phi = \{(x, y) \in \mathbb{R}^2 \mid \phi(x, y) = 0\}.$$

With the level set formulation it is not necessary to know the exact location of the interfaces. It can be found by locating Γ_ϕ for which ϕ vanishes. This approach allows for a more complex topology, and additional interfaces can be added by merely introducing additional level set functions, e.g. for a second interface (a third phase), a level set function ψ can be defined as

$$\psi(x, y) = \pm d_\psi,$$

where d_ψ is the shortest distance to the second interface Γ_ψ . Similarly to Γ_ϕ , the second interface is now defined as

$$\Gamma_\psi = \{(x, y) \in \mathbb{R}^2 \mid \psi(x, y) = 0\}.$$

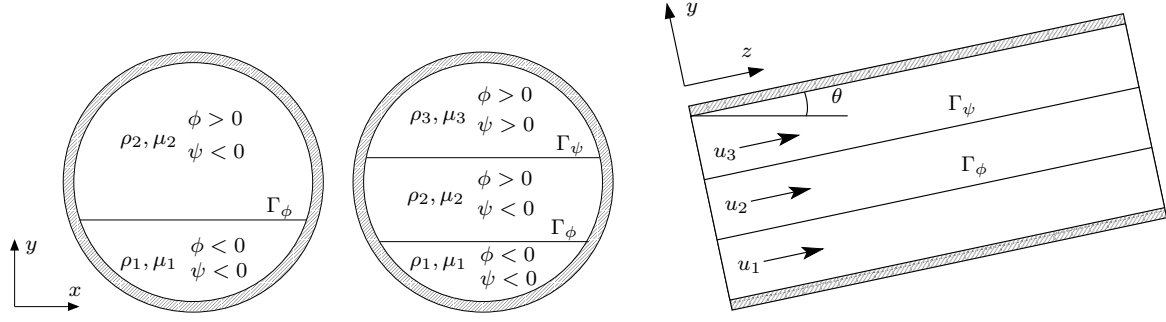


Figure 1: Illustration of stratified smooth two- and three-phase pipe flow with inclination angle θ .

2.2 Governing equations

Consider a fully developed, incompressible and unidirectional pipe flow of stratified fluids. The time averaged, steady state axial momentum equation for each phase can be written as

$$\frac{\partial}{\partial x} \left[(\mu + \mu_t) \frac{\partial u}{\partial x} \right] + \frac{\partial}{\partial y} \left[(\mu + \mu_t) \frac{\partial u}{\partial y} \right] - \frac{dp}{dz} - \rho g \sin \theta = 0, \quad (1)$$

where u is the axial velocity, ρ is the density, g is the gravitational acceleration, θ is the pipe inclination angle and dp/dz is the pressure gradient in the axial direction. The molecular and turbulent viscosities are denoted by μ and μ_t , respectively. Adopting the level set formulation above, assuming the interfaces to be infinitely thin, the fluid properties can be defined directly from the level set functions as

$$\rho(\phi, \psi) = \begin{cases} \rho_1 & \text{if } \phi < 0, \psi < 0, \\ \rho_2 & \text{if } \phi \geq 0, \psi < 0, \\ \rho_3 & \text{if } \phi > 0, \psi \geq 0, \end{cases} \quad \text{and} \quad \mu(\phi, \psi) = \begin{cases} \mu_1 & \text{if } \phi < 0, \psi < 0, \\ \mu_2 & \text{if } \phi \geq 0, \psi < 0, \\ \mu_3 & \text{if } \phi > 0, \psi \geq 0, \end{cases}$$

for two- and three-phase flow (see Figure 1). For simplicity, the interfaces are assumed to be smooth and no interfacial disturbances occur.

The two-layer turbulence model of Chen and Patel (1988) is used to mimic turbulent stresses. In this turbulence model, the standard $k - \varepsilon$ model is used only in the fully turbulent region, while the viscous affected region is resolved with a one-equation turbulence model. For the latter case, a simpler length scale model is used to replace the equation of dissipation. The equation of dissipation is also known as the weakest modelled equation of the $k - \varepsilon$ model, in particular in the viscous sub layer. Generally, the eddy viscosity relation can be written as

$$\mu_t = C_\mu \rho \sqrt{k} l_\mu,$$

where C_μ is a dimensionless constant (see Table 1), k is the turbulent kinetic energy and l_μ is the turbulence length scale.

The turbulence length scale is in the fully turbulent region determined from the dissipation rate ε as

$$l_\mu = \frac{k^{3/2}}{\varepsilon},$$

and in the viscous affected regions the length scale is adopted from the model by Wolfshtein (1969),

$$l_\mu = \frac{\kappa d}{C_\mu^{3/4}} \left[1 - \exp \left(-\frac{R_y}{A_\mu} \right) \right],$$

where R_y is defined as $\rho\sqrt{k}d/\mu$, κ is the von Karman constant and A_μ is a model coefficient. The distance d is defined as the shortest distance to a surface, either the pipe wall or an interface. This definition of d is based on the assumption that the presence of an interface acts to dampen turbulence.

The turbulent kinetic energy is modelled by the following governing equation:

$$\frac{\partial}{\partial x} \left[\left(\mu + \frac{\mu_t}{\sigma_k} \right) \frac{\partial k}{\partial x} \right] + \frac{\partial}{\partial y} \left[\left(\mu + \frac{\mu_t}{\sigma_k} \right) \frac{\partial k}{\partial y} \right] + \mu_t \left[\left(\frac{\partial u}{\partial x} \right)^2 + \left(\frac{\partial u}{\partial y} \right)^2 \right] - \rho\varepsilon = 0 \quad (2)$$

in both the fully turbulent and viscous affected regions. In the fully turbulent region, the rate of dissipation is determined from the following governing equation:

$$\frac{\partial}{\partial x} \left[\left(\mu + \frac{\mu_t}{\sigma_\varepsilon} \right) \frac{\partial \varepsilon}{\partial x} \right] + \frac{\partial}{\partial y} \left[\left(\mu + \frac{\mu_t}{\sigma_\varepsilon} \right) \frac{\partial \varepsilon}{\partial y} \right] + C_{1\varepsilon} \frac{\varepsilon}{k} \mu_t \left[\left(\frac{\partial u}{\partial x} \right)^2 + \left(\frac{\partial u}{\partial y} \right)^2 \right] - C_{2\varepsilon} \rho \frac{\varepsilon^2}{k} = 0, \quad (3)$$

while the dissipation rate is described as

$$\varepsilon = \frac{k^{3/2}}{l_\varepsilon} \quad (4)$$

in the viscous affected region. The length scale l_ε is used as proposed by Wolfshtein (1969),

$$l_\varepsilon = \frac{\kappa d}{C_\mu^{3/4}} \left[1 - \exp \left(-\frac{R_y}{A_\varepsilon} \right) \right].$$

The values used for the turbulent coefficients A_μ , A_ε , C_μ , $C_{1\varepsilon}$, $C_{2\varepsilon}$, σ_k , σ_ε and κ are summarized in Table 1.

Table 1: Values for the turbulence model coefficients.

C_μ	A_μ	A_ε	κ	$C_{1\varepsilon}$	$C_{2\varepsilon}$	σ_k	σ_ε
0.09	70.0	5.08	0.418	1.44	1.92	1.0	1.3

The two models should be matched in a region where viscous effects become negligible. Chen and Patel (1988) found that the results were insensitive to the matching criterion as long as R_y was greater than 200, and they suggested $R_y = 250$ as a suitable matching criterion. The same criterion has been adopted here to match the two models.

Another advantage in using the level set approach is that the distance to the nearest interface is given explicitly as the minimum of the absolute values of the level set functions. This becomes useful when calculating d in the expressions above.

The $k - \varepsilon$ model assumes isotropic turbulence and is incapable of producing secondary motion. Secondary flows are known to appear in non-circular ducts (Demuren and Rodi 1984) and can also be observed in stratified gas-liquid pipe flow (e.g. Strand 1993). However, modelling this phenomenon would require calculations of all the Reynolds stresses, involving more sophisticated turbulence models. Meknassi et al. (2000) used an algebraic stress model to simulate the anisotropy of the turbulence in gas-liquid pipe flow using a body-fitted bipolar coordinate system. A similar approach can be adopted with the present model, but is neglected in this study due to the increase in complexity and computational cost.

2.3 Boundary conditions

To exploit the symmetry of the flow and increase computational efficiency the following boundary conditions are used on the vertical axis:

$$\frac{\partial u}{\partial n} = 0, \quad \frac{\partial k}{\partial n} = 0 \quad \text{and} \quad \frac{\partial \varepsilon}{\partial n} = 0,$$

where $\partial/\partial n$ denotes the derivatives normal to the boundary.

At the solid pipe wall, the velocity, turbulent kinetic energy and eddy viscosity vanish due to the natural no-slip condition, i.e.

$$u_w = 0, \quad k_w = 0 \quad \text{and} \quad \mu_{t,w} = 0,$$

where the subscript w denotes the boundary value at the wall. The dissipation rate is expressed by Eq. (4) in the near-wall region and does not require any boundary value to make the problem well-defined.

Since the interface between two phases is assumed to be smooth, it can be treated as a moving wall. This assumption suggests that the interface reduces the length scale of turbulence, decreasing the turbulent viscosity in a similar manner as the presence of a solid surface. Therefore, the following boundary conditions are imposed at the interface:

$$k_{i,p} = k_{i,q} = 0 \quad \text{and} \quad \mu_{t,i,p} = \mu_{t,i,q} = 0,$$

between phase p and q. The subscript i denotes the interfacial boundary value. The dissipation rate is again given by Eq. (4). Further, continuity in velocity and shear stress at the interface yields

$$u_{i,p} = u_{i,q} \quad \text{and} \quad \mu_p \frac{\partial u_{i,p}}{\partial n} = \mu_q \frac{\partial u_{i,q}}{\partial n}.$$

2.4 Closing relations

The set of equations are closed by the equations for the phase flow rates. The relations are given as

$$\int_{A_q} u(x, y) dA = Q_q \quad \text{for} \quad q = (1, 2, 3),$$

where A_q is the phase cross-sectional area, Q_q is the phase flow rate and the subscript q denotes the phase. This way, the phase area, pressure gradient dp/dz , velocity field u and the turbulent quantities k and ε can be determined for given phase flow rates. The phase flow rate is commonly represented by the phase superficial velocity defined as $U_{qs} = Q_q/A$.

2.5 Numerical method

The governing equations (1)–(3) are discretized using a finite difference scheme on a composite, overlapping grid (Chesshire and Henshaw 1990) with adaptive grid refinements (Martin and Cartwright 1996) near the interfaces and near solid boundaries. The overlapping grid (see Figure 2) consists of two structured curvilinear base component grids describing the cross section of a pipe. Each component grid has its own mapping function,

$$(x, y) = \Phi(\xi, \eta),$$

transforming the computational space (ξ, η) into the physical space (x, y) . The component grids are coupled through higher order interpolations on the interior boundary cells. The interpolations are done in computational space allowing for simpler interpolation techniques on rectangular grids to be used (see Figure 3).

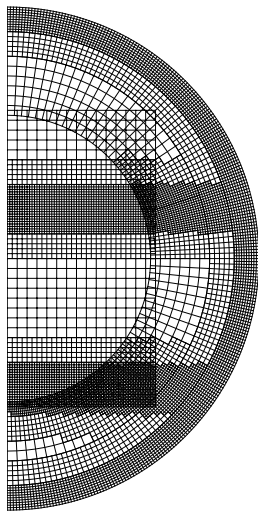


Figure 2: The composite overlapping grid with local grid refinements near the pipe wall and near the interfaces in a three-phase flow.

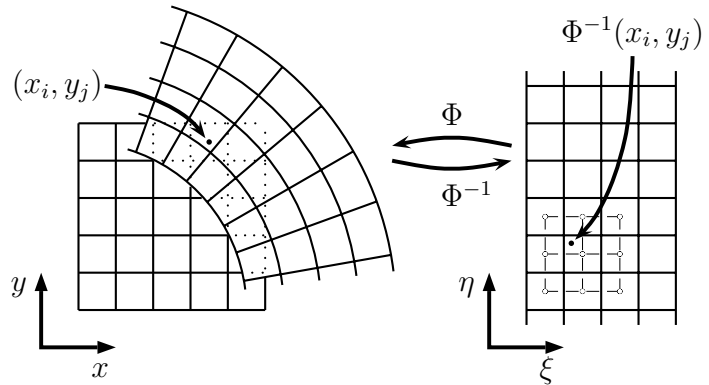


Figure 3: The interpolation points in computational space for coupling between overlapping composite grids.

A local grid refinement technique is adopted to obtain adequate resolution without increasing the computational expenses tremendously. This is done by adding block-structured subgrids to regions where the grid is to be refined (Berger and Rigoutsos 1991). These refined subgrids use information from coarser grid levels by updating the boundary cells using higher order interpolation. Information from refined levels is passed to the coarser level using the *refined flux* at the coarse/fine interface (see Martin and Cartwright 1996). The discrete equations are solved iteratively and separately on each subgrid. Interior boundary cells are updated as information is passed between the grids after every iteration step.

The boundary conditions at the interface are treated properly by applying a sharp interface technique. The decomposed immersed interface method as presented by Berthelsen (2004) is used. This method adds componentwise correction terms to the finite difference stencil to make the discretization well-defined across the interface. With this approach, the interface is decoupled from the grid, which allows for using more complex interface configurations than with body-fitted grid.

3 Numerical Results and Discussion

3.1 Gas-liquid flow

The present model is compared with the experimental results of Espedal (1998) and a one-dimensional mechanistic model using the friction factors proposed by Taitel and Dukler (1976). Espedal performed experiments on stratified air-water flow in a 0.06 m diameter pipe at small inclination angles. A large number of experiments were conducted for different combinations of air and water flow rates where the liquid holdup, H_L , and the pressure gradient were measured.

Wave probes were used to identify the interfacial structure in the experiments and the following characteristics were defined: smooth flow, small amplitude waves, small amplitude 2D waves, large amplitude 2D waves and large amplitude 3D waves. To be consistent with the assumptions made in the

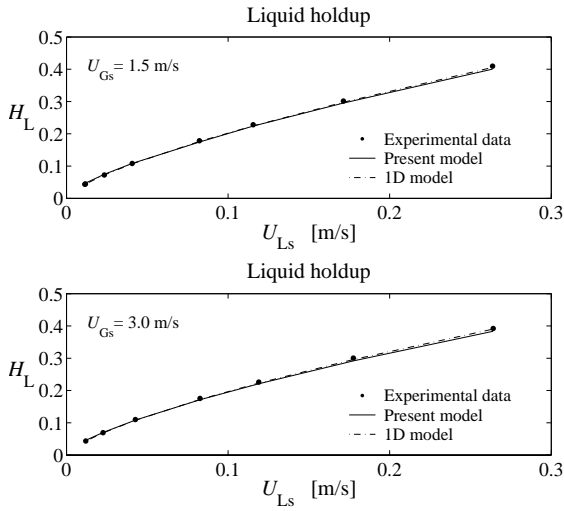


Figure 4: Comparison of predicted and measured liquid holdup.

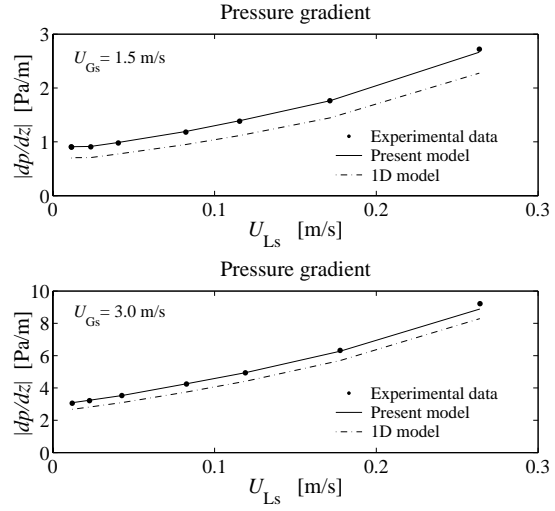


Figure 5: Comparison of predicted and measured pressure gradient.

present approach, only data from the experiments where no waves occurred or only small amplitude waves (less than <0.5 mm) were observed are used for comparisons. The presence of small amplitude waves shows only small effect on the results presented here.

In Figure 4 and 5, the predictions of liquid holdup and the pressure gradient are compared with the measurements for a downward inclined pipe with inclination angle $\theta = -0.5^\circ$. The gas superficial velocity, U_{Gs} , is held constant at 1.5 m/s and 3 m/s, while the liquid superficial velocity, U_{Ls} , varies from 0.01 m/s to 0.27 m/s. The pressure gradient and the liquid holdup are plotted against the liquid superficial velocity.

The results show good agreement for predicting both liquid holdup and pressure gradient. The predicted liquid holdup is almost identical for the present model and the one-dimensional model. The present approach shows a small tendency of under-prediction as the holdup increases, though the difference is negligible. In predicting the pressure gradient, the discrepancy between the two models becomes more significant. The present approach agrees quite well with the measurements, but deviates slightly at higher liquid flow rates. The simpler one-dimensional model estimates too low values for the pressure gradient.

Espedal measured the wall shear stress and reported the average wall shear stress in the gas phase, τ_G . The average liquid wall shear stress, τ_L , and interfacial shear stress, τ_i , are calculated from a momentum balance using the measured liquid holdup, pressure gradient and gas wall shear stress. Figure 6 compares a selection of predicted friction factors with values obtained from the experiments. The friction factors f_G , f_L and f_i are defined as

$$f_G = \frac{\tau_G}{\frac{1}{2}\rho_G \bar{u}_G^2}, \quad f_L = \frac{\tau_L}{\frac{1}{2}\rho_L \bar{u}_L^2} \quad \text{and} \quad f_i = \frac{\tau_i}{\frac{1}{2}\rho_G (\bar{u}_G - \bar{u}_L)^2},$$

where \bar{u}_G and \bar{u}_L are the bulk velocities in the gas phase and liquid phase, respectively.

The modified Blasius formula, $f = 0.046\text{Re}^{-0.2}$, under-estimates the friction factors at the wall and interface, which also explains the lower predicted pressure gradient in Figure 5. The present model predicts the gas wall and interfacial friction factors quite well compared to the simpler one-dimensional approach. However, in the liquid phase the model under-predicts the wall friction factor, and the discrepancy seems to increase as the liquid Reynolds number increases. The assumption $f_i \cong f_G$ for stratified smooth flow as a first approximation is supported by the calculated results and experimental data given in this example. Though, it is noticed that the interfacial value is actually slightly higher.

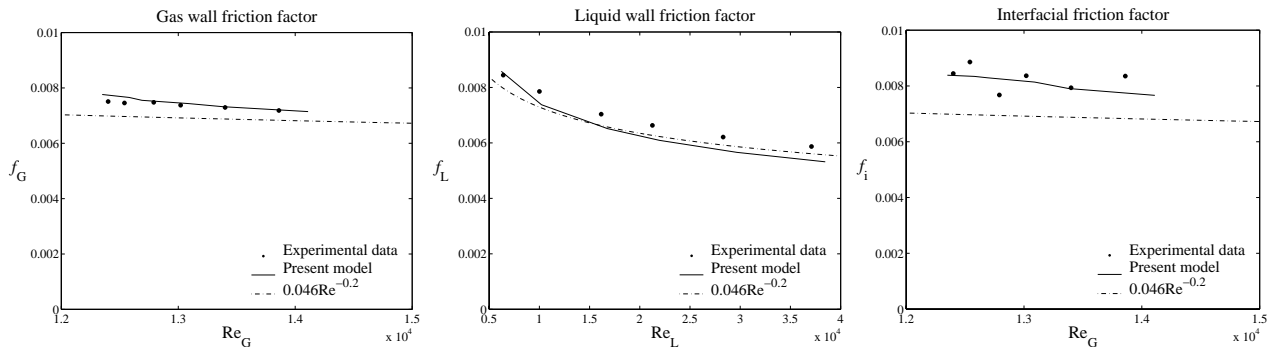


Figure 6: Calculated average friction factors as function of phase Reynolds number using the present model compared with experimental results and the Blasius type equation used by Taitel and Dukler (1976).

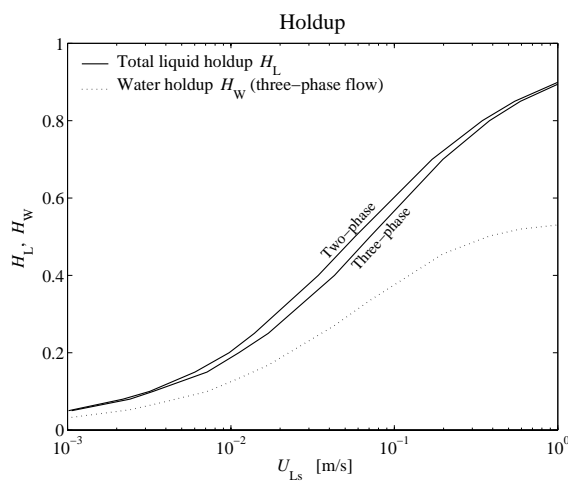


Figure 7: Calculated liquid holdup for stratified smooth two- and three-phase flow where the oil-layer is given same properties as water.

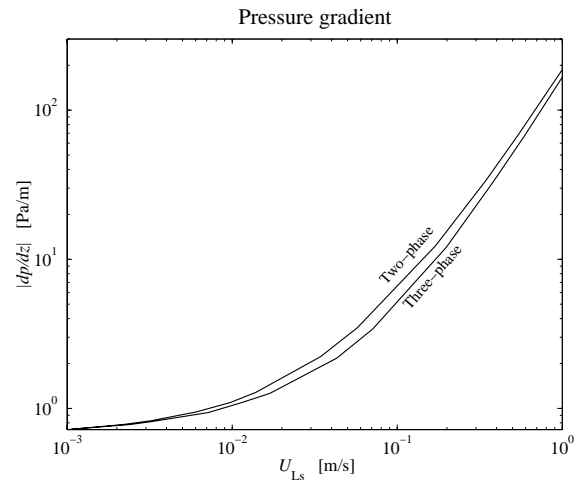


Figure 8: Calculated pressure gradient for stratified smooth two- and three-phase flow where the oil-layer is given same properties as water.

3.2 Gas-liquid-liquid flow

The lack of measured data available on stratified three-phase flow with smooth interfaces makes comparison with experimental results difficult. Therefore, this subsection will only provide some typical examples of gas-liquid-liquid flow in a horizontal pipe to demonstrate the capability of using the present method for calculating stratified smooth three-phase flow in pipes.

In the examples below, the pipe diameter is 0.05 m, and the gas-liquid-liquid system consist of air, oil and water. The subscript A, O and W are used to denote air, oil and water, respectively. The density of air is set to $\rho_A = 1.2 \text{ kg/m}^3$ and of water $\rho_W = 1000 \text{ kg/m}^3$. The air viscosity is rounded to $\mu_A = 2.0 \times 10^{-5} \text{ Pa}\cdot\text{s}$ and for water it is $\mu_W = 0.001 \text{ Pa}\cdot\text{s}$. If not else stated the oil density is $\rho_O = 800 \text{ kg/m}^3$ and the oil-to-water viscosity ratio, $\tilde{\mu} = \mu_O/\mu_W$, varies between 2 and 10.

The first example demonstrates the effect of introducing a smooth interface in the liquid phase. A two-phase air-water system is compared with a three-phase system where the oil layer is given the same material properties as water. The total liquid holdup, $H_L = H_O + H_W$, for both cases are compared in Figure 7 and the pressure gradients are compared in Figure 8. The results are plotted as functions of total liquid superficial velocity, $U_{Ls} = U_{Os} + U_{Ws}$. The gas superficial velocity, $U_{Gs} = U_{As}$, is held constant at 1 m/s and the volumetric water fraction, $WF = U_{Ws}/U_{Ls}$, is equal to 0.5.

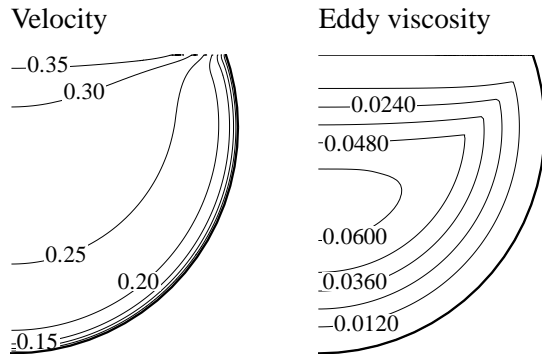


Figure 9: Contour plots of the velocity field [m/s] and eddy viscosity [Pa·s] in the liquid phase in a gas-liquid two-phase system. Liquid holdup is 0.7.

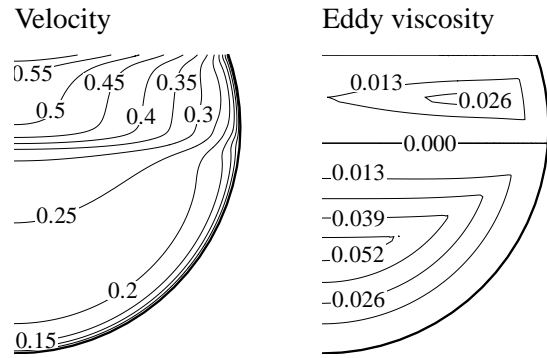


Figure 10: Contour plots of the velocity field [m/s] and eddy viscosity [Pa·s] in the liquid phase in a gas-liquid-liquid three-phase system where both liquid layers have same material properties. Total liquid holdup is 0.7.

The curves for total liquid holdup and the pressure gradient coincide for low liquid flow rates for both cases. In this region, the liquid phases are laminar and the smooth liquid-liquid interface should have no effect on the flow. As the liquid flow rate increases and turbulent stresses becomes noticeable, the curves starts to deviate from each other. The total liquid holdup is lower for the three-phase flow case. This is because the turbulent stresses are damped towards the smooth liquid-liquid interface yielding a higher flow rate for equal pressure gradient. For high liquid rates, where turbulent stresses dominate, the laminar zone near the interface becomes thinner and the two cases seem to approach each other. The water holdup curve in the three-phase flow follows the same trend as the total liquid holdup curve, but for low liquid rates it is relatively high. This was also observed by Taitel et al. (1995) for $\tilde{\mu} = 1$. They explained this by the faster moving gas dragging the oil layer to higher velocities than the water layer, requiring lower oil holdup to maintain the same flow rate in the oil layer as in the water layer.

Figure 9 and 10 show the velocity distribution and the turbulent eddy viscosity distribution in the liquid layers when total liquid holdup is 0.7. The contour plots clearly demonstrate how the turbulent viscosity is damped towards the liquid-liquid interface causing a laminar zone near the interface in the three-phase flow.

In Figure 11 and 12, the gas superficial velocity is held constant at $U_{Gs} = 1$ m/s and the oil density is 800 kg/m^3 , while the oil-water viscosity ratio, $\tilde{\mu}$, varies between 2 and 10. The volumetric water fraction, WF , is still equal to 0.5. The total liquid level increases for increasing oil viscosity, particularly at low liquid flow rates. This is because the more viscous oil moves slower, which leads to an increase in the oil holdup and the total liquid holdup to maintain the liquid flow rate. This effect is greater at low liquid rates, since the effect of higher viscosity is larger when turbulent stresses are small. Also, at lower liquid rates, the water holdup will increase as the oil viscosity increases. This is expected since the dragging effect from the oil layer decreases when the oil layer moves slower, thus making the water level to increase in order to maintain the water-to-oil flow rate ratio constant.

For higher liquid flow rates, turbulent stresses are dominating the oil layer, and the effect of increased viscosity becomes smaller as the curves approach each other. However, the water holdup is reduced as a result of increased oil viscosity. At these rates, the water layer is mostly driven by the pressure gradient, and not the interfacial shear stress caused by the faster moving oil layer. Since increased oil viscosity increases the pressure gradient, the water flow rate will also increase, reducing the necessary water level to maintain the water-to-oil flow rate ratio at constant liquid rates.

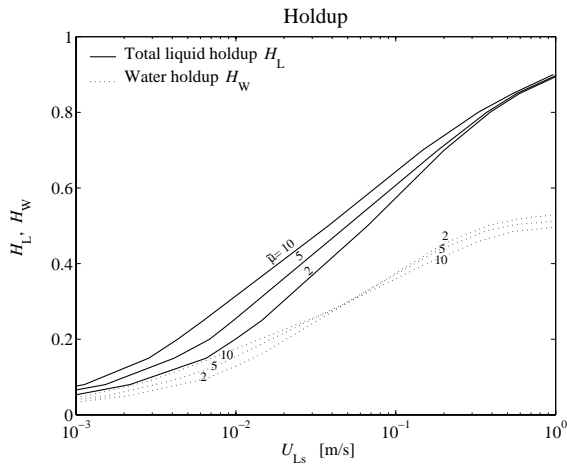


Figure 11: Calculated liquid holdup for stratified smooth three-phase flow where the oil-to-water viscosity ratio $\tilde{\mu}$ is 2, 5 and 10.

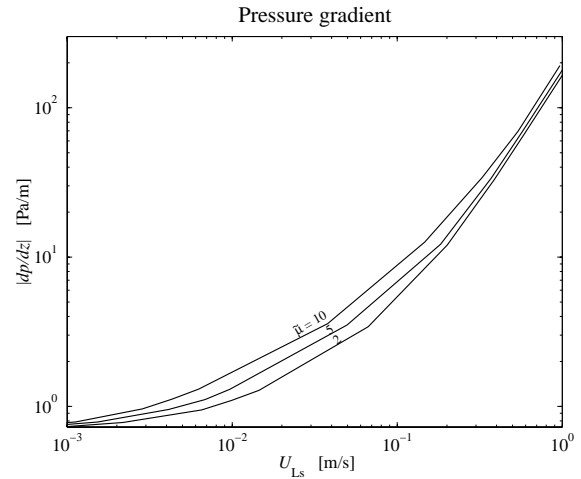


Figure 12: Calculated pressure gradient for stratified smooth three-phase flow where the oil-to-water viscosity ratio $\tilde{\mu}$ is 2, 5 and 10.

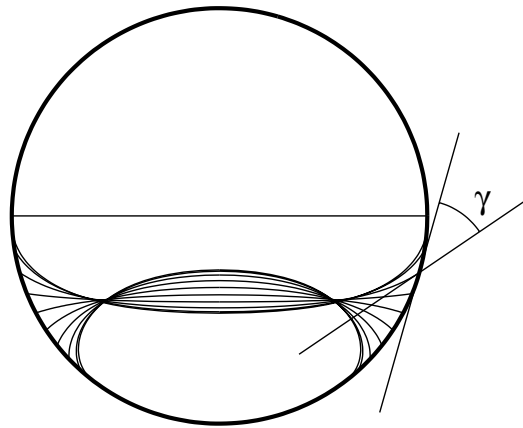


Figure 13: A selection of prescribed shapes for the liquid-liquid interface, where $H_W = H_O = 0.25$. For a convex shaped interface the pipe wall is water wetted, while for a concave shaped interface the pipe wall is oil wetted.

In the next example, the effect of a curved liquid-liquid interface is studied by applying a set of prescribed interface shapes (see Figure 13), while the liquid holdups, H_W and H_O , are held constant for a given pressure gradient. Curved liquid-liquid interfaces were observed in the experiments of Roberts (1996). The curvature is here characterized by a contact angle γ , where $\gamma \rightarrow 0^\circ$ denotes a convex shape and $\gamma \rightarrow 180^\circ$ denotes a concave shape, while a plane interface is somewhere in between.

The calculated liquid superficial velocities, U_{Ls} , U_{Ws} and U_{Os} , normalised by the total liquid superficial velocity obtained with a plane interface, U_{Ls}^0 , are shown in Figure 14 as functions of γ . Figure 15 shows the calculated volumetric water fraction, WF , normalised by the water fraction obtained with a plane interface, WF^0 , as a function of γ . The water holdup and oil holdup are both equal to 0.25, the oil-to-water viscosity ratio, $\tilde{\mu}$, is 4 and the pressure gradient is held constant at 15 Pa/m.

For convex shaped interfaces, the wetted wall perimeter in the oil phase is less than for a concave shaped interface. That results in less wall friction and higher oil liquid rates for given pressure gradient. The total liquid flow rates decrease monotonically as the interface goes from a convex shape

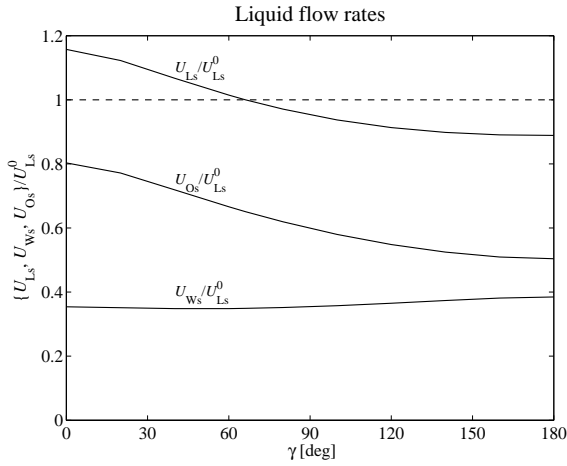


Figure 14: Normalised liquid flow rates for curved interfaces where $U_{Ls}^0 = 0.1639$ m/s.

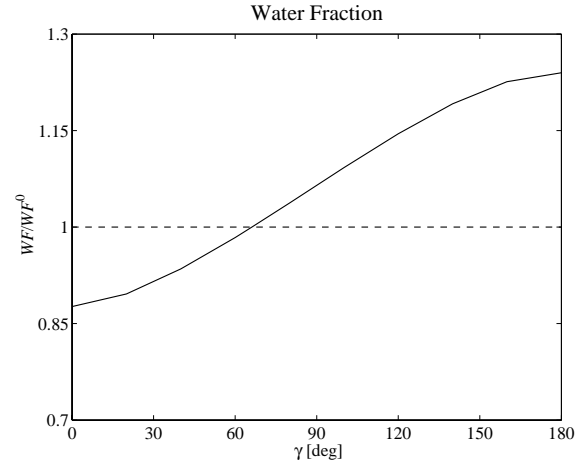


Figure 15: Normalised water fractions for curved interfaces where $WF^0 = 0.349$.

towards a concave shape. Most of this reduction is done by the oil phase, while the water flow rate remains nearly constant. Only a small reduction in the water flow rate can be observed when the interface approach the plane interface, $\gamma \cong 66^\circ$, thereafter a small increase in water flow rate as the shape becomes more concave. The minimum seems to be located slightly to the left for the plane case. The larger relative decrease in the oil flow rate compared to the water flow rate leads to an increase in the volumetric water fraction as the interface becomes more concave.

The wall and interfacial shear stresses are averaged and average friction factors are calculated from

$$f_A = \frac{\tau_A}{\frac{1}{2}\rho_A \bar{u}_A^2}, \quad f_O = \frac{\tau_O}{\frac{1}{2}\rho_O \bar{u}_O^2}, \quad f_W = \frac{\tau_W}{\frac{1}{2}\rho_W \bar{u}_W^2}, \quad f_i = \frac{\tau_i}{\frac{1}{2}\rho_A (\bar{u}_A - \bar{u}_O)^2}, \quad \text{and} \quad f_j = \frac{\tau_j}{\frac{1}{2}\rho_O (\bar{u}_O - \bar{u}_W)^2},$$

where τ_i and τ_j are the interfacial shear stresses at the air-oil interface and oil-water interface, respectively, τ_q ($q = A, O, W$) is the wall shear stress and \bar{u}_q is the bulk velocity in phase q . A selection of calculated friction factors are compared with the modified Blasius formulation used by Taitel et al. (1995) for wall friction factors, $f = CRe^{-n}$, in Figure 16. The interface is plane for all friction factors presented here. The phase Reynolds numbers are defined as suggested by Khor et al. (1997),

$$Re_A = \frac{\rho_A \bar{u}_A A_A}{\mu_A (S_A + S_i)}, \quad Re_O = \frac{\rho_O \bar{u}_O A_O}{\mu_O (S_O + S_j)} \quad \text{and} \quad Re_W = \frac{\rho_W \bar{u}_W A_W}{\mu_W S_W},$$

where A_q and S_q ($q = A, O, W$) are the phase cross sectional area and the wetted wall perimeters for phase q , respectively. The interfacial perimeters are denoted S_i and S_j for the air-oil interface and the oil-water interface, respectively.

The water layer wall friction factor is nearly identical to the formulation used by Taitel et al. (1995). The gas wall friction factor obtained with the present method gives higher values than the Blasius type equation while the calculated wall friction factors in the oil layer is considerable lower than the modified Blasius equation. For smooth interfaces, as considered here, the air-oil interfacial friction factor is very close to the gas wall friction factor. A similar relation can be observed for the oil-water interface and the oil layer wall friction factor.

The momentum correction factors, defined as

$$MCF_q = \frac{\int_{A_q} u(x, y)^2 dA}{\bar{u}_q^2 A_q} \quad \text{for} \quad q = (A, O, W),$$

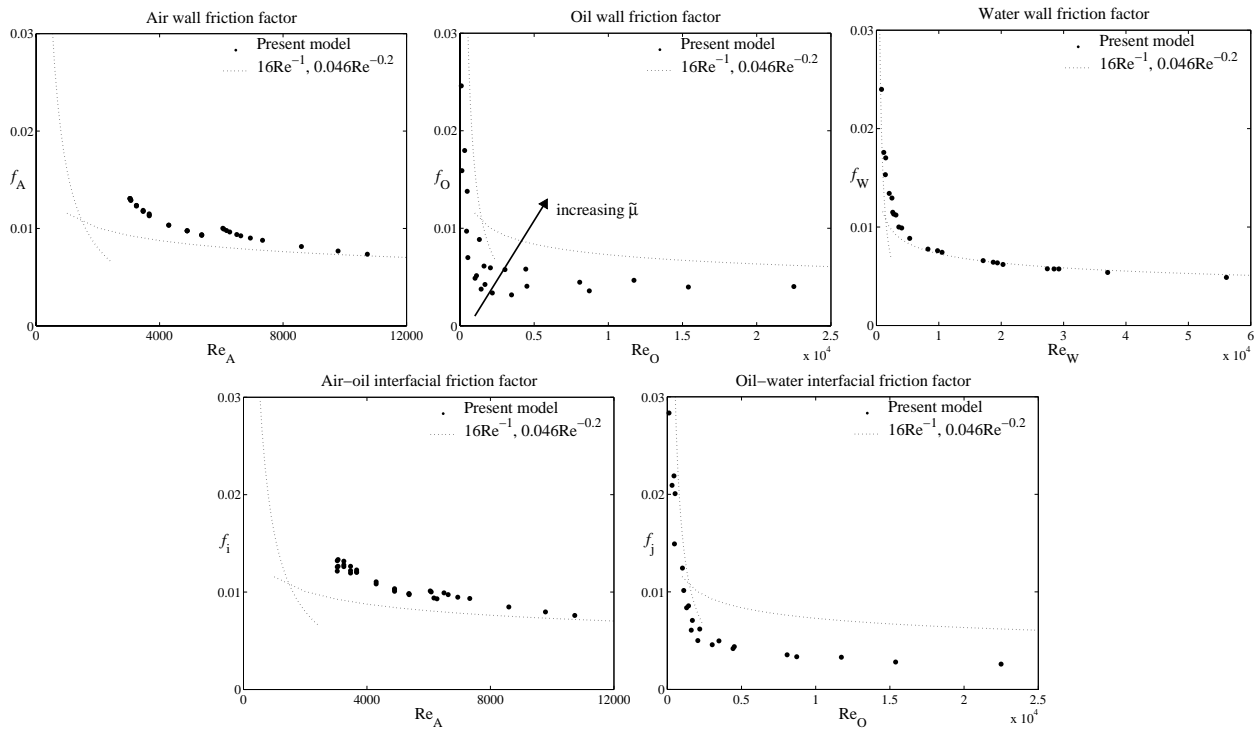


Figure 16: Calculated averaged friction factors as function of phase Reynolds number for stratified smooth three-phase flow in horizontal pipes using the present model compared with the Blasius type equation used in Taitel et al. (1995).

are plotted in Figure 17. A selection of data for $U_{Gs} = 1$ m/s and 2 m/s is given. Newton and Behnia (2000, 2001) reported that the momentum correction factors for two-phase flow were higher than those for turbulent single-phase pipe flow and the data approached a constant value of approximately 1.06 in the gas phase as the Reynolds number increased. In the present calculation, the momentum correction factors decreases as the Reynolds number increases and it seems like they are approaching a constant value. However, it should be noticed that in the gas phase the momentum correction factor makes a jump for increased gas superficial velocity at about $Re_A = 6000$.

In the higher Reynolds number region it is likely that a transition from the stratified flow regime would occur making these results doubtful. But, for the time being, such calculations as presented here still give new and valuable information about stratified smooth three-phase flow.

4 Summary

A numerical model of turbulent, stratified smooth two- and three-phase pipe flow has been presented. Turbulent stresses were modelled using a two-layer $k - \varepsilon$ turbulence model. The interface has been decoupled from the numerical grid utilising the immersed interface method. This technique allows for using multiple and arbitrary shaped interfaces.

The method has been tested and compared with experimental data for two-phase flow in a downward inclined pipe with a small inclination angle. Predictions of liquid holdup and pressure gradient showed acceptable agreement with the measured data. Calculations of gas wall and interfacial friction factors matched the results from the experiments well. In the liquid phase, a small under-estimation of the wall friction factor was observed. A parametric study of horizontal three-phase pipe flow was done to demonstrate the capability of the method.

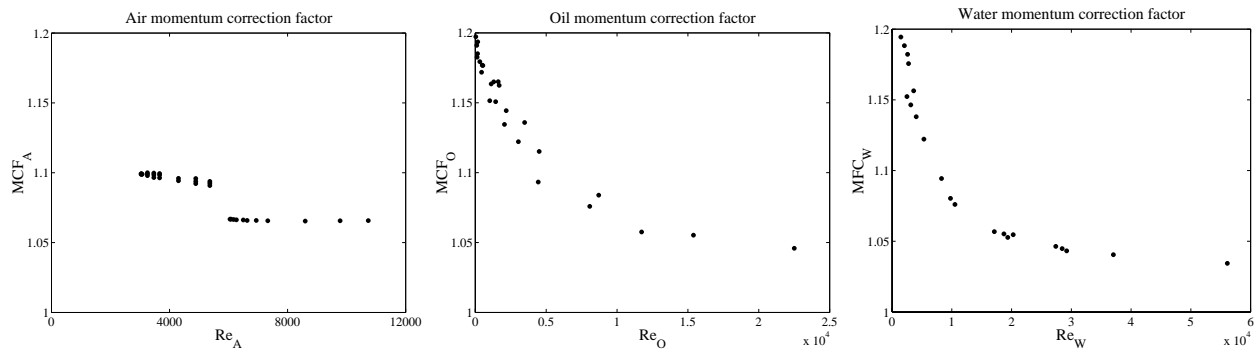


Figure 17: Calculated momentum correction factors in stratified smooth three-phase flow.

The model offers great flexibility in addressing turbulent stratified multiphase flow in pipes. It does not rely on empirical data other than those involved in turbulence models. The calculations presented here are restricted to smooth interfaces only, limiting the immediate applicability of the results, but the effect of interfacial waves is considered to be a modelling issue more than a part of the numerical method, and later studies will show how the immersed interface method can be applied to predict stratified wavy multiphase pipe flow.

Acknowledgement

This work was supported by the Norwegian Research Council through the Petronics programme for doctoral studies.

References

- Andritsos, N., Hanratty, T.J., 1987. Influence of interfacial waves in stratified gas-liquid flows. *AIChE Journal* 33(3), 444–454.
- Berger, M., Rigoutsos, I., 1991. An algorithm for point clustering and grid generation. *IEEE Transaction on System, Man and Cybernetics* 21(5), 1278–1286.
- Berthelsen, P.A., 2004. A decomposed immersed interface method for variable coefficient elliptic equations with non-smooth and discontinuous solutions. *Journal of Computational Physics* 197(1), 364–386.
- Berthelsen, P.A., Ytrehus, T., 2004. Stratified smooth two-phase flow using the immersed interface method. Submitted to *Computers & Fluids*.
- Biberg, D., 1999. Two-phase stratified pipe flow modelling - A new expression for the interfacial shear stress. The 2nd International Symposium on Two-Phase Flow Modelling and Experimentation, Pisa, Italy, May 22–26.
- Chen, H.C., Patel, V.C., 1988. Near-wall turbulence models for complex flows including separation. *AIAA Journal* 26(6), 641–648.
- Chesshire, G., Henshaw, W.D., 1990. Composite overlapping meshes for the solution of partial differential equations. *Journal of Computational Physics* 90(1), 1–64.

- Demuren, A.O., Rodi, W., 1984. Calculation of turbulence-driven secondary motion in non-circular ducts. *Journal of Fluid Mechanics* 140, 189–222.
- Espedal, M., 1998. An experimental investigation of stratified two-phase pipe flow at small inclinations. Dr.Ing.-thesis, Norwegian University of Science and Technology, Department of Applied Mechanics, Thermo- and Fluid Dynamics, Trondheim, Norway.
- Issa, R.I., 1988. Prediction of turbulent, stratified, two-phase flow in inclined pipes and channels. *International Journal of Multiphase Flow* 14(2), 141–154.
- Khor, S.H., Mendes-Tatsis, M.A., Hewitt, G.F., 1997. One-dimensional modelling of phase holdups in three-phase stratified flow. *International Journal of Multiphase Flow* 23(5), 885–897.
- Martin, D.F., Cartwright, K., 1996. Solving Poisson's equation using adaptive mesh refinement. Technical Report UCB/ERI M96/66, U.C. Berkeley, California, USA. <http://seesar.lbl.gov/ANAG/staff/martin/AMRPoisson/>
- Meknassi, F., Benkirane, R., Line, A., Masbernat, L., 2000. Numerical modeling of wavy stratified two-phase flow in pipes. *Chemical Engineering Science* 55, 4682–4697.
- Newton, C.H., Behnia, M., 2000. Numerical calculation of turbulent stratified gas-liquid pipe flows. *International Journal of Multiphase Flow* 26(2), 327–337.
- Newton, C.H., Behnia, M., 2001. A numerical model of stratified wavy gas-liquid pipe flow. *Chemical Engineering Science* 56, 6851–6861.
- Roberts, I.F., 1996. Modelling and experimental studies of transient stratified multiphase flows. PhD-thesis, Imperial College, London, England.
- Spedding, P.L., Hand, N.P., 1997. Prediction in stratified gas-liquid co-current flow in horizontal pipelines. *International Journal of Heat and Mass Transfer* 40(8), 1923–1935.
- Strand, Ø., 1993. An experimental investigation of stratified two-phase flow in horizontal pipes. Dr.Scient.-thesis, University of Oslo, Department of Mathematics, Mechanics Division, Oslo, Norway.
- Shoham, O., Taitel, Y., 1984. Stratified turbulent-turbulent gas-liquid flow in horizontal and inclined pipes. *AIChE Journal* 30(3), 377–385.
- Taitel, Y., Barnea D., Brill J.P., 1995. Stratified three phase flow in pipes. *International Journal of Multiphase Flow* 21(1), 53–50.
- Taitel, Y., Dukler, A.E., 1976. A model for predicting flow regime transitions in horizontal and near horizontal gas-liquid flow. *AIChE Journal* 22(1), 47–55.
- Wolfshtein, M., 1969. The velocity and temperature distribution in one-dimensional flow with turbulence augmentation and pressure gradient. *International Journal of Heat and Mass Transfer* 14, 301–318.

Paper IV

Calculations of stratified wavy two-phase flow in
pipes

P. A. Berthelsen & T. Ytrehus

Submitted to
International Journal of Multiphase Flow